Graduate School Form 30
(Updated 11/20/2014)

PURDUE UNIVERSITY
GRADUATE SCHOOL
Thesis/Dissertation Acceptance

This is to certify that the thesis/dissertation prepared

By Tanya Lynn Katzman

Entitled THE USE OF STABLE ISOTOPES AND PARTICULATE MATTER IN THE INVESTIGATION OF LOCAL AND REGIONAL ATMOSPHERIC CHEMISTRY

For the degree of Doctor of Philosophy

Is approved by the final examining committee:

Greg Michalski

Paul B. Shepson

Garth J. Simpson

Linda Lee

To the best of my knowledge and as understood by the student in the Thesis/Dissertation Agreement, Publication Delay, and Certification/Disclaimer (Graduate School Form 32), this thesis/dissertation adheres to the provisions of Purdue University's "Policy on Integrity in Research" and the use of copyrighted material.

Greg Michalski

Approved by Major Professor(s): _____

_____

Approved by: Timothy Zwier 07/18/2016

Head of the Department Graduate Program Date

THE USE OF STABLE ISOTOPES AND PARTICULATE MATTER IN THE INVESTIGATION OF LOCAL AND REGIONAL ATMOSPHERIC CHEMISTRY

A Dissertation

Submitted to the Faculty

of

Purdue University

by

Tanya Lynn Katzman

In partial Fulfillment of the

Requirements of the Degree

of

Doctor of Philosophy

August 2016

Purdue University

West Lafayette, Indiana

To my family and friends, both near and far.

ACKNOWLEDGMENTS

First and foremost, I'd like to thank my family and friends for their endless love, support, and endless optimism. Their support means the world to me, and keeps me going every day. I'd like to thank my parents for letting me thoroughly confuse them when I needed to vent about my research. My board game family here at Purdue, for entertaining, distracting, supporting, and encouraging me.

This work would not have been possible without the guidance and assistance from my advisor, Dr. Greg Michalski. To thank Dr. Bethany Theiling, thank you for your patience and expertise when it came to instrumentation. My lab mates over the years have been a crucial part of the process, as sounding boards and as teachers: Dr. Krystin Riha, Dr. Fan Wang, Dan McMahon, Mike King, Wendell Walters, Benjamin Wilkins, and Huan Fang. To my PSI lab colleagues, Dr. Tim Berry and Christy Gibson, your friendship, support, and assistance means a lot to me. I'd also like to thank the undergraduate researchers that I've worked with over the years, who's assistance has been invaluable.

Last but not least, I'd like to thank my New Zealand collaborators, Dr. Perry Davy and Dr. Mike Harvey. Thank you so much for sponsoring me during EAPSI, and making my New Zealand projects possible. I can't wait to see how it all turns out! I'd also like to

thank Pam Rodgers, for assistance in weighing and dispensing filters, Dr. Travis Ancelet, for his assistance with XRF, and the NIWA staff who have/are continuing my Baring Head sampling program now that I am back stateside. You all were extremely helpful during my time in New Zealand, and I had a great, albeit productive, time during my visit.

TABLE OF CONTENTS

Page

LIST OF TABLES vii

LIST OF FIGURES ix

ABSTRACT xii

CHAPTER 1: INTRODUCTION AND OVERVIEW 1

1.1 Aerosol Background 1
1.2 Stable Isotopes 4
1.2.1 Nitrogen Isotopes and the Nitrogen Cycle 6
1.2.2 NOx Oxidation 8
1.2.3 Oxygen Isotopes 11
1.3 Chapter Organization 13
1.4 References 14

CHAPTER 2: ANALYTICAL METHODS 16

2.1 Ion Chromatography 16
2.2 Isotope Ratio Mass Spectrometry 18
2.3 Denitrifier Method 19
2.4 BrF_5 Laser Decomposition 21
2.5 ICP-OES 23
2.6 X-Ray Fluorescence 23
2.7 Black Carbon 25
2.8 Nutrient Analysis of NH_3 25
2.9 References 27

CHAPTER 3: DETERMINATION OF NO + O2 REACTION MECHANISM USING STABLE ISOTOPES 28

3.1 Introduction 28
3.2 Method 33
3.3 Results and Discussion 35
3.4 Conclusion 42
3.5 References 44

Page

CHAPTER 4: 2007 CALIFORNIA AEROSOL STUDY: EVALUATION OF $\delta^{15}N$ AS A TRACER OF NOX SOURCES AND CHEMSITRY 46

4.1 Introduction....46
4.2 Methods....53
4.2.1 Site Description....53
4.2.2 2007 California Wildfire Season 56
4.2.3 Sample Analysis....57
4.3 Results....59
4.4 Discussion....65
4.5 Conclusion 80
4.6 References....81

CHAPTER 5: SEASONAL VARIATIONS IN PARTICULATE MATTER AT A COASTAL URBAN CENTER....86

5.1 Introduction....86
5.2 Sampling Site....87
5.2.1 Materials and Sampling Conditions....89
5.3 Analysis Methods....89
5.3.1 Black Carbon 89
5.3.2 Ion Chromatography 90
5.3.3 X-ray Fluorescence 90
5.3.4 Stable Isotope Analysis....91
5.4 Results and Discussion 91
5.5 Conclusions....100
5.6 References....102

CHAPTER 6: CONCLUSIONS 105

APPENDICES

Appendix A: Investigating Sulfur Sources and Oxidation Chemistry in Sulfate Aerosol Production in the Southern Ocean and New Zealand Mainland 108
Appendix B: Laser Decomposition Isotope Interface (LADII) 121

VITA....126

PUBLICATION....128

LIST OF TABLES

Table Page

1.1 National Ambient Air Quality Standards as set forth by the U.S. Environmental Protection Agency 2

1.2 Natural abundances of stable isotopes used in biogeochemistry 4

1.3 Absolute isotope ratios of international standards 5

1.4 The nitrogen cycle 8

1.5 Source $\delta^{15}N$ values from literature 10

2.1 Working nitrate isotope lab standards 20

2.2 Isodat control code settings for LADII 30

3.1 Summary of trial conditions 34

3.2 Calculated reaction temperature and Rayleigh calculated enrichment and fractionation factors 35

3.3: Root-mean-square speeds of NO and O_2 isotopologues 37

3.4 Summary of reaction rates used in the Kintecus model 39

3.5 Kintecus model parameters 40

4.1 Site Demographics as recorded by the US Census Bureau and California Air Resources Board 55

4.2 Power Plants in San Diego County and Imperial County by fuel/operation type as of 2015 56

4.3 Proportion of NOx sources (f) by category (in bold) and sub-category (italics) 68

4.4 Mass balance source $\delta^{15}N$-NOx values 68

Table Page

4.5 List of sampling days impacted by wildfires, as recorded in the CARB sampling notes at each sampling site. 76

Appendix Table

B.1: Isodat Control Code Settings for LADII 124

LIST OF FIGURES

Figure Page

1.1 Summary of nitrogen cycling and subsequent oxidation/reduction processes that occur in the atmosphere 7

1.2 Oxygen isotopic composition of atmospheric compounds. 12

2.1 Dual inlet system of the IRMS.....18

2.2 Laser Decomposition Isotope Interface (LADII) Mode A (top) and Mode B (bottom). The 3-Port valve has 2 functions: connecting to He #1 (purple arrow) and bypassing He #1 (orange arrow).....27

3.1 Schematic of the gas line used in this experiment 33

4.1 Satellite image of Southern California, taken October 22, 2007. Image show fires burning (red) and presence of strong Santa Ana winds pushing smoke offshore. Sampling sites are numbered as follows: Chula Vista (1), El Cajon (2), El Centro (3), and Brawley (4). Image courtesy of NASA/MODIS Rapid Response 53

4.2 Comparison of anion concentrations as measured by the California Air Resources Board in 2007 and the Purdue Stable Isotope Lab in 2015. Filled in triangles are samples showing NH_4NO_3 loss, and red trend line indicates the agreement of non-volatilized samples. 60

4.3 $\delta^{15}N_{NO3}$ (left) values and anion concentrations (right) in PM_{10} collected in Chula Vista, California. Noted wildfire activity during PM_{10} sampling is circled/boxed.....61

4.4 $\delta^{15}N_{NO3}$ values as observed in El Cajon (left) and El Centro (right). 62

4.5 CO (left) and O_3 (right) 24-hour average concentrations at Chula Vista, California. Noted wildfire activity during PM_{10} sampling is circled.....64

Figure Page

4.6 EGU fuel usage for San Diego and Imperial Counties, California....66

4.7 Seasonality of unknown $\delta^{15}N$ source for El Centro (top), El Cajon (middle) and Chula Vista (bottom), California....70

4.8 Hourly $\delta^{15}N_{NO2}$ (top) and NO_2 mole ratio (bottom) for Chula Vista, CA. In the top figure, trace represents a 24-point moving average. Stars represent observed aerosol NO_3 $\delta^{15}N$ values....74

4.9 PM_{10} (left) and $PM_{2.5}$ (right) concentrations in Chula Vista, California in 2007. Fire days are circled in orange. 77

4.10 NOx, NO, and NO_2 concentrations as observed in Chula Vista, California during the year of 2007. Fire days are circled in orange. 78

5.1 Location of the Whangarei, New Zealand sampling site....88

5.2 PM_{10} (left) and BC (right) concentrations and daily average temperatures for Whangarei, New Zealand....92

5.3 Daily average K^+ concentration and temperature for Whangarei, New Zealand....94

5.4 Cl and S concentrations for Whangarei, New Zealand....95

5.5 Nitrate concentrations and daily average temperatures for Whangarei, New Zealand....96

5.6 $\delta^{15}N$ (top) and $\Delta^{17}O$ (bottom) for NO_3^- collected in Whangarei, New Zealand 98

Appendix Figure Page

A.1 New Zealand aerosol sampling locations. Warmer colors indicate areas of high biological productivity and DMS fluxes. The 8 most common back trajectories from Baring Head (% occurrences) indicate shifts in terrestrial and oceanic SO_4^{2-} loading. Modified from Sievering et al., 2004 109

A.2 $\Delta^{17}O$ vs. $\delta^{34}S$ in sulfate from different sources and oxidation pathways. Mass dependent fractionation follow $\delta^{17}O = 0.52 \times \delta^{18}O$ and produce $\Delta^{17}O \approx 0‰$. Mass independent fractionation follows $\Delta^{17}O = \delta^{17}O - 0.52 \times \delta^{18}O$, where $\Delta^{17}O > 0‰$. Terrestrial SO_4^{2-} should be isotopically distinct from Southern Ocean SO_4^{2-}. My working hypothesis suggests these two isotopic "end-members" (dashed boxes) will be found in aerosols with different air mass trajectories and in different aerosol sizes, or as mixture between the two end-members 110

A.3 pH dependent of SO_2 oxidation and its impact on the product SO_4^{2-} and $\Delta^{17}O$ value 112

A.4 Whangarei SO_4^{2-} concentrations (circles, right) peak in the summer, whereas Cl^- (red diamond) does not, indicating a large DMS flux rather than an increase in sea salt. Statistical analysis of HySplit back trajectories suggests secondary SO_4^{2-} in Whangarei (left) originates in the Tasman Sea or the western Pacific. Baring Head secondary SO_4^{2-} originates in the Southern Ocean, and allows for the comparison of regional S cycles (Subtropics vs. Southern Ocean) 113

A.5 Baring Head Atmospheric Research Station at Baring Head Lighthouse. 115

A.6 The 15m tower located at Baring Head (left) will have one sampler at the top and one at the bottom. A previously installed Lear Siegler sampler with PM10 inlet at the top of the tower will sample only southerly events. A second sampler, installed at the base of the tower (right) during EAPSI, will continuously sample all air masses 116

B.1: Laser Decomposition Isotope Interface (LADII) Mode A (top) and Mode B (bottom). The 3-Port valve has 2 functions: connecting to He #1 (purple arrow) and bypassing He #1 (orange arrow) 123

ABSTRACT

Katzman, Tanya Lynn. Ph.D., Purdue University, August 2016. The Use of Stable Isotopes and Particulate Matter in the Investigation of Local and Regional Atmospheric Chemistry. Major Professor: Greg Michalski.

The chemical composition of particulate matter (PM), a known contributor to air pollution, is highly variable, and elemental analysis reveals information about local and regional sources, as well as how air masses and climate influence PM compositions. Seasonal changes in climate, such as temperature, amount of daylight, or meteorological patterns influence source emissions (increased residential heating activities, decreased natural soil emissions) and the relative importance of certain chemical pathways in the atmosphere. Since the magnitude of these seasonal changes are highly dependent on location, each sampling site is unique and the chemical composition of PM provides valuable insight into local and regional atmospheric chemistry. Elemental analysis was used to evaluate local atmospheric chemistry at four sites in Southern California (Chula Vista, El Cajon, El Centro, and Brawley) and in Whangarei, New Zealand. PM in Southern California sites revealed seasonal trends, but also how emissions from the 2007 wildfire season impacted local chemistry, producing elevated PM and trace gas concentrations and low O_3 concentrations. Analysis of PM collected in Whangarei, New Zealand revealed that local atmospheric chemistry is heavily influenced by marine air masses, seasonal shifts

in source contributions (e.g. residential heating activities), and changes in boundary layer height.

Stable isotope ratios are often applied as tracers of sources and local chemistry, which is extremely useful for deciphering PM. As the main NOx sink, the stable isotope composition of NO_3^- reflects NOx sources contributions, oxidation pathways, and other processes that effect the isotope distribution (e.g. equilibrium exchange). However, the use of N isotopes ($\delta^{15}N$) as a tracer is usually split between two schools of thought: the source hypothesis and the chemistry hypothesis. The source hypothesis claims that the $\delta^{15}N$ value of NO_3^- is solely determined by NOx source $\delta^{15}N$ values, and observed variations are due to shifts in source emissions. Alternatively, the chemistry hypothesis argues that the $\delta^{15}N$ value of NO_3^- is impacted by source contributions and chemical reactions occurring in the atmosphere. Here, variations in observed $\delta^{15}N$ values are attributed to changes in reaction pathway contribution, as well as shifts in source emissions. Stable isotope analysis of NO_3^- collected in Southern California and Whangarei, New Zealand was used to evaluate these hypotheses. Using source emission data, known $\delta^{15}N$ values of NOx sources, and observed $\delta^{15}N$ values of NO_3^- collected in Chula Vista, CA, isotope mass balance suggests that the source $\delta^{15}N$ value is not conserved, requiring a NOx source with an unreasonably large $\delta^{15}N$ value (~ 280‰) to explain observed values. Isotope exchange equilibrium was found to explain observed $\delta^{15}N$ values well, but deviations did exist, particularly in the winter. These deviations are likely due to shifts in the importance of this exchange and additional fractionation effects associated with reaction pathways. Additionally, the inverse correlation between $\delta^{15}N$ and solar radiation observed in Whangarei further supports the chemistry hypothesis. The research presented in this dissertation is the first known

evaluation of these two stable isotope hypotheses, with the results strongly support the chemistry hypothesis.

While the oxidation of NO_2 is well understood, the mechanism of the oxidation of NO to NO_2 is highly uncertain, and so stable isotopes were utilized to determine this reaction mechanism. Laboratory studies found that the remaining O_2 became depleted relative to the O_2, and followed a strict mass dependent relationship. Complimented by kinetic modeling, results strongly suggest that this reaction proceeds in two steps, with the formation of a peroxynitrate intermediate being favored due to the observed mass dependent relationship. This research is the first to offer support to the peroxynitrate intermediate, whereas previous works favored the energetically more stable nitrogen trioxide form.

CHAPTER 1: INTRODUCTION AND OVERVIEW

1.1 Aerosol Background

Aerosols, more specifically particulate matter (PM), are a major contributor to air pollution, causing reduced visibility, contributing to acid deposition, and have been linked to cardiac and respiratory diseases, including lung cancer.[1–3] For this reason, the EPA regulates PM emissions, setting daily and annual limits (Table 1.1). Although particles can range from a few nanometers to tens of micrometers in diameter, two size categories in particular are monitored: fine aerosol ($PM_{2.5}$), which consists of particles with a diameter of 2.5μm or less, and course aerosol (PM_{10}), with diameters less than 10μm. These aerosols can be directly emitted from a source (primary aerosols) or formed in the atmosphere due to chemical and physical reactions in the atmosphere (secondary aerosol).[1,3] The chemical composition of particulate matter is highly dependent on local and regional sources, local meteorology, and mechanical processes, such as wind, which includes particles such as pollen, dust, and sea salt, and thus contains a wealth of knowledge about their source as well as the environments and reactions that shaped the particle. They tend to have short lifetimes (few days to a few weeks), as they are rapidly removed by wet (precipitation, fog) or dry (settling) deposition, and so reflect the chemistry of the region.[1] Aerosol composition varies by location since sources, atmospheric processes, prevailing meteorology, and seasonality are all non-uniform.

Table 1.1: National Ambient Air Quality Standards as set forth by the U.S. Environmental Protection Agency

Pollutant		Averaging Time	Concentration Limit
Carbon Monoxide (CO)		1 hour	35 ppm
Lead (Pb)		Rolling 3-month average	0.15 μg/m^3
Nitrogen Dioxide (NO_2)		1 year	53 ppb
Ozone (O_3)		8 hours	0.070 ppm
Particular Matter (PM)	$PM_{2.5}$	24 hours	35 μg/m^3
	PM_{10}	24 hours	150 μg/m^3
Sulfur Dioxide (SO_2)		1 hour	75 ppb

Despite their problems, aerosols also play an important role in regulating climate, through direct and indirect means[1]. Aerosol components can both scatter and absorb radiation, and the overall effect depends on the aerosol mixture. Ammonium sulfate scatters radiation, whereas black carbon absorbs radiation, thus the makeup of the mixture determines the net direct effect of the aerosol mass.[1] Indirectly, aerosol concentrations influence the number of cloud condensation nuclei (CCN), which in turn influence the formation of clouds (influencing the droplet size and number), cloud lifetime, and Earth's albedo.

However, there is some disagreement as to how exactly the Earth's climate will respond. The CLAW hypothesis, named after its authors Robert Jay Charlson, James Lovelock, Meinrat Andreae and Stephen G. Warren, proposes a negative feedback loop, where ocean warming enhances dimethyl sulfide (DMS) production, SO_4^{2-} aerosol, and thus CCN. The end result would be homeostasis: warming oceans would lead to an increase in the Earth's albedo which would in turn would cool the Earth.[4] A more recent theory proposes a positive feedback loop, commonly referred to as the Anti-CLAW hypothesis.

This theory suggests that ocean warming will deprive phytoplankton of nutrients, leading to a decrease in DMS production, SO_4^{2-} aerosol, and CCN. The net effect would result in a reduction of albedo, warmer and warmer oceans, and an enhancement of the feedback loop.[5]

In general, aerosols can be categorized by their environment. Urban aerosols are heavily dominated by anthropogenic aerosols, specifically from industrial processes, motor vehicles, and power generation, with natural sources such as pollen and dust contributing a much smaller proportion. Rural continental aerosols are a mixture of natural and anthropogenic influences, whereas remote continental aerosols tend to be more fine than coarse with a mixture of natural aerosols and transported oxidation products. Marine aerosols that lack continental transport influence are typically of remote ocean origins, with sea spray being the main contributor to the mass of both coarse and fine particles. Although aerosols of different origins have different compositions, aerosols at one location can also differ by season, day, or even diurnally as source contributions, chemistry or weather patterns change.

Despite their similar relative size, PM_{10} and $PM_{2.5}$ are produced by different processes, have different chemical compositions, are removed from the atmosphere by different processes, and impact the respiratory system very differently.[1] Coarse particles tend to contain sea salt, soil dust, crustal materials, volcanic ash, pollen, and/or tire wear particles, whereas fine particles tend to contain combustion products, such as soot, NO_3^-, SO_4^{2+}, NH_4^+, secondary organic aerosols (SOAs), and coagulated smaller particles. Composition is not only locally and regionally dependent, but also varies with seasons.

Table 1.2: Natural abundances of stable isotopes used in biogeochemistry[19]

Isotope	Natural Abundance
^{2}H	0.0115%
^{13}C	1.07%
^{15}N	0.37%
^{17}O	0.038%
^{18}O	0.205%
^{33}S	0.75%
^{34}S	4.20%
^{36}S	0.01%

Although sources such as motor vehicle emissions vary very little during the year, sources such as pollen and volatile organic compounds (VOCs) are seasonally dependent. The extent of the seasonal dependence is dependent on local climate, and as a result, regions that experience large seasonal temperature and photochemical swings experience the most seasonality. For example, photochemical dependent product concentrations (NO, DMS from phytoplankton) tend to peak in the summer, whereas nitrate tends to peak in the winter when the amount of solar radiation and boundary layer height are at a minimum, and lower temperatures cause HNO_3 to be less volatile.[1]

1.2 Stable Isotopes

Stable isotope ratios are often used as tracers of sources and chemical or physical processes, which is extremely useful for deciphering aerosol mixtures. Hydrogen (^{2}H), carbon (^{13}C), nitrogen (^{15}N), oxygen (^{17}O, ^{18}O), and sulfur (^{34}S) all have stable isotopes that are routinely used as a tracer. As the concentration of these isotopes is incredibly small compared the their lighter, more abundant counter parts (Table 1.2), sample isotope

Table 1.3: Absolute isotope ratios of international standards[19]

Standard	Isotope	Accepted Atomic Ratio
Standard Mean Ocean Water (SMOW)	D/H	0.00015576
	$^{18}O/^{16}O$	0.00200520
	$^{17}O/^{16}O$	0.000373
PeeDee Belemnite (PDB)	$^{13}C/^{12}C$	0.0112372
	$^{18}O/^{16}O$	0.0020671
	$^{17}O/^{18}O$	0.000379
Air N_2	$^{15}N/^{14}N$	0.0036765
Canyon Diablo Troilite (CDT)	$^{34}S/^{32}S$	0.0450045

composition is reported as a comparison to reference material with known isotope composition (Table 1.3) and reported in units of per mil (‰):

$$\delta(‰)=\left(\frac{R_{sample}}{R_{standard}}-1\right)\times 1000 \qquad \text{(Eq. 1)}$$

R refers to the atomic ratio of the heavy isotope to the light isotope (e.g. $^{17}O/^{16}O$). Although the natural abundance is the main influence of isotope composition, natural variations occur as the result of chemical or physical processes and conditions which influence the distribution. It is this behavior that allows stable isotope ratios to be such good tracers.

Compounds with the same molecular formula and connectivity, but possess different isotopes (e.g. $^{14}N^{16}O$ and $^{14}N^{17}O$) are known as isotopologues. An isotopologue's slightly heavier mass has an impact on the thermodynamic and physical properties of the molecule, referred to as an isotope effect. A heavier isotope, for example, reacts at a slower rate than a lighter isotope, which can cause a particular isotope to accumulate on one side of a reaction more than the other. Isotope effects are especially pronounced in lighter isotopes such as H, C, N, O, and S. The extent of this effect is quantified by a fractionation factor (α), defined as the ratio of the isotopologue atomic ratios or reaction rates:[6]

$$\alpha_{A\text{-}B} = \frac{R_A}{R_B} \quad \text{(Eq. 2)}$$

$$\alpha_{A\text{-}B} = \frac{k_A}{k_B} \quad \text{(Eq. 3)}$$

Partitioning has also been described using an enrichment factor (ε), which is related to α as follows:[6]

$$\varepsilon(‰) = (\alpha_{A\text{-}B} - 1) \times 1000 \quad \text{(Eq. 4)}$$

Isotopes can fractionate one of two ways: through equilibrium exchange or as the result of kinetic preference. Equilibrium exchange processes show no net change in chemical species, but rather there is an isotopologue shift as isotopes shift between molecules (e.g. $^{14}N^{16}O + {}^{16}O^{17}O \leftrightarrow {}^{14}N^{17}O + {}^{16}O^{16}O$). Kinetic isotope effects result in situations where the reaction is unidirectional (e.g. evaporation in an open container) or in situations where a unidirectional rate of a reaction is sensitive to mass at a specific position in an isotopologue. Isotope effects will be utilized in Chapter 3.

1.2.1 Nitrogen Isotopes and The Nitrogen Cycle

Nitrogen aerosols are a part of the global nitrogen cycle, a key biogeochemical cycle in the Earth system. Nitrogen is essential to life, as it is an essential part of the nucleic acids that make up DNA.[1,7] However, N_2, the most abundant form of nitrogen in the atmosphere, is not biologically useful due to the stability of the N≡N bond. However, the process of fixation transforms N_2 into NO:[1]

$$N_2 \rightarrow \text{NO or } NH_4^+ \quad \text{(R1)}$$

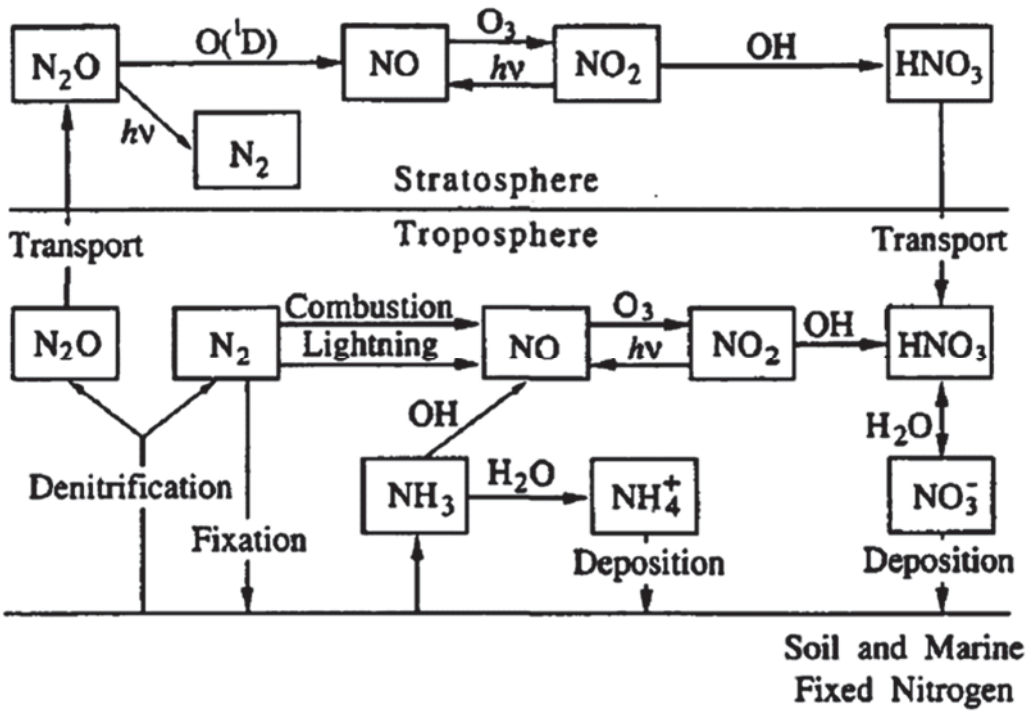

Figure 1.1: Summary of nitrogen cycling and subsequent oxidation/reduction processes that occur in the atmosphere.[1]

Fixation can occur naturally, through ionization by solar radiation or lightning or transformed into NH_4^+ by microorganisms, or as a byproduct of anthropogenic combustion processes. Once fixed, nitrogen is processed and transformed into other nitrogen forms, both inorganic (e.g. nitrate) and organic (e.g. amino acids).[7] The nitrogen transformation processes are together referred to as The Nitrogen Cycle. The nitrogen cycle (Figure 1.1) is important for primary productivity in many ecosystems, but human activities have dramatically increased the amount of biologically available nitrogen, thus altering the nitrogen cycle. This alteration can be detrimental to the environment, as nitrogen plays a critical role in environmental issues such as the greenhouse effect, ozone depletion, and acid deposition.[8] The nitrogen cycle is comprised of five major transformation processes:

Table 1.4: The nitrogen cycle[1]

Process	Reaction
N_2 fixation	$N_2 \rightarrow RN$
Nitrification	$NH_4^+ \rightarrow NO_3^- \rightarrow NO_2^-$
Denitrification	$NO_3^- \rightarrow NO_2^- \rightarrow NO/N_2O \rightarrow N_2$
N assimilation	$NH_4^+ \rightarrow RN$ $NO_3^- \rightarrow RN$
N Mineralization (ammonification)	$RN \rightarrow NH_3 \rightarrow NH_4^+$

fixation, nitrification, denitrification, mineralization, and assimilation. These transformations are influenced by bacteria and other microorganisms, and so there are many environmental factors influencing these processes. The use of nitrogen isotopes ($\delta^{15}N$) is useful in tracing how nitrogen compounds are transformed in the environment. Nitrogen cycle transformation processes and their associated isotope effects are summarized in Table 1.4.

1.2.2 NOx Oxidation

Nitrogen oxides (NOx = NO + NO_2) are responsible for regulating the oxidation capacity of the atmosphere, as they influence both the formation and destruction of O_3 and OH radicals, both of which are important oxidizers. For this reason, NOx is highly reactive, with an atmospheric lifetime of less than a day to a week at best. Lifetimes of other atmospheric trace gases are influenced by NOx.[9,10] NOx is a product of both natural (lightning, soil nitrification/denitrification, wildfires) and anthropogenic emissions (fossil fuel combustion in motor vehicles, power generation, and industrial processes).[11–13] Since the Industrial Revolution, anthropogenic emissions have exceeded natural emissions.[11]

However, with the implementation of the Clean Air Act and similar legislation globally, NOx emission in North America and Europe have declined, although concentrations in Asia are increasing. HNO_3 and aerosol NO_3^- are the main sinks of NOx, both of which contribute to environmental acidification, eutrophication, and biodiversity shifts in terrestrial ecosystems.[8,11–13]

NOx is oxidized by a variety of oxidants in the atmosphere to NO_2, and ultimately into a variety of nitrate forms, both organic and inorganic. The Leighton Cycle describes how NOx cycles photochemically between NO and NO_2 during the daytime:

$$NO + O_3 \rightarrow NO_2 + O_2 \quad \text{(R2)}$$

$$NO_2 + h\upsilon \rightarrow NO + O\left(^3P\right) \quad \text{(R3)}$$

$$O\left(^3P\right) + O_2 \rightarrow O_3 \quad \text{(R4)}$$

NO is also oxidized by peroxy radicals (HO_2 or ROO) to form NO_2:

$$NO + HO_2 \text{ (or ROO)} \rightarrow NO_2 + OH \text{ (or RO)} \quad \text{(R5)}$$

NO_2 is further oxidized by OH radicals or O_3 to form NO_3^- or HNO_3, the major sinks for NOx.

$$NO_2 + O_3 \rightarrow NO_3 + O_2 \quad \text{(R6)}$$

$$NO_2 + OH + M \rightarrow HNO_3 + M \quad \text{(R7)}$$

However, as the NO_3 radical is readily photolyzed,[14] daytime oxidation favors the OH radical, whereas O_3 is favored at night. Additionally, NO_2 accumulates at night, due to the lack of photolysis,[15,16] and reacts with NO_3 radical to form N_2O_5. N_2O_5 can hydrolyze on aerosol surfaces to produce HNO_3.

Table 1.5: Source $\delta^{15}N$ values from literature.

Source	$\delta^{15}N$ range	Reference
Coal Fired Power Plants	+6 to +25.6‰	Walters et al., 2015b; Heaton, 1990; Felix et al., 2012
Natural Gas Power Plants	-18.2 to -14.8‰	Walters et al., 2015b
Motor Vehicle - gas	-19.1 to 17‰	Walters et al., 2015a
Motor Vehicle - diesel	-5 to 0‰	Walters et al., 2015b
Off-Road Vehicles - gas	-14.2 to -8.8‰	
Airplanes	-0.9‰*	
Ships/Trains	-19‰*	
Soils	-48.9 to -19.9‰	Walters et al., 2015b; Li & Wang, 2008; Felix & Elliott, 2014
Wildfires	-7 to 12‰	Fibiger et al., 2014
* predicted		

$$NO_2 + NO_3 \rightarrow N_2O_5 \quad \text{(R8)}$$

$$N_2O_5 + H_2O_{(l,\ aerosol)} \rightarrow 2HNO_3 \quad \text{(R9)}$$

NO_3 radical can also react with VOCs to form HNO_3 by abstracting a hydrogen atom.

$$NO_3 + VOC \rightarrow HNO_3 + R \quad \text{(R10)}$$

HNO_3 is highly soluble and thus readily removed from the atmosphere by wet and dry deposition. Additionally, both NOx and NO_3 radicals can react with VOCs to produce a variety of organic nitrates:[17]

$$NO_2 + RO_2 + M \rightarrow RONO_2 + M \quad \text{(R11)}$$

$$NO_2 + R(O)O_2 + M \rightarrow R(O)OONO_2 + M \quad \text{(R12)}$$

$$NO_3 + VOC \rightarrow RONO_2 \quad \text{(R13)}$$

As the main sinks of NOx, analysis of the isotope composition of nitrates reflect the contributing NOx sources and transformation processes.

The isotopic composition of isotopes is really a mixture of its contributing sources or processes.[18] In the case of nitrate, the main NOx sink, the nitrogen isotope value ($\delta^{15}N_{NO3}$) reflects the sources, subsequent transformations or chemical reactions, and any post-depositional effects that the NO_3^- sample has undergone.[9] Table 1.5 summarizes previously measured source $\delta^{15}N$ values, which can be used with isotope mass balance techniques to assess and quantify the influences to the nitrate product. Isotope mass balance of NO_3^- is calculated by:

$$\delta^{15}N_{NO3} = \sum f_i \delta^{15}N_i \qquad \text{(Eq. 5)}$$

Here, $\delta^{15}N_i$ is the measured nitrogen isotope value for a contributing source, sink, or transformation process, and f_i is the fraction that the source, sink, or transformation contributes to the overall nitrate. Isotope mass balance will be discussed further and used in Chapter 4.

1.2.3 Oxygen Isotopes

Oxygen has three stable isotopes, ^{16}O, ^{17}O, and ^{18}O. $\delta^{18}O$ values are often used to monitor variations in ocean temperature and to monitor Earth's hydrologic cycle[19]. Use of triple oxygen isotopes of nitrate is commonly used to determine the relative importance of different oxidants in the formation of NO_3^-.[20] In most cases, oxygen isotopes fractionate in a mass dependent manner, which adheres to the following relationship:

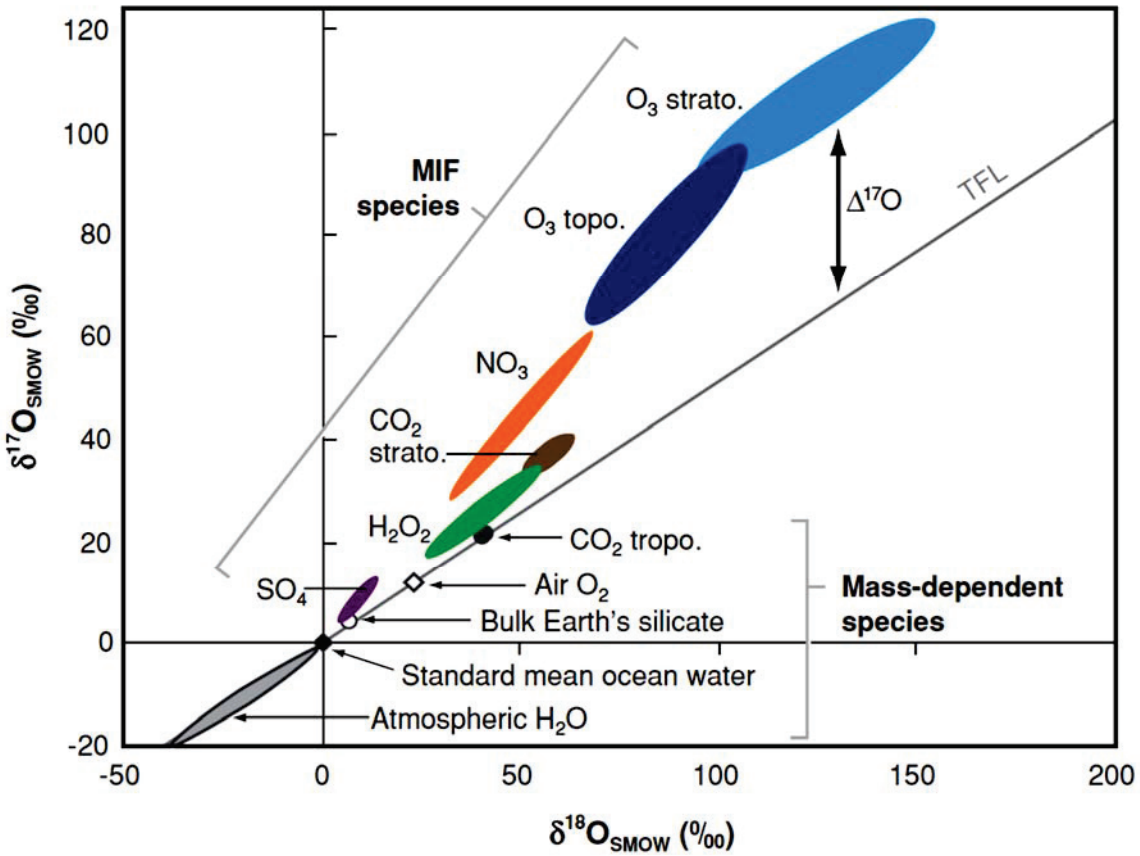

Figure 1.2: Oxygen isotopic composition of atmospheric compounds.[21]

$$\delta^{17}O = 0.52 \times \delta^{18}O \qquad \text{(Eq. 6)}$$

One notable exception to this relationship has been observed in ozone, which possesses roughly equivalent proportions of $\delta^{17}O$ and $\delta^{18}O$, a phenomena known as mass independent fractionation which is quantified by the following relationship:

$$\Delta^{17}O = \delta^{17}O - 0.52 \times \delta^{18}O \qquad \text{(Eq. 7)}$$

Figure 1.2 plots $\delta^{17}O$ vs $\delta^{18}O$ of the main oxygen reservoirs on Earth, producing the terrestrial fractionation line (TFL). Deviations from the TFL ($\Delta^{17}O \neq 0‰$) reflect mass independent fractionation and ozone oxidation influence.

As with N isotopes, oxygen isotope ratios reflect a mixture of inputs. Non-zero $\Delta^{17}O$ values in NO_3^- indicates O_3 oxidation of some degree, whereas $\Delta^{17}O = 0‰$ reflects oxidation by OH radicals, primarily. The larger the $\Delta^{17}O$, the greater the proportion of O_3 oxidation. The impact of $\Delta^{17}O$ will be discussed further in Chapters 5 and 6.

1.3 Chapter Organization

This dissertation is comprised of six chapters, including this introduction, and organized as follows:

- CHAPTER 2: This chapter presents a summary of analytical methods used in the process of completing this dissertation work.
- CHAPTER 3: An investigation into the $NO + O_2$ reaction mechanism using stable isotopes of nitrogen and oxygen is presented.
- CHAPTER 4: This chapter presents an evaluation of the use of $\delta^{15}N$ as an environmental tracer, using particulate matter collected in Southern California during 2007.
- CHAPTER 5: This chapter presents an investigation into the atmospheric chemistry at a coastal urban site using particulate matter collected in Whangarei, New Zealand.

1.4 References

(1) Seinfeld, J. H.; Pandis, S. N. *Atmospheric Chemistry and Physics: From Air Pollution to Climate Change, 2nd Edition* -; 2nd ed.; 2006.

(2) Katzman, T. L.; Rutter, A. P.; Schauer, J. J.; Lough, G. C.; Kolb, C. J.; Van Klooster, S. *Aerosol Air Qual. Res.* **2010**, *10*, 140–U13.

(3) Finlayson-Pitts, B. J.; Pitts, J. N.; Jr. *Chemistry of the Upper and Lower Atmosphere: Theory, Experiments, and Applications*; Academic Press, 1999; Vol. 17.

(4) Charlson, R. J.; Lovelock, J. E.; Andreae, M. O.; Warren, S. G. *Nature* **1987**, *326*, 655–661.

(5) Lovelock, J. *The revenge of Gaia : earth's climate in crisis and the fate of humanity*; Basic Books, 2006.

(6) Hoefs, J. *Stable Isotope Geochemistry*; Springer International Publishing: Cham, 2015.

(7) Bernhard, A. *Nat. Educ. Knowl.* **2010**, *3*, 25.

(8) Galloway, J. N.; Dentener, F. J.; Capone, D. G.; Boyer, E. W.; Howarth, R. W.; Seitzinger, S. P.; Asner, G. P.; Cleveland, C. C.; Green, P. A.; Holland, E. A.; Karl, D. M.; Michaels, A. F.; Porter, J. H.; Townsend, A. R.; V□osmarty, C. J. *Biogeochemistry* **2004**, *70*, 153–226.

(9) Hastings, M. G. *IOP Conf. Ser. Earth Environ. Sci.* **2010**, *9*, 012002.

(10) Hastings, M. G.; Jarvis, J. C.; Steig, E. J. *Science* **2009**, *324*, 1288.

(11) Walters, W. W.; Goodwin, S. R.; Michalski, G. *Environ. Sci. Technol.* **2015**, *49*, 2278–2285.

(12) Walters, W. W.; Michalski, G. *Geochim. Cosmochim. Acta* **2015**, *164*, 284–297.

(13) Walters, W. W.; Tharp, B. D.; Fang, H.; Kozak, B. J.; Michalski, G. *Environ. Sci. Technol.* **2015**, *49*, 11363–11371.

(14) Russell, A. G.; Cass, G. R.; Selnfeld, J. H. *Environ. Sci. Technol.* **1986**, *20*, 1167–1172.

(15) Walters, W. W.; Simonini, D. S.; Michalski, G. *Geophys. Res. Lett.* **2016**, *43*, 440–448.

(16) Freyer, H. D.; Kley, D.; Volz-Thomas, A.; Kobel, K. *J. Geophys. Res.* **1993**, *98*, 14791.

(17) Romer, P. S.; Duffey, K. C.; Wooldridge, P. J.; Allen, H. M.; Ayres, B. R.; Brown, S. S.; Brune, W. H.; Crounse, J. D.; de Gouw, J.; Draper, D. C.; Feiner, P. A.; Fry, J. L.; Goldstein, A. H.; Koss, A.; Misztal, P. K.; Nguyen, T. B.; Olson, K.; Teng, A. P.; Wennberg, P. O.; Wild, R. J.; Zhang, L.; Cohen, R. C. *Atmos. Chem. Phys. Discuss.* **2016**, 1–25.

(18) Kendall, C. In *Isotope Tracers in Catchment Hydrology*; Elsevier Science, 2012; p. 870.

(19) Thiemens, M. H. *Proc. Natl. Acad. Sci. U. S. A.* **2013**, *110*, 17631–17637.

(20) Michalski, G.; Bhattacharya, S. K.; Mase, D. F. *Handbook of Environmental Isotope Geochemistry*; Baskaran, M., Ed.; Springer Berlin Heidelberg: Berlin, Heidelberg, 2012.

(21) Riha, K. M. The Use of Stable Isotopes to Constrain the Nitrogent Cycle, Purdue University, 2013.

CHAPTER 2: ANALYTICAL METHODS

This chapter summarizes the theory and operating specifics of the instruments and techniques used during the completion of this dissertation. Several techniques were used in multiple projects (IC, IRMS, Denitrifier Analysis), whereas some techniques had flaws that made data collected unusable.

2.1 Ion Chromatography

Ion Chromatography is a separation method that separates ions based on their interactions with a mobile phase (eluent) and a stationary phase (separation column). Sample components are separated based on their affinities for the mobile and stationary phase. A component with a greater affinity for the stationary phase than the mobile phase will be retained by the column longer than a component that responds better to the mobile phase. Eluent and separation columns are chosen based on the intended separation target, and can only separate only the type of ion its design allows. For anion analysis, a carbonate eluent, created using a mixture of carbonate and bicarbonate salts, and an anion exchange column is traditionally used.[1] Sample anions in the sample are attracted to cations, typically ammonium, of the separation column. The retention times are dependent on the strength of the ionic interactions between the sample, the column and the eluent. An anion that is more strongly attracted to the column will elude later than an anion that is more strongly attracted

to the eluent. Ion chromatography systems typically have the same general set up and operation. Sample is pumped from a container, through a guard column, and onto a separation column. A guard column serves to protect the separation column from large particles, such as organic matter, that would clog up and ruin a separation column. Eluent is then pumped onto the separation column to elude components off and send them to the suppressor. The suppressor acts to remove or dampen the conductivity of the eluent background, which is high due to its salt content. Removing the background allows for easier detection of the sample conductivity. From the suppressor, separated components arrive at the detector, which measures the electrolytic conductivity of the solution as it arrives at the detector.

Anion concentrations (Cl^-, NO_3^-, and SO_4^{2-}) of particulate matter samples from Whangarei, New Zealand were determined by ion chromatography, using 5 mL of diluted aerosol solution. During analysis, sample was pumped through a 100μL injection loop, which rinsed and prepared for column injection. A 100μL portion was injected on to a Dionex IonPac AG11 guard column prior to loading onto a Dionex IonPac AS11 analytical column. 2.0 mM $NaHCO_3/Na_2CO_3$ eluent was used for the separation. A self-regenerating suppressor (Dionex ASRS 300) reduces the conductivity of the eluent prior to analysis by the conductivity detector (Dionex CD20). Standards of known NO_3^-, SO_4^{2-} and Cl^- concentrations were used to calibrate the IC and determine the sample concentrations. The entire system was automated and analyzed one sample every 20 minutes.

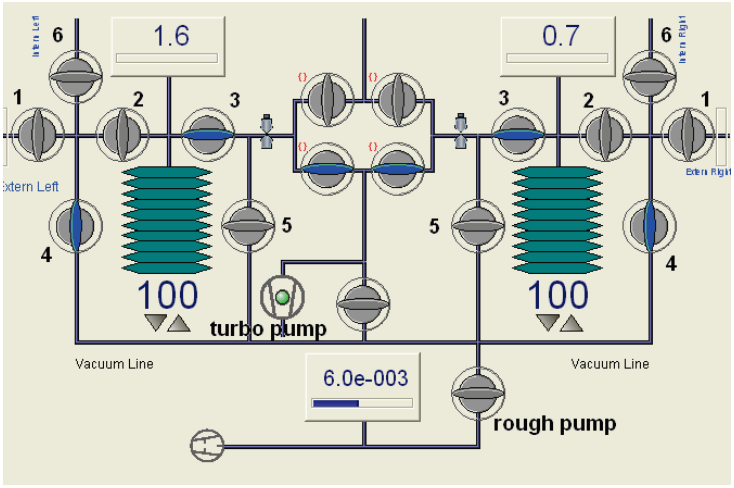

Figure 2.1: Dual inlet system of the IRMS

2.2 Isotope Ratio Mass Spectrometry

Isotopic analysis is conducted using an Isotope Ratio Mass Spectrometer (IRMS), first developed by A.O. Nier in 1947. Although technological advances have led to the development of components that are smaller, faster, and more stable, very few changes have been made to the original design. The components of the IRMS can be divided into four general categories: the inlet system, the ion source, the mass analyzer, and the detection system.

The inlet system is the first component that the sample gas comes into contact with. In the original design, the IRMS used a dual inlet system (Figure 2.1), but current instruments can also have a continuous flow inlet system. A continuous flow system has the ability to analyze on-line whereas dual inlet systems are often used for off-line sample preparation methods. In a dual inlet system, analysis is done by comparing a sample gas contained in the left bellows with a reference gas in the right bellows. The changeover block, shown in between the two bellows, switches back and forth and sends each gas

aliquot to the ion source for analysis. Dual inlet analysis cycles back and forth between the sample and reference bellows several times, completing a set number of cycles, and the results of each replicate cycle are averaged together. In a continuous flow system, an open split system is utilized to inject both samples and standards. The sample split receives sample as it eludes off the Gas Chromatograph (GC) column at the end of the sample preparation system.

Once through the inlet system, the sample arrives at the ion source. In the source, the sample gas is ionized, accelerated, and focused into a narrow ion beam that is sent toward the mass analyzer. The conditions of the ion source are such that only singly ionized particles are produced. The mass analyzer in the IRMS is a magnetic sector, so isotopes are separated based on how the magnetic field influences their momentum. The ion beam is bent, with the angle dependent on momentum, and directed toward the detector. Faraday cups are used for ion detection in an IRMS. Cups are calibrated to collect specific sample masses, simultaneously (e.g. masses 32, 33, and 34 during O_2 analysis). The ion beam is measured as a voltage (in mV), which corresponds to the isotope concentration in the sample. Concentrations are given in delta notation, which was detailed in Chapter 2.2.

2.3 Denitrifier Method

Isotopes of nitrate ($\delta^{15}N$, $\delta^{18}O$, and $\Delta^{17}O$) are frequently used to assess changes in nitrogen sources, and decipher the biogeochemical and oxidation processes impacting a sample. The denitrifier method allows for the analysis of natural abundance samples (as opposed to labeled samples), thus allowing for the analysis of environmental samples

Table 2.1: Working nitrate isotope lab standards

Sample Type	Reference Material	$\delta^{15}N$ (‰) vs air N_2	$\delta^{18}O$ (‰) vs SMOW	$\Delta^{17}O$ (‰) vs SMOW	Fraction NC32	Fraction 20H
Pristine Biosphere	NC32	15.3	-18.8	0	1	0
	1H	14.6	15.2	1	0.95	0.05
	2H	3.7	-11.1	2	0.91	0.09
Polluted Biosphere	5H	11.5	0.15	5	0.76	0.24
	10H	7.9	17.6	10	0.53	0.47
Atmospheric	20H	0.5	54.1	19.8	0	1
	Antarctic	-20	72.3	32		

(seawater, precipitation, aerosols), which generally have very low NO_3^- concentrations. *Pseudomonas aureofaciens*, a naturally occurring denitrifying bacteria lacking an active N_2O reductase,[2] converts NO_3^- to N_2O. If conversion is complete and no additional nitrogen pool is available, the bacteria produce N_2O with the same $\delta^{15}N$ value as the original NO_3^- (per mass balance). However, oxygen is much more complicated, as only one of the initial 6 O atoms is present in the resultant N_2O and O atoms can exchange with H_2O during incubation. Standards of known isotopic composition are used to correct these issues.

Each sample or standard is injected into vials containing the denitrifying bacteria in a tryptic soy broth (TSB) medium, which has been purged with N_2 to remove any residual NO_3^- or N_2O. The vials incubate overnight, and lysed with a 5% NaOH solution, allowing N_2O to collect in the headspace of the sample vial. The headspace can be analyzed using two different methods. The first method extracts the N_2O, purifies it, and sends it to an IRMS to measure the isotope ratios ($\delta^{15}N$ and $\delta^{18}O$).[2,3] The second method extracts the headspace, purifies the N_2O, decomposes it to N_2 and O_2 in a gold tube at 900°C, and separates the gases in a molecular sieve capillary GC column prior to analysis

by IRMS. The gold tube thermal reduction method allows for the measurement of the $\delta^{15}N$, $\delta^{17}O$, $\delta^{18}O$, and thus $\Delta^{17}O$ values.[4]

As mentioned previously, denitrification steps do show fractionation. In order to account for these effects, nitrate isotope lab standards are used (Table 2.1). Except for the Antarctic standard, the standards are created by mixing an international reference, NC32, with Hoffman fertilizer, a $NaNO_3$ fertilizer with a known $\Delta^{17}O$ of 20‰. Standards are treated the same way that samples are, ensuring to account for any fractionation that occurs, and samples are calibrated using these standards. Overall, this method allows for the analysis of low concentration samples in the absence of a significant blank[2] or memory effect.[4]

2.4 BrF_5 Laser Decomposition

Oxygen isotopes of SO_4^{2-} ($\delta^{17}O$, $\delta^{18}O$, and $\Delta^{17}O$) were analyzed using a CO_2-laser fluorination method.[5] The method analyzes SO_4^{2-} in the form of crystalline $BaSO_4$, which are ultimately decomposed into O_2 gas for analysis. One important characteristic of this method is its non-quantitative conversion of $BaSO_4$ to O_2. However, the $\delta^{18}O$ value is not correlated to the O_2 yield, nor BrF_5 pressure. The method allows for analysis of small sample sizes (down to 4 mg) with analytical error of ±0.05‰ for $\Delta^{17}O$ and ±0.8‰ for $\delta^{18}O$ on average.[5] The $\delta^{18}O$ value, however, is consistently too low and requires the application of a 9.4 ± 0.8‰ correction factor. The CO_2-laser approach requires less than half an hour for O_2 decomposition and purification, which is a key advantage over other SO_4^{2-} isotope analysis methods.[5]

$BaSO_4$ samples were prepared by precipitating SO_4^{2-} containing solutions with a $BaCl_2$ solution. The $BaSO_4$ precipitate was separated from the remaining solution and dried in an ~100°C oven overnight. The crystals must be completely dry, as any residual water would dilute the O isotopes. Particle size is critical for analysis, as larger crystals are likely to splatter in the reaction chamber and produce very little O_2, and smaller particles form lumps during precipitation and do not dry out thoroughly. Both of these particle size issues can lead to contamination and so crystals in the 0.2-5 μm range are optimal.[5] On the day prior to analysis, 6-12 mg (ideally) of sample were loaded into sample wells on the target. The target was loaded into the reaction chamber, which is evacuated and allowed to equilibrate overnight.

In the evacuated chamber, 25-30 torr of BrF_5 gas is expanded into the metal line and to a liquid nitrogen trap. The liquid nitrogen condenses the BrF_5 from any impurities (N_2, Ar), which are vacuumed out of the line. The purified BrF_5 is added to the reaction chamber and exposed to the samples. A 30W CO_2-laser is used to heat the sample. The laser beam is pulsed to minimize sample sputtering. The sample melts as the laser heated reaction occurs, and the stabilization of chamber pressure indicates reaction completion. Gases in the reaction chamber (BrF_5, O_2, other by products) are allowed to expand into the liquid nitrogen trap. The liquid nitrogen is rapidly switched out for a -90°C ethanol slush, which selectively allows O_2 to pass through the trap. O_2 then expands into a previously evacuated gas line, where it is collected by a molecular sieve (5A) trap in liquid nitrogen. The trap, which is detached from the line, is then transferred to the IRMS for isotope analysis using the dual inlet system.

2.5 ICP-OES

Inductively Coupled Plasma-Optical Emission Spectroscopy (ICP-OES) is an atomic emission spectroscopy technique that determines the concentration of trace elements using the photons emitted by excited atoms.[6] Liquid and gas samples are injected into the instrument, where they are aerosolized and directed into the center channel of the plasma. The plasma, which can reach 10,000 K, provides enough energy to vaporize the aerosol, ionizes the aerosol components, and promotes the ions to an excited state. The energy given off as the ions return to the ground state is characteristic of each elemental component. Each wavelength corresponds to a specific element, and the number of photons emitted correlates with its concentration.

The ICP-OES located in the Purdue Rare Isotope Measurement (PRIME) Laboratory was used to analyze aerosols collected at Whangarei, New Zealand. A standard containing 15 elements in a 5% HNO_3 solution was used to calibrate for elemental concentrations. Samples were also prepared in a 5% HNO_3 solution. Although the standard contained 15 elements, only Na, K, and Mg were targeted for analysis. However, data obtained revealed that the filters used for collection were made of glass fiber, not quartz as we had believed. Glass fiber filters are notoriously dirty, and even when washed prior to use, can still have a large blank. Therefore, XRF data was used instead.

2.6 X-Ray Fluorescence

X-Ray Fluorescence (XRF) is a fast, non-destructive analytical method used for the determination of elemental concentrations. The method requires very little sample preparation and can be used to analyze samples in solid, liquid, or powder forms.[7] XRF

systems fall into two categories based on their method of analysis: energy dispersive (EDXRF) and wavelength dispersive (WDXRF) systems. EDXRF and WDXRF system setups only differ in their method of detection. EDXRF systems measure energies emitted directly from the sample, whereas WDXRF systems add an analyzing crystal for indirect detection. The difference in detection impacts the analytical range, spanning Na to U for EDXRF as opposed to Be to U for WDXRF. In addition to a broad elemental range, XRF can measure concentrations in the high ppb – low ppm range, with better limits of detection for heavier elements.[7]

At its core, XRF is an atomic emission method. An x-ray source irradiates the sample and the sample components respond by fluorescing x-rays at discrete wavelengths, which are characteristic of a particular element.[7] Measurement of the emitted wavelengths divulges the elements present in the sample, whereas the intensity of the wavelength corresponds to the concentration of the element present. The wavelength of the emitted x-ray corresponds to the energy difference between the excited state, created by the source x-ray, and the ground state. An element has more than one discrete energy level, and thus can emit at more than one wavelength, or line, essentially creating a unique signature or fingerprint for that element.[7]

Elemental analysis at GNS Science (a New Zealand Crown Research Institute) was conducted using a Panalytical Epsilon 5 EDXRF. Analysis was conducted using the parameters laid out in the EPA Method IO-3.3 (June 1999).[8] The XRF uses a 100 kV Sc/W X-Ray tube, allowing for the analysis of elements from Na to U. Emitted x-rays are detected using a high performance Ge detector. Calibration standards for each element of

interest were used to determine concentrations, and a NIST reference standard was utilized to verify the results.

2.7 Black Carbon

Black carbon (BC) concentrations were determined by GNS Science using a M43D Digital Smoke Stain Reflectometer. Filters are placed over a light source, and the amount of light absorbed by the BC on the filter is measured. The amount of light absorbed is proportional to the amount of BC on the filter. Samples are measured with respect to standards, which were created by collecting acetylene soot on the filters, with standard BC mass determined gravimetrically.

2.8 Nutrient Analysis of NH_3

Analysis of NH_3 was conducted on a Seal AQ2 Discrete Analyzer. Using a robotic arm and step-driven motor, the analyzer measures and mixes precise amounts of sample and reagent in reaction wells, which are allowed to react for a programmed length of time, and analyzed using spectroscopic methods. Analysis methods adhered to established EPA approved methods, specifically EPA-103-A Rev 10.[9] NH_3 standards of known concentration were used by the AQ2 to automatically create a calibration curve, which was utilized by the software to determine sample concentrations.

The reaction[9] within the wells takes place at alkaline conditions (typically pH > 12). At these conditions, NH_3 reacts with $HClO^-$ (typically commercial bleach is used) to form chloramine. Alkaline phenol (formed by mixing phenol with NaOH in solution) reacts

with the chloramine to form the dye, indophenol blue. Nitroferricyanide is added to the dye to intensify the color for analysis. The concentration of the dye is determined based on the absorbance of the at 660nm, and corresponds to the concentration of NH_3 in the original sample.

2.9 References

(1) *A Practical Guide to Ion Chromatography:An Introduction and Troubleshooting Manual*; 2nd ed.; SeQuant AB: Umea, Sweden, 2007.

(2) D. M. Sigman K. L. Casciotti, M. Andreani, C. Barford,M. Galanter, and J. K. Bolhlke. *Anal. Chem.* **2001**, 4145–4153.

(3) K. L. Casciotti M. Galanter Hastings, J. K. Bo1 hlke, and A. Hilkert, D. M. S. *Anal. Chem.* **2002**, 4905–4912.

(4) Kaiser, J.; Hastings, M. G.; Houlton, B. Z.; Röckmann, T.; Sigman, D. M. *Anal. Chem.* **2007**, *79*, 599–607.

(5) Bao, H.; Thiemens, M. H. *Anal. Chem.* **2000**, *72*, 4029–4032.

(6) Hou, X.; Jones, B. T. Inductively Coupled Plasma/Optical Emission Spectrometry. *Encyclopedia of Analytical Chemistry*, 2000, 9468–9485.

(7) Brouwer, P. *THEORY OF XRF: Getting acquainted with the principles*; 3rd ed.; PANalytical B.V.: Almelo, The Netherlands, 2010.

(8) **1999**.

(9) SEAL Analytical. AQ2 Method: EPA-103-A Rev. 10, 2012, 1–10.

CHAPTER 3: DETERMINATION OF NO + O_2 REACTION MECHANISM USING STABLE ISOTOPES

3.1 Introduction

One of the most recognizable reactions in chemistry is the reaction between NO_2 and O_2:

$$2NO + O_2 \rightarrow 2NO_2 \qquad \text{(R1)}$$

This reaction serves as an intermediate in the synthesis of commercial nitric acid[1,2], influences the photochemical oxidation of hydrocarbons in the atmosphere which contribute to urban smog,[3,4] and influences the oxidative capacity of the atmosphere by controlling concentrations of O_3, OH radicals and influencing lifetimes of greenhouse gases[4,5]. The color change caused by NO_2 formation is used as a visual example of gas rates laws in most general chemistry texts. As written (R1), the reaction is often used as an example of a termolecular reaction in kinetics chapters in general chemistry texts. The true reaction mechanism, however, has long been the subject of a debate with no overall consensus. For over 200 years[1], numerous studies have been conducted to try to resolve the reaction mechanism, and while there is a consensus on certain details, definitive proof of the reaction sequence is still debated.[6]

Since the first kinetic study was conducted in 1918 by Bodenstein and Wackenheim,[6,7] numerous kinetic studies have been conducted, most of which agree on

the reaction order: second order in NO and first order in O_2. However, despite the vast number of studies conducted, no reaction mechanism has been agreed upon.[6] Adding to the complexity of the reaction is the slight negative temperature dependence, first noted by Foerster and Blich in 1910.[7] In an attempt to address both the mechanism and its negative temperature dependence, Kassel[8,9] used three-body collision frequency calculations and concluded that, although infrequent, R1 would be sufficient enough to explain the observed rate of reaction and this rate could possibly decrease with an increase in temperature and thus would be an example of a true termolecular reaction. Gershinowitz and Eyring[10] supported Kassel and applied transition state theory to propose a transition state where the O_2 added is partially bonded to the N in both NO molecules. However, several studies arguing for the termolecular reaction often describe the formation of a complex prior to colliding with a third body to produce NO_2.[10] If this is the case, the reaction would not be a classical termolecular reaction. The termolecular has not been completely disregarded, however more recent experimental and computational evidence has generally led scientists away from the termolecular mechanism.[6,11] The two mechanisms that have been proposed to explain the apparent termolecular kinetics of the reaction are a NO dimer intermediate reaction mechanism (R2a, R2b), and an NO_3 intermediate reaction mechanism (R3).

The NO dimer based mechanism is a two-step process (R2a, R2b) that assumes that there is a fast equilibrium forming a NO dimer (R2a) prior to the slower rate determining reaction with O_2 that yields NO_2 (R2b).[6] NO has been shown to exist solely in dimer form in the solid and liquid phases, but can also be found in the gas phase at low concentrations and cryogenic temperatures.[11]

$$NO + NO \leftrightarrow (NO)_2 \qquad \text{(R2a)}$$

$$(NO)_2 + O_2 \rightarrow 2NO_2 \qquad \text{(R2b)}$$

This mechanism was supported by Trautz, who explained that the observed slight negative temperature coefficient was a result of the competing steps; the second step possessing a positive temperature coefficient, but being overruled by the first steps negative coefficient which is larger in magnitude.[8] In addition, Hasche and Patrick's studies at 0° and 30°C[7] determined that the negative temperature coefficient points toward the formation of an intermediate compound in equilibrium with the starting material. The authors argued that the equilibrium of this step would shift left as temperature increased, thus producing the observed negative temperature coefficient. Guggenheim[12] also supported this mechanism, and by applying the principle of corresponding states determined that the NO dimer would have a lifetime $10^5 - 10^6$ times that required for the collision, thus supporting the feasibility of this mechanism as a whole.

The third proposed mechanism (R3a, R3b) involves the formation of an NO_3 radical. A fast equilibrium forms a NO_3 intermediate (R3a) before a second NO reacts with the NO_3 to form two NO_2 (R3b).[6] Two structures of NO_3 have been proposed in literature: (a) nitrogen trioxide, in which all oxygen atoms are equivalently bonded to the N atom[13,14] and (b) the peroxynitrate radical, with the structure O-O-N-O.[11,15,16]

$$NO + O_2 \leftrightarrow NO_3 \qquad \text{(R3a)}$$

$$NO_3 + NO \rightarrow 2NO_2 \qquad \text{(R3b)}$$

To our knowledge, no experimental evidence exists which conclusively favors one intermediate structure over another. Utilizing ab initio calculations, Eisfeld and Morokuma[13] argued against peroxynitrate radical, concluding that this isomer would not

result in a bound structure. Additionally, they argue that in order to form this isomer, an additional energy barrier would need to be overcome, which is not possible with the thermal energies in the atmosphere. Conversely, an infrared spectroscopy study by Guillory and Johnson[16,17] revealed a new absorption band at 1840 cm^{-1} which they attributed to peroxynitrate. More specifically, the authors attribute this band to the N=O stretching motion, reasoning that the symmetrical form did not return vibrational frequencies higher than 1500 cm^{-1}. Clyne and Thrush[18] observed that isotopic exchange between NO_2 and ^{18}O produced a mixed isotopic distribution, and conclude that only the symmetrical nature of nitrogen trioxide could produce this result. However, Klein and Herron found that the NO_3 intermediate that forms is relatively long lived (on the order of 10^{-7}s), which would allow for rearrangement of peroxynitrate.[18] However, majority of studies supporting the NO_3 intermediate theory do not favor one NO_3 isomer over the other, often discussing their results without specifying an isomer, or justifying both forms.

The $2NO + O_2$ reaction has also been of interest to computational chemists because it involves radical species and the he complex nature of these electronic structures presents challenges for quantum chemical methods. Recent ab initio calculations seem to favor the mechanism set forth by McKee[19], where the mechanism proceeds through two intermediates prior to forming NO_2:

$$O_2 + NO \leftrightarrow NO \cdot O_2 \qquad \text{(R4a)}$$

$$NO \cdot O_2 + NO \rightarrow ONOONO \qquad \text{(R4b)}$$

$$ONOONO \rightarrow 2NO_2 \qquad \text{(R4c)}$$

In this mechanism, $k_{-4a} >> k_{4b}$ with R4b serving as the rate determining step. The mechanism agrees with both the experimental rate order and the observed overall activation barrier (second order in NO and first order in O_2 with a slightly negative overall activation barrier).[19] However, due to its negative bond dissociation energy, ONOONO has never been observed experimentally.[20]

Despite numerous experimental and ab initio studies, no clear mechanistic consensus has been reached. The work presented here will employ stable isotopes to evaluate proposed mechanisms for NO oxidation by O_2. In general, the partitioning of isotopes during chemical reactions or physical processes (e.g. diffusion) are due to a difference in isotopologue masses. Compounds with the same molecular formula but different isotopic composition (e.g. $^{16}O^{18}O$ vs $^{16}O^{16}O$) are called isotopologues, which result in slight differences in their chemical thermodynamics.[21,22] These differences are classified as two main types of isotope fractionation processes: equilibrium isotope exchange[21] and kinetic isotope effects (KIE).[23] In equilibrium exchange reactions, there is no net change in chemical species, but the isotopes may exchange between the molecules. KIE often result when the rate of the reaction is sensitive to the atomic mass at specific positions in a molecule and the reaction is essentially unidirectional. Together, these two types of fractionation allow for stable isotopes to be used as tracers of sources and chemical and physical processes, and thus can reveal details about how a reaction proceeds.[23] Since the only difference in the proposed mechanisms is how the O_2 adds, focusing on the distribution of the O isotopes (^{16}O, ^{17}O, and ^{18}O) should allow for the elucidation of the NO oxidation mechanism.

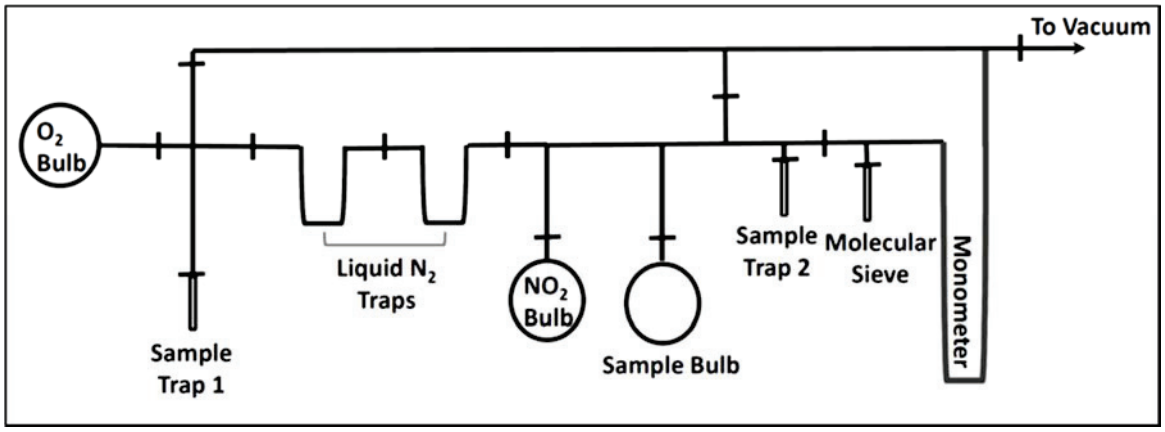

Figure 3.1: Schematic of the gas line used in this experiment.

3.2 Method

In order to determine how the isotopic distribution responds to temperature, Ultra High Purity O_2 (added in excess) was allowed to expand into an evacuated reaction bulb, measured, and closed off. Any O_2 remaining in the line was collected on a 5A Molecular Sieve using liquid nitrogen. This sample will serve as the pre-reaction sample. To vary the temperature, trials were conducted by placing the reaction bulb in liquid nitrogen (77K), an ethanol slush (201K), ice water (277K), or left on the bench for room temperature. With the reaction bulb isolated, NO was allowed to expand into the evacuated line. Once the pressure was measured, the NO was added to the reaction bulb, sealed off, and allowed to react in the dark for 25 minutes. Once the reaction time was reached, the reaction bulb was quenched with liquid nitrogen in order to freeze out the NO_2 formed. The conditions of each trial are summarized in Table 3.1.

Table 3.1: Summary of trial conditions.

Temperature (K)	mmol O_2	mmol NO	Fraction O_2 Recovered	$\delta^{17}O$ (‰)	$\delta^{18}O$ (‰)
77	3.85 ± 0.24	4.10 ± 0.06	0.568 ± 0.030	-6.862 ± 0.674	-13.460 ± 1.181
201	1.53 ± 0.02	1.66 ± 0.02	0.570 ± 0.029	-2.403 ± 0.460	-4.943 ± 0.726
277	1.22 ± 0.01	1.26 ± 0.02	0.582 ± 0.028	-1.585 ± 0.061	-3.341 ± 0.258
297	1.04 ± 0.06	1.12 ± 0.03	0.595 ± 0.026	-1.532 ± 0.869	-2.975 ± 1.400
297	6.24	4.65	0.246	-1.574 ± 0.178	-2.679 ± 0.307
297	5.24	4.67	0.214	-3.814 ± 0.162	-6.997 ± 0.343
297	4.64	7.45	0.128	-7.422 ± 0.151	-13.848 ± 0.308
297	4.43	2.72	0.244	-1.109 ± 0.250	-1.819 ± 0.506

Excess O_2 was recovered using 5A molecular sieve and liquid nitrogen and served as the post-reaction sample. Both samples were analyzed for $\delta^{17}O$ and $\delta^{18}O$ on a Thermo Delta V dual inlet isotope ratio mass spectrometer (IRMS). Dual inlet measurements are collected by comparing the isotopic composition of a sample against that of a reference, with the sample located in one bellow and the reference located in a separate bellow. In this work, the post-reaction sample was measured against the pre-reaction sample, thus the reported values reflect the change in isotope distribution only from reaction with NO at the conditions summarized in Table 3.1. Oxygen isotope data is reported in per mil (‰) relative to Vienna Standard Mean Ocean Water (VSMOW), as follows (where x = 17 or 18)

$$\delta^{x}O(‰) = \frac{\left(\frac{^{x}O}{^{16}O}\right)_{sample} - \left(\frac{^{x}O}{^{16}O}\right)_{VSMOW}}{\left(\frac{^{x}O}{^{16}O}\right)_{VSMOW}} \times 1000 \qquad \text{(Eq. 1)}$$

Table 3.2: Calculated reaction temperature and Rayleigh calculated enrichment and fractionation factors.

Bath Temperature (K)	Reaction Temperature (K)	$^{18}\varepsilon$	$^{17}\varepsilon$	$^{18}\alpha$	$^{17}\alpha$
77	192	22.556	12.896	1.0226	1.0129
201	252	13.067	8.4803	1.0131	1.0085
277	287	5.2811	1.1859	1.0053	1.0012
297	297	-31.440	-18.946	0.96856	0.98105

The reaction bulb and the O_2 were equilibrated to the temperature of the bath when mixing began, but the NO was at room temperature. Once added to the reaction bulb, the NO begins to equilibrate with the bath temperature. However, the reaction begins upon mixing, so the reaction temperature lies between room temperature and the temperature of the bath. The final temperature of the reaction was calculated using thermodynamic methods and summarized in Table 3.2. It is worth noting that the reaction temperatures still cover a relatively large temperature range, and thus the reaction conditions are still distinct.

3.3 Results and Discussion

Oxygen isotopes can fractionate in one of two manners: mass dependently or mass independently. In mass dependent fractionation, the isotopes adhere to the following relationship,

$$\delta^{17}O = 0.52 \cdot \delta^{18}O \qquad \text{(Eq. 2)}$$

Mass independent fractionation deviate from this relationship, with the degree of deviation measured by $\Delta^{17}O$:

$$\Delta^{17}O = \delta^{17}O - 0.52 \cdot \delta^{18}O \qquad \text{(Eq. 3)}$$

Fractionation factors (α) describe how a reaction or process distributes the isotopes, and those of measured data can be determined using a Rayleigh relationship. The Rayleigh equation determines enrichment factor,

$$\delta_f = \varepsilon \ln f + \delta_i \quad \text{(Eq. 4)}$$

which is related to the fractionation factor as follows:

$$\varepsilon = (\alpha - 1) \cdot 1000 \quad \text{(Eq. 5)}$$

Experiments were conducted over a range of temperatures and showed that the remaining O_2 was depleted in both ^{17}O and ^{18}O relative to the initial O_2, yet the isotopes maintained a mass dependent distribution. The data also reveals that the heavy isotopologues of O_2 were reacting preferentially to form NO_2 rather than the light isotopologues. This is opposite to most KIEs where normally the lighter isotope reacts more rapidly and is preferentially incorporated into products, leaving isotopically heavy reactants.[23]

Since the NO_2 preferentially retains the heavier isotopes this reaction is an example of an inverse isotope effect. Inverse isotope effects generally occur when the reaction pathway includes a reaction intermediate. Perhaps the most studied inverse isotope effect occurs during the $O + O_2 \rightarrow O_3$ reaction during which the product O_3 isotopologue becomes extraordinarily enriched.[24,25] As an inverse isotope effect was observed in our data, we can disregard the termolecular mechanism (R1), since this reaction assumes no intermediate is formed. Additionally, the speed at which molecules of NO and O_2 travel is proportional to the collision probability for that molecule, and a molecules speed is inversely proportional

Table 3.3: Root-mean-square speeds of NO and O_2 isotopologues.

Isotopologues	Mass (kg)	υ_{rms} (m/s)
NO	4.98×10^{-26}	499
$N^{17}O$	5.15×10^{-26}	491
$N^{18}O, O_2$	5.31×10^{-26}	484
$O^{17}O$	5.45×10^{-26}	476
$O^{18}O$	5.65×10^{-26}	469

to its mass. The root-mean-square speed (υ_{rms}) is calculated as follows

$$\upsilon_{rms} = \sqrt{\frac{3kT}{m}} \qquad \text{(Eq. 6)}$$

where k is the Boltzmann constant, and m is the mass of a single molecule in kg. The lighter isotopologues of NO and O_2 have faster velocities than their heavier isotopologue counterparts (Table 3.3), and thus are more likely to collide and react. Therefore, in a termolecular reaction, the lighter isotopologues would collide more frequently and thus react more rapidly resulting in a normal isotope effect. Due to the presence of an inverse isotope effect in our data, further eliminates the possibility of a termolecular reaction.

The negative temperature effect and inverse isotope effect can help with understanding the chemical mechanism occurring during (R1). In both intermediate steps (R2, R3), the first step proceeds through a rapid equilibrium to form an intermediate, which is essential to produce the negative temperature effect. Kinetically, the light isotopes will react first to form the intermediate leaving the reactants heavy. However, the light isotopes also react first as the intermediate decomposes back into the starting reactants. The net effect is that the heavy isotope ends up concentrated in the intermediate, and thus translated forward to the ultimate product, NO_2. Additionally, the intermediate formed is less stable

as temperature increases, thus a decrease in the overall rate of reaction. Due to the observed depletion in the excess O_2, we can disregard the NO_2 dimer mechanism (R2), as the equilibrium step doesn't include O_2. The equilibrium leads to the concentration of heavy isotopes in the intermediate, thus causing the O_2 excess to be depleted of heavy isotopes. This, combined with the instability of the intermediate with increasing temperature, results in the excess O_2 being more depleted at lower temperatures.

In an attempt to distinguish between the two intermediate forms, peroxynitrate and nitrogen trioxide, we consider the $\delta^{17}O$ and $\delta^{18}O$ in the excess O_2 and note a strict mass-dependent relationship. In studying the origin of the mass-independent enrichment in ozone, Hathorn and Marcus[26] noted that symmetry impacted the availability of reactive states and thus the fractionation. The authors found that symmetrical isotopologues of O_3 had fewer reactive states available to distribute energy, and experienced some degree of mass-independent fractionation as a result. The more "chaotic" nature of asymmetrical isotopologues allows for fractionation to occur in a mass-dependent manner. Applying this concept to the NO_3 intermediates, we note that all isotopologues of nitrogen trioxide are symmetrical in some manner, and thus should undergo some degree of mass-independent fractionation. Additionally, it is possible that the temperature is significantly high enough to favor the nitrogen trioxide intermediate over the peroxynitrate, which would become more unstable as temperature increases. However, if this was the case, the symmetrical nature of nitrogen trioxide should still result in some degree of mass independent fractionation. As our study returned a strict mass-dependent relation, we conclude that reaction must proceed through the asymmetrical peroxynitrate intermediate.

Table 3.4: Summary of reaction rates used in the Kintecus model.

Temperature	k_{3a}	k_{-3a}	k_{3b}	k_{5c}	k_{5d}	k_{5e}	k_6
77	1.066E-22	201.8	6.073E-13	4.567E-52	4.567E-52	6.073E-13	7.189
201	1.072E-22	203.0	6.548E-13	8.498E-28	8.498E-28	6.548E-13	11.62
277	1.029E-22	194.8	1.858E-12	1.159E-23	1.159E-23	1.858E-12	1.364E-25
297	9.756E-23	184.7	1.754E-12	6.319E-23	6.319E-23	1.754E-12	1.412E-25

To confirm our predicted mechanism, Kintecus,[27] a computer box model that models kinetics of chemical reactions, was utilized in an attempt to replicate the observed results. To start off, R3a and R3b were modeled, utilizing the peroxynitrate form of NO_3. Fractionation factors (α) and reduced partition function ratios (β) for mono-substituted isotopologues were calculated in the Q-Chem 4.2 program suite using both the B3LYP and EDF2 hybrid density functional theory (DFT) methods. This model was specifically used to determine the equilibrium exchange fractionation factors for peroxynitrate. As the non-peroxy oxygen is double bonded to the nitrogen, this oxygen was not factored into the equilibrium exchange. Reaction rates and model parameters are summarized in Tables 3.4 and 3.5, respectfully.

The Kintecus model was originally run with calculated fractionation factors in the forward reaction of the equilibrium step. The model returned isotopic values which trended similar to the observed experimental results. To apply a kinetic isotope effect, the $NO\text{-}O_2$ collisional frequency was applied, but this did not change the isotopic value significantly (~0.5‰). While the trend (depletion of heavy isotopes, which increases with decreasing temperature) was similar to our observations, the measured values were significantly different. For this reason, we believe that our simple two step mechanism does not completely describe the process.

Table 3.5: Kintecus Model Parameters

Formation of peroxynitrate intermediate; k_{3a}[28]	NO + OO ==> OONO	Modified to replicate observed reaction speed; based on $4.8\times10^{-22}\ \frac{cm^3}{molecules\cdot s}$
	$N^{18}O$ + OO ==> $OON^{18}O$	
	NO + ^{18}OO ==> $^{18}OONO$	
	NO + ^{18}OO ==> $O^{18}ONO$	
Decomposition of peroxynitrate intermediate; k_{-3a}[3,28]	OONO ==> NO + OO	$K_{eq}=\frac{k_3}{k_{-3}}=5.28\times10^{-25}$
	$OON^{18}O$ ==> $N^{18}O$ + OO	
	$^{18}OONO$ ==> NO + ^{18}OO	
	$O^{18}ONO$ ==> NO + ^{18}OO	
Formation of NO_2 from peroxynitrate and NO; k_{3b}[1]	OONO + NO ==> ONO + ONO	$k=Ae^{\frac{-Ea}{RT}}$ $A=4.39\times10^{7}\ \frac{cm^3}{molecules\cdot s}$ $Ea=7.4kJ/mol$
	$^{18}OONO$ + NO ==> ONO + $ON^{18}O$	
	$O^{18}ONO$ + NO ==> ONO + $ON^{18}O$	
	$OON^{18}O$ + NO ==> ONO + $ON^{18}O$	
	$^{18}OONO$ + $N^{18}O$ ==> ONO + $ON^{18}O$	
	$O^{18}ONO$ + $N^{18}O$ ==> $ON^{18}O$ + $ON^{18}O$	
	$OON^{18}O$ + $N^{18}O$ ==> ONO + $^{18}ON^{18}O$	
	OONO + $N^{18}O$ ==> ONO + $ON^{18}O$	
Formation of NO_4 from NO_2 and excess O_2; k_{5c}[15]	ONO + OO ==> OONOO	$k=Ae^{\frac{-Ea}{RT}}$ $A=1\times10^{-12}\ \frac{cm^3}{molecules\cdot s}$ $Ea=57990\ kJ/mol$
	$ON^{18}O$ + OO ==> $OONO^{18}O$	
	$ON^{18}O$ + OO ==>$OON^{18}OO$	
	ONO + ^{18}OO ==> $OON^{18}OO$	
	ONO + ^{18}OO ==> $OONO^{18}O$	
Decomposition of NO_4; k_{5d}[15]	OONOO ==> ONO + OO	$k_{5d}=2.92\times10^{16}\ \frac{cm^3}{molecules\cdot s}$
	$OON^{18}OO$ ==> ONO + ^{18}OO	
	$OON^{18}OO$ ==> $ON^{18}O$ + OO	
	$OONO^{18}O$ ==> ONO + ^{18}OO	
	$OONO^{18}O$ ==> $ON^{18}O$ + OO	
Exchange between NO_4 and peroxynitrate; k_{5e}[15]	$OONO^{18}O$ + OONO ==> $^{18}OONO$ + OONOO	k_{5e} set equal to k_{3b}
	$^{18}OONO$ + OONOO ==> $OONO^{18}O$ + OONO	
	$OON^{18}OO$ + OONO ==> $^{18}OONO$ + OONOO	
	$^{18}OONO$ + OONOO ==> $OON^{18}OO$ + OONO	
	$O^{18}ONO$ + OONOO ==> $OONO^{18}O$ + OONO	
	$OONO^{18}O$ + OONO ==> $O^{18}ONO$ + OONOO	
Removal of NO_2 from gas phase; k_6[29,30]	ONO ==> AONO	$k_6=\frac{1}{4}C_{NO2}S\gamma$
	$ON^{18}O$ ==> AONO	
	$^{18}ON^{18}O$ ==> AONO	

Ogg[15] studied peroxy radicals of NO_4 and NO_3 at 0° and 25°C and determined experimentally that, at these temperatures, NO_2 does not undergo isotopic exchange with O_2. Instead Ogg proposed the following mechanism:

$$N_2O_5 \rightarrow NO_2 + NO_3 \quad \text{(R5a)}$$

$$NO_2 + NO_3 \rightarrow N_2O_5 \quad \text{(R5b)}$$

$$NO_2 + O_2 \rightarrow NO_4 \quad \text{(R5c)}$$

$$NO_4 \rightarrow NO_2 + O_2 \quad \text{(R5d)}$$

$$^{O}oNO^{18}O + ONo\ ^{O} \rightarrow\ ^{O}oN^{18}O + OONo^{O} \quad \text{(R5e)}$$

R5e was spelled out to identify the specific structural formula and exchange. Factoring in Ogg's exchange[15] to the Kintecus model, we found that the formation of NO_4 (R5c), its exchange with peroxynitrate (R5e) and subsequent decomposition (R5d) shifted the isotope distribution. Without exchanging with NO_4, the model predicted the inverse isotope effect, but the remaining O_2 was too depleted. By factoring in exchange with NO_4, the model reduced the depletion and correctly predicted the observations at low temperatures (77 and 201K), but the fractionation pattern at ambient temperatures (277 and 297K) was still a bit off.

Ogg's exchange mechanism neglected to address the NO_2 that was freezing to the sides of the reaction vessel and removed from the reaction. Riemer et al.[29] experienced the same issue with N_2O_5 as it hydrolyzes on the surface of aerosol particles. To account for this loss, the author calculated a rate constant for the hydrolyzation of N_2O_5 using the mean molecular velocity (C_{N2O5}), the aerosol surface area (S), and the reaction probability (γ_{N2O5}). Applying this to the frozen removal of NO_2 (k_{wall}),

$$k_{wall} = \frac{1}{4} C_{NO2} S \gamma_{NO2} \quad \text{(Eq. 7)}$$

and factoring these new reactions (see Table 3.3) into our Kintecus model, we were able to account for the slight change in fractionation at ambient temperatures. Whereas the mean molecular speed is mostly dependent on molecular mass, the reaction probability (whether or not it will freeze to the wall) is solely dependent on the temperature. For this reason, we applied two different γ, one for temperatures below the freezing and condensation points and the other for trials above. Factoring in this effect, our model nearly matched our observed results.

3.4 Conclusion

NO_x (NO_x = NO + NO_2) is produced by both natural and anthropogenic sources and is extremely important to atmospheric chemistry. One of the most prevalent sources of NOx is from the combustion of fossil fuels, making up over 60% of the total N budget.[31] NO is extremely reactive, and oxidizes rapidly in the troposphere by various reactions. Frequently, the first step of NO oxidation is to form NO_2, which is either reduced back to NO by photolysis or further oxidized into species such as NO_3^-, HNO_3, N_2O_5, etc. While the oxidation of NO_2 is well understood, the mechanism of the oxidation of NO to NO_2 is highly uncertain.

Laboratory experiments complimented by kinetic modeling suggest that the reaction proceeds through the formation of a NO_3 radical intermediate. Stable isotope analysis of excess O_2 was found to be lighter than the initial O_2 added and followed a strict mass dependent relationship. The depleted O_2 means that the NO_2 formed is enriched in

heavier isotopes of O_2. Additionally, the mass dependent relationship suggests that the intermediate formed is asymmetrical. As the nitrogen trioxide intermediate is symmetrical, the peroxynitrite radical must be the intermediate that forms.

3.5 References

(1) Zakharov, I. I.; Minaev, B. F. *Theor. Exp. Chem.* **2011**, *47*, 93–100.

(2) Treacy, J. C.; Daniels, F. *J. Am. Chem. Soc.* **1955**, *77*, 2033–2036.

(3) Morrison, M. E.; Rinker, R. G.; Corcoran, W. H. *Ind. Eng. Chem. Fundam.* **1966**, *5*, 175–181.

(4) Walters, W. W.; Goodwin, S. R.; Michalski, G. *Environ. Sci. Technol.* **2015**, *49*, 2278–2285.

(5) Eisfeld, W.; Morokuma, K. *J. Chem. Phys.* **2001**, *114*, 9430–9440.

(6) Olbregts, J. *Int. J. Chem. Kinet.* **1985**, *17*, 835–848.

(7) Hasche, R. L.; Patrick, W. A. *J. Am. Chem. Soc.* **1925**, *47*, 1207–1215.

(8) Kassel, L. S. *The kinetics of homogeneous gas reactions*; New York, 1932.

(9) Kassel, L. *J. Phys. Chem.* **1930**, *34*, 1777–1796.

(10) Gershinowitz, H.; Eyring, H. *J. Am. Chem. Soc.* **1935**, *57*, 985–991.

(11) Tsukahara, H.; Ishida, T.; Mayumi, M. *Nitric Oxide* **1999**, *3*, 191–198.

(12) Guggenheim, E. A. *Mol. Phys.* **1966**, *10*, 401–404.

(13) Eisfeld, W.; Morokuma, K. *J. Chem. Phys.* **2003**, *119*, 4682–4688.

(14) Schott, G.; Davidson, N. *J. Am. Chem. Soc.* **1958**, *80*, 1841–1853.

(15) Ogg, R. a. *J. Chem. Phys.* **1953**, *21*, 2079.

(16) Guillory, W.; Johnston, H. **1963**, 1695–1696.

(17) Guillory, W. A.; Johnston, H. S. *J. Chem. Phys.* **1965**, *42*, 2457.

(18) Clyne, M. A. A.; Thrush, B. A. *Proc. R. Soc. A Math. Phys. Eng. Sci.* **1961**, *261*, 259–273.

(19) Mckee, M. L. *J. Am. Chem. Soc.* **1995**, *117*, 1629–1637.

(20) Beckers, H.; Zeng, X.; Willner, H. *Chemistry* **2010**, *16*, 1506–1520.

(21) Urey, H. C. *J. Chem. Soc.* **1947**, 562.

(22) Bigeleisen, J.; Mayer, M. G. *J. Chem. Phys.* **1947**, *15*, 261.

(23) Hoefs, J. *Stable Isotope Geochemistry*; Springer International Publishing: Cham, 2015.

(24) Thiemens, M. H. *Science (80-.).* **1999**, *283*, 341–345.

(25) Mauersberger, K. *Science (80-.).* **1999**, *283*, 370–372.

(26) Hathorn, B. C.; Marcus, R. A. *J. Chem. Phys.* **1999**, *111*, 4087.

(27) Ianni, J. C. Kintecus, 2014.

(28) Riemer, N. *J. Geophys. Res.* **2003**, *108*, 4144.

(29) Seinfeld, J. H.; Pandis, S. N. *Atmospheric Chemistry and Physics: From Air Pollution to Climate Change, 2nd Edition* -; 2nd ed.; 2006.

CHAPTER 4: 2007 CALIFORNIA AEROSOL STUDY: EVALUATION OF $\delta^{15}N$ AS A TRACER OF NOX SOURCES AND CHEMSITRY

4.1 Introduction

Nitrogen oxides (NOx = NO + NO_2) are extremely important trace gases in the atmosphere. They play a role in regulating the oxidative capacity of the atmosphere[1–3] and determining the chemical composition of the atmosphere by participating in chemical reactions such as the photochemical production of O_3.[2–6] As a result, NOx influences the formation of particulate matter, impacting regional air quality and the Earth's radiative balance. The modern NOx cycle is dominated by anthropogenic emissions,[1,4,5,7,8] although natural NOx sources do contribute regionally.[1,5,6] The strength of these sources varies regionally and seasonally, producing significant differences in air quality between urban and rural environments on an annual basis. The relatively short lifetime of NOx (few days at most[1,9]) in addition to the regional variability of NO_x emissions also means that NOx mixing ratios are globally highly variable.[3,9] For this reason, chemical transport models are utilized to decipher NOx cycling and its impact on the environment, often using local NO_3^- or O_3 measurements to evaluate the model.[3,10,11]

NOx has four major source categories: fossil fuel combustion, biomass burning, soil emissions, and lightning.[5] Fossil fuel combustion dominates the current NOx budget and is the primary source in urban areas, where as rural areas are often a mixture of

combustion sources and soil emissions. In agricultural regions, NOx produced as a by-product of nitrification/denitrification can be significantly enhanced by the application of N fertilizers. Once emitted, NOx cycles back and forth between its two forms via the Leighton Cycle during the day.[6,9,12]

$$NO + O_3 \rightarrow NO_2 + O_2 \quad \text{(R1a)}$$

$$NO_2 + h\upsilon \rightarrow NO + O\left(^3P\right) \quad \text{(R1b)}$$

$$O\left(^3P\right) + O_2 \rightarrow O_3 \quad \text{(R1c)}$$

The above reactions, and NO oxidation by oxygenated radicals, establish steady state mixing ratios of NO, NO_2 and O_3.[6,9] Volatile organic compounds (VOCs) react with OH radicals and O_2 during the day to produce organic peroxy radicals:

$$VOC + OH \xrightarrow{[O_2]} RO_2 + H_2O \quad \text{(R2)}$$

Organic peroxy radicals further react to oxidize NO to NO_2:

$$NO + RO_2 \rightarrow NO_2 + RO \quad \text{(R3)}$$

Hydroperoxyl radicals (HO_2) and other organic peroxy radicals (ROO) derived from VOCs, form NO_2 without the loss of O_3. During the day, the VOC-oxidized NO_2 will be added to the Leighton Cycle, where it will photolyze into NO and contribute to the formation of new O_3 molecules. Thus this photochemical cycle involving NOx and VOCs, are responsible for regulating elevated O_3 concentrations in the atmosphere.[1,4–6,13]

NOx is removed from the atmosphere by conversion to HNO_3 via different chemical pathways during the day and night. During the daytime, NOx is removed from

the Leighton cycle by reacting with photochemically produced OH radicals to form HNO_3.[14]

$$NO_2 + OH + M \rightarrow HNO_3 + M \quad \text{(R4)}$$

NOx can also be removed from the atmosphere by VOCs producing organic nitrates:

$$NO_2 + RO_2 + M \rightarrow RONO_2 + M \quad \text{(R5)}$$

$$NO_2 + R(O)O_2 + M \rightarrow R(O)OONO_2 + M \quad \text{(R6)}$$

During the night, NO_2 photolysis and OH radical production ceases and the OH radical pathway to HNO_3 shuts down. Any NO present in the troposphere reacts rapidly with O_3 to form NO_2 (R1a) followed by the formation of NO_3 radical

$$NO_2 + O_3 \rightarrow NO_3 + O_2 \quad \text{(R7)}$$

R5 is the only significant source of NO_3 radical in the atmosphere. At night, the NO_3 radical acts as the major oxidant thus influencing trace gases in the atmosphere.[6] VOCs and dimethyl sulfide (DMS) can react with NO_3 radicals to form HNO_3 by hydrogen abstraction.[14]

$$NO_3 + VOC\ (DMS) \rightarrow HNO_3 + R\cdot \quad \text{(R8)}$$

This pathway is especially important at night when NO_3 radical concentrations are high. Marine phytoplankton have been shown to produce DMS, which is emitted from the surface of the ocean,[14–17] therefore this reaction is of particular interest in the coastal and marine air masses. In addition, NO_3 radicals can add to VOCs to form organic nitrates:

$$NO_3 + VOC \rightarrow RONO_2$$

Additionally, due to the lack of NO at night, NO_3 radical reacts with NO_2 to form N_2O_5[6]

$$NO_2 + NO_3 + M \rightarrow N_2O_5 + M \quad \text{(R9)}$$

with the reverse reaction triggered by thermal decomposition. N_2O_5 can undergo heterogeneous hydrolysis on aerosol surfaces to form HNO_3

$$N_2O_5 + H_2O + \text{surface} \rightarrow 2HNO_3 \qquad \text{(R10)}$$

and serves as the major nighttime NOx sink.[6]

Nitrogen chemistry is highly dependent on local N emissions and meteorology, as well as the presence of other trace gases. These dependencies are largely responsible for regional differences, especially across climates. In urban areas, anthropogenic N emissions overwhelm natural emissions due to a high concentration of motor vehicle traffic, industrial activities, and power generation processes.[6,18,19] On the other hand, rural areas experience significant natural emissions, but also a moderate influence of anthropogenic NOx sources, such as motor vehicle traffic.[6] In agriculture areas, N emissions tend to be in reduced forms (NH_3, NH_4^+), arising from fertilizer application and livestock operations.[20] Emissions in remote areas are primarily from natural sources, such as lightening and dust, but transported secondary aerosol products (NO_3^-, SO_4^{2-}) can be present, depending on regional meteorology.

In addition to regional land uses, climate has a significant influence on N chemistry. Temperatures, amount of precipitation, elevation, amount of solar radiation, and other trace gases and particles all impact local chemistry and atmospheric processing. Arid and semi-arid climates receive very little precipitation throughout the year, thus promoting dry deposition processes.[20] These areas also tend to have a significant input of mineral dust, which tends to be more alkaline than other particles.[21] This in turn influences oxidation and other chemical pathways, which can be pH dependent. Coastal areas experience a mixture of continental and marine air masses, with chemistry being influenced by the presence of

sea salt particles. Sea salt particles provide gases with a surface to condense on, and undergo aqueous phase reactions rather than gas phase reactions.[22] Additionally, as sea salt particles are larger than fine particles, dry deposition occurs much more rapidly and often locally. However, the impact of sea salt on NOx is only significant in urban influenced coastal areas, as the concentration of NOx in the marine boundary layer (MBL) is too low.[23] Chemistry in areas with high concentrations of VOCs is distinct from areas with low or non-existent VOC concentrations.[24] Polar chemistry tends to be highly seasonal, due to the lack of photochemistry during the winter and low concentrations year-round. However, snowpack photolysis during the arctic spring, recycles reactive N species (NOx, HONO) back into the atmosphere.[25]

This study investigates aerosols collected during 2007 in San Diego, USA which is a coastal urban area influenced by sea salt aerosols, anthropogenic combustion emissions, and seasonal wildfires. Wildfires also have a significant influence on local atmospheric chemistry and 2007 was notable for being the worst fire season in the San Diego region on record. In addition to NOx emissions, wildfires emit precursors to O_3 formation, such as CO and VOCs,[26,27] which can in turn influence oxidation pathways.[19,28] Wildfires also influences the partitioning between reactive nitrogen species (NOx, HNO_3, HONO, particulate-NO_3^-).[28] Additionally, as atmospheric chemistry varies by location, the effect wildfire NOx emissions have on NO_3^- formation is also of interest. Given the connection between nitrate (as HNO_3 or particulate NO_3^- (p-NO_3)) and NOx, it is readily accepted that the sources of NOx must influence the isotopic composition of the resulting nitrate. Due to this effect, it has been suggested that nitrogen stable isotopes could be utilized as tracers in order to understand how NOx cycles through the

environment,[1,4,5,12,29,30] to evaluate chemical models, and to decipher the historical climate record.

Although stable isotopes of N are commonly used as a source tracer, how this tracer is applied is a point of contention. The "source" hypothesis argues that the $\delta^{15}N$ value of NO_3^- reflects the $\delta^{15}N$ value of NOx source inputs into the environment, and any variation is the result of difference in source contributions. Proponents of this hypothesis argue that the $\delta^{15}N$ value of the resultant NO_3^- reflects the $\delta^{15}N$ value of the original NOx source, as the N atom is conserved during the oxidation process.[31–33] Therefore, the observed variations in NO_3^- $\delta^{15}N$ values are the result of changes in source emissions due to seasonal changes or regional influences. Any potential physical or chemical processing after emission is ignored or assumed to have negligible effect on $\delta^{15}N$ values.[30] The "chemistry" hypothesis argues that N isotopes are influenced by chemical reactions, atmospheric or biologic processing, and post-depositional effects.[1] As relative mass differences are most pronounced for the lightest elements (H, C, N, O, S),[34] N is often subject to kinetic and equilibrium isotope fractionation effects,[5,9] which vary based on temperature. In the case of equilibrium exchange between nitrogen oxide forms, equilibrium favors ^{15}N enrichment in the more oxidized form.[9,35] Kinetic fractionations are also predicted to vary by season, due to shifts in reaction pathways and equilibrium systems (summer dominance of NO_2 + OH pathway vs winter $NO_2/NO_3^-/N_2O_5$ equilibrium).[9] Previous studies often apply the source hypothesis, writing off the chemistry hypothesis as "minor,"[29,36] but others have noted the impact chemistry should has on $\delta^{15}N$ values.[1,9,37]

Stable isotope studies in regions with consistent NOx sources throughout the year could be used to settle this debate, as each hypothesis would produce different behavior. The source hypothesis would predict that a simple source mixing model and isotope mass balance would explain observed $\delta^{15}N$ values in nitrate samples. Since anthropogenic emissions are monitored and regulated by the U.S. Environmental Protection Agency (EPA), local and regional emissions can be used to quantify and calculate expected $\delta^{15}N$ values for local NO_3^- sample, due to the conservation of source $\delta^{15}N$ values. Since NO_3^- results from the oxidation of a mixture of contributing NOx sources, the observed $\delta^{15}N$ value of NO_3^- (henceforth referred to as $\delta^{15}N_{NO3}$) would be a result of mixing NOx sources based on the source's contributing fraction. The chemistry hypothesis would predict that reactions or processes would shift the $\delta^{15}N$ values from their original source $\delta^{15}N$ values, with the magnitude of the shift dependent on atmospheric and/or meteorological conditions and the energetics of the reaction or process.

Given the known complications, this work seeks to assess the use of stable isotopes as tracers, specifically, the assumption that the $\delta^{15}N$ value is a tracer of source alone without significant influence from chemical reactions. Using source emission data and known source $\delta^{15}N$ values, isotope mass balance should be able to approximate measured $\delta^{15}N_{NO3}$ values and determine the $\delta^{15}N$ value associated with wildfire derived NOx, which is currently unknown. Significant deviations from observed values would support the significance of isotope effects associated with chemical reaction and processing in the atmosphere. Aerosols collected in Southern California, emission data, and isotopic analysis were utilized to determine the utility of $\delta^{15}N$ as tracer of NOx sources.

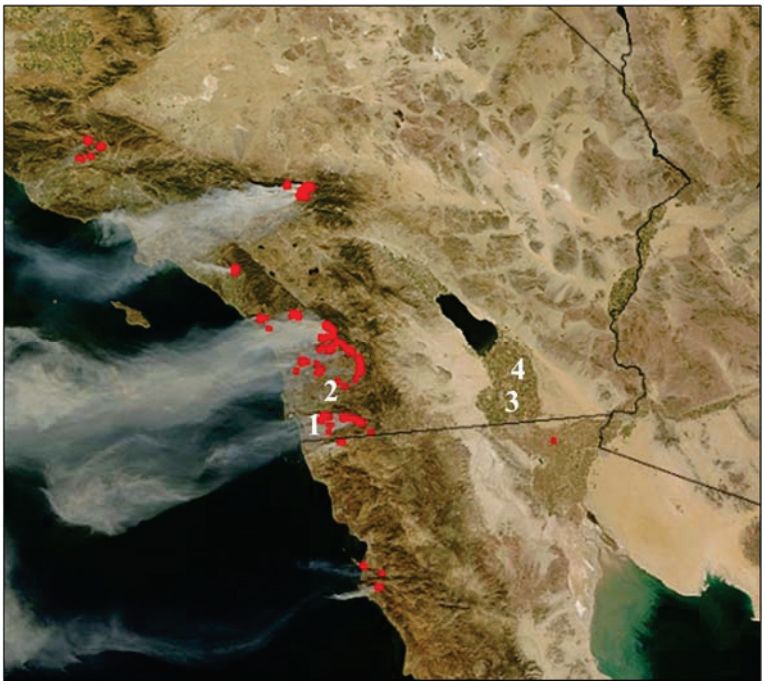

Figure 4.1: Satellite image of Southern California, taken October 22, 2007. Image show fires burning (red) and presence of strong Santa Ana winds pushing smoke offshore. Sampling sites are numbered as follows: Chula Vista (1), El Cajon (2), El Centro (3), and Brawley (4). Image courtesy of NASA/MODIS Rapid Response.[38]

4.2 Methods

4.2.1 Site Description

The study area was the Southern California region near San Diego and the Mexican border during 2007. Particulate matter with diameters less than 10 μm and other air quality data was collected by the San Diego and Imperial County Air Pollution Control Districts and the California Air Resources Board (CARB). Four monitoring locations from two different counties (Figure 4.1) were chosen for this study: Chula Vista and El Cajon in San Diego County and Brawley and El Centro in Imperial County. Imperial County locations are located between the Salton Sea and the US-Mexico Border in the Imperial Valley and

the Colorado Desert. Despite the desert climate, irrigation has made land-use in this region highly agricultural; thus, soil NO emissions may be important in the Valley. These valley locations are also less populated than San Diego locations, with a combined population of 179,091. San Diego County locations are part of the greater San Diego metropolitan area, much closer to the Pacific coast (~7.5 km and 29.5 km from the Chula Vista and El Cajon sampling sites, respectfully), and experience a Mediterranean climate. These areas are also much more densely populated, with a metropolitan population of approximately 3.3 million and local NOx emissions are dominated by residential and metropolitan sources. Seasonal and daily shifts in temperature and NOx emissions are more apparent in the Imperial County locations, due to the coastal influence on the San Diego County sites. Additionally, the Port of San Diego has two cargo terminals, one cruise terminal, two ship repair yards, the West Coast's only shipyard, and serves as the base for the largest naval complex in the world. In 2013, the Port recorded 556 arriving vessels.[39] Table 4.1 further summarizes site demographics.

Imperial County has 489,137 acres of agricultural, with over 95% of this acreage lying in the Imperial Valley. Alfalfa, onions, head lettuce, and broccoli dominate field and vegetable crops, and cattle dominates livestock operations although sheep operations are also significant. The valley's climate allows for multiple harvests per year for some planted crops.[40] Agricultural operations and other non-farm applications used 271,239 tons of fertilizer in 2012.[41] As the county receives very little precipitation throughout the year (2.61" annually),[42] the region depends heavily on irrigation from the Colorado River.[43] San Diego County also has significant agriculture industry, with 268,592 acres of planted crops

Table 4.1: Site Demographics as recorded by the US Census Bureau and California Air Resources Board.

	Chula Vista	El Cajon	Brawley	El Centro
Latitude	32.63123	32.7912	32.97831	32.79215
Longitude	-117.05905	-116.9421	-115.53904	-115.56299
Elevation (m)	55	144	-15	9
Population	260988	103091	25820	43763
Area (sq mi)	49.63	14.43	7.68	11.08
Distance from Pacific Ocean (km)*	7.5	29.5	162	158
Air Basin	San Diego	San Diego	Salton Sea	Salton Sea
County	San Diego	San Diego	Imperial	Imperial
Climate	Mediterranean	Mediterranean/ Semi-arid	Low Desert	Desert
Land Use	Residential/ Metropolitan	Residential/ Metropolitan	Residential/ Agriculture	Residential/ Agriculture
ARB Site	80 E. J St.	1155 Redwood Ave	220 Main St.	150 9th St
Monitoring Site Maintained by:	San Diego Air Pollution Control District	San Diego Air Pollution Control District	Imperial County Air Pollution Control District	Imperial County Air Pollution Control District
* Estimated using Google Earth				

(80.6%), vegetables (1.7%), fruit and nut trees and shrubs (13.0%), and nursery and cut flowers (4.7%), with avocados utilizing the most acreage. In 2012, San Diego County used 163,785 tons of fertilizer, which included agricultural uses as well as non-farm uses (gardening, landscaping).[41] Cattle operations are also prevalent in San Diego County, with hog operations also significant.[44] Although the county receives more precipitation than Imperial County (10.13" annually), 80% of San Diego County's water is imported from Northern California and the Colorado River.[45]

Although 10% of the California's power is supplied by coal, San Diego and Imperial Counties, which lie along the US-Mexico border, do not rely on coal for power generation. Instead, power plants located in San Diego and Imperial counties use natural

Table 4.2: Power Plants in San Diego County and Imperial County by fuel/operation type as of 2015[45]

Powered by:	San Diego County	Imperial County
Natural Gas	60	1
Hydro	10	10
Wind	2	1
Solar	29	13
Biomass	0	1
Geothermal	0	20
Digester Gas	3	0
Landfill Gas	8	0

gas, wind, water, solar energy, and biomass to produce energy (Table 4.2). A few plants in Imperial County also utilize geothermal energy for power generation.[46] However, plants using renewable power generation methods (hydro, wind solar, geothermal) do not use combustion for power generation, and therefore do not emit NOx.

4.2.2 2007 California Wildfire Season

Although wildfires are common to the Western United States, 2007 was a particularly explosive season for Southern California. Rainfall and snow pack levels were at historic lows causing to live fuel moistures levels to reach all-time lows. These conditions, along with the larger than normal dead fuel accumulations resulted in the rapid spread of the fires, especially during the month of October.[47,48] The first wildfire of the season, the Zaca Fire, began two months early than normal, on July 4, 2007 in Santa Barbara County. The fire burned for two months, scorching 240,207 acres before it was finally contained. The season continued with several small fires throughout September and early October, before Ranch Fire, fed by as strong Santa Ana winds, set off a chain of

events that sparked 23 fires in rapid succession.[47] Although some fires continued through early November, the first three days were the most destructive as the Santa Ana Winds were the strongest during this period. These late October fires burned through half a million acres of land, impacting populated areas, wildlife reserves, and watersheds, displacing hundreds of thousands of residents.[47,48]

Fires in San Diego County consumed more acres than fires in other counties, with some fires burning in for 10 days prior to containment. Fueled by extremely dry conditions, brought about by below average winter precipitation and very little summer rain, and strong (40-70 mph) Santa Ana winds, wildfires spread rapidly.[48] Harris Fire, located along the U.S. – Mexico border, started October 21, 2007. Pushed west by Santa Ana winds, the fire reached the Chula Vista city limits by October 23. Containment strategies were hampered by strong winds, and it was 6 days before significant containment was obtained. Harris fire was fully contained by October 31, but not before consuming 90,440 acres.[48] Witch Fire, located approximately 25 miles NE of El Cajon, CA, also started October 21, 2007. As with Harris Fire, Santa Ana winds grounded air crews and hampered suppression methods. The fire merged with Poomacha Fire, which began October 23 on the La Jolla Indian Reservation, on October 25 before containment was reached on October 31. Witch Fire was the largest of the Fire Siege, consuming 197,990 acres. Poomacha Fire was mostly contained by October 31, but full containment wasn't reached until November 13.[48]

4.2.3 Sample Analysis

Aerosol filters were collected on 8x10" Quartz Microfiber filters using a high volume PM_{10} inlet sampler on a 1-in-6-day basis by the San Diego County and Imperial

County Air Pollution Control Districts. Samples were collected for 24 hours at a flow rate of approximately 1.05 m^3/min. Initial analysis was conducted by the CARB, using a quarter of the exposed filter, in order to determine overall PM mass by Electronic Analytical Balance (ARB Analysis Method 016) as well as the nitrate, sulfate, chloride, ammonium, and potassium concentrations by Ion Chromatography (ARB Analysis Methods 007 and 023).[49] Most collection sites also monitor trace gas concentrations (CO, NO_2, O_3) and meteorological conditions (temperature, wind direction speed, humidity) using standard protocols,[50] thus adding data that was useful for interpreting the isotopic results. The remaining portion of each filter was placed in a folder and boxed away, before procurement by Purdue University in 2015.

A secondary ion analysis was conducted in 2015 at Purdue University using standard protocols. Briefly, the filters were soaked in 100 mL of Millipore water (EMD Millipore, Fischer Scientific) to dissolve the collected particulates and ions. This extract was split into 6 – 15 mL centrifuge tubes (VWR), each portion containing ~13 mL. One portion was utilized for anion analysis using Ion Chromatography. Anions (chloride, nitrate, and sulfate) were determined using a Dionex IonPac AS14 analytical column with a Omnifit SPE Sorbant C18 chromatographic column and 3.5 mM $NaHCO_3$/1 mM Na_2CO_3 eluent. A Dionex AMMS300 suppressor with 50mN H_2SO_4 was used prior to detection with an Alltech Model 650 Conductivity Detector. Standards of known NO_3^-, SO_4^{2-} and Cl^- concentration were used to calibrate the IC and determine the sample concentrations.

Another portion of the filter extract was used for isotopic analysis of N and O. The sample was concentrated using a freeze dryer down to final volume of ~1-2 mL. This portion was injected into a 12 mL vial containing a denitrifying strain of bacteria (P.

Aureofaciens).[51–53] The bacteria convert nitrate in the sample into nitrous oxide (N_2O). The N_2O is extracted from the headspace, purified, and analyzed for $\delta^{15}N$ and $\delta^{18}O$ values using a Thermo Delta V Isotope Ratio Mass Spectrometer.[51–53] Working lab standards, calibrated against USGS34 and USGS35, were used to account for isotopic fractionation during bacteria denitrification and N_2O purification. The working standards had an average standard deviation of 1.6‰.

4.3 Results

In order to verify the aerosol ion composition had not changed while in storage, filters were re-analyzed using Ion Chromatography and compared to the results obtained by CARB in post-sampling (Figure 4.2). The NO_3^-, Cl^-, and SO_4^{2-} concentrations measured in 2015 agreed with concentrations measured in 2007, but four samples showed significant NO_3^- loss. Two of these samples, collected November 8th and 20th, correspond to filters with relatively large concentrations of aerosol NH_4^+, suggesting that the NO_3^- loss may have been due to NH_4NO_3 volatilization during storage. Previous studies conducted by the CARB found that filters stored in open containers for over six days experienced significant NO_3^- volatilization. Additionally, the study found that at temperatures elevated above room temperature volatilization occurred in both a sealed and open container.[54] The other two samples do not have any (November 2nd) or very little (October 27th) NH_4^+ to explain this loss. Another study noted that HNO_3 and NH_4^+ could react with fine organic matter, leading to NH_4NO_3 being associated with organic matter.[55] As organic matter was filtered out of extracted samples, it is possible that associated NH_4NO_3 would also be removed. However, the impact this loss has on the $\delta^{15}N$ value of the remaining NO_3^-, can be accounted for

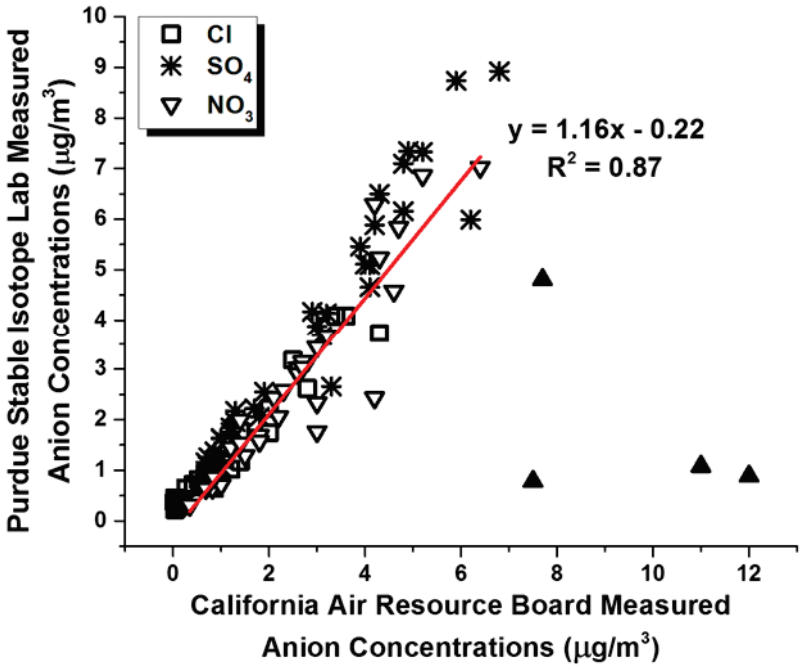

Figure 4.2: Comparison of anion concentrations as measured by the California Air Resources Board in 2007 and the Purdue Stable Isotope Lab in 2015. Filled in triangles are samples showing NH_4NO_3 loss, and red trendline indicates the agreement of non-volatilized samples.

using the Rayleigh distillation equation, and thus will still provide valuable data about wildfire NOx emissions.

Chula Vista NO_3^- concentrations (Figure 4.3) averaged 3.0 ± 2.3 µg/m^3, and showed no consistent seasonality. However, concentrations in the days after the fire, NO_3^- concentrations increased, reaching concentrations 2-4 times the annual average. In contrast with previous studies, which observed a winter increase in NO_3^- concentrations, NO_3^- concentrations at Chula Vista showed no apparent increase. However, it is possible that the wildfire NOx emissions could be obscuring any seasonal NO_3^- concentration shifts. Previous studies[56–58] attribute the winter increase in NO_3^- concentrations to a lower boundary layer height, which would trap NOx and oxidants closer to the surface,

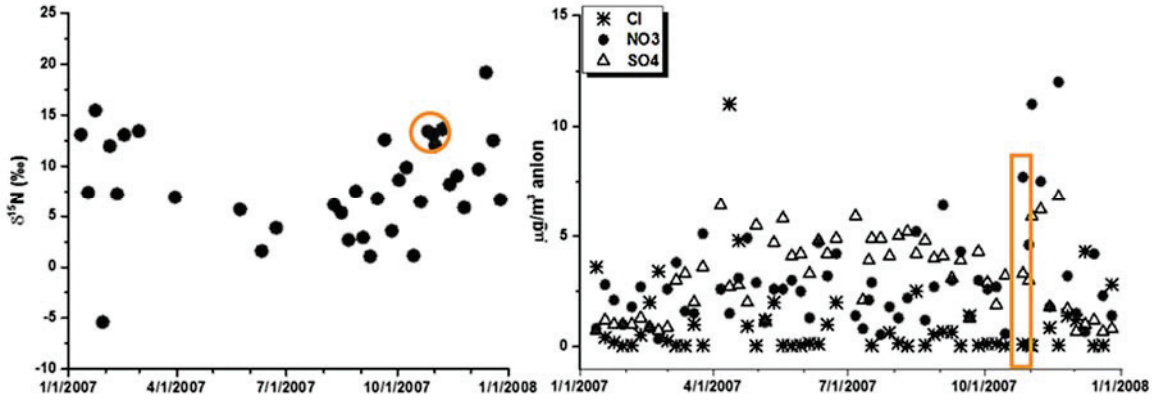

Figure 4.3: $\delta^{15}N_{NO3}$ (left) values and anion concentrations (right) in PM_{10} collected in Chula Vista, California. Noted wildfire activity during PM_{10} sampling is circled/boxed.

promoting oxidation.[10,31,56–58] However, the relatively narrow temperature range, which averages 17.6 ± 4.1°C (68.7 ± 39.4°F), likely would not change the boundary layer height significantly, suggesting a seasonal shift in NO_3^- concentrations is likely absent at Chula Vista.

The annual average nitrate $\delta^{15}N$ value in Chula Vista was 8.3 ± 5.0‰, with summer minimums (4.1‰ average) and winter maximums (10.0‰). This seasonal trend echoes a study by Freyer,[59] which observed summer minima and winter maxima in NO_3^- collected in rain samples (-5% and 0‰, respectfully) and particulate samples (3‰ and 7%, respectfully). Conversely, studies by Hastings[60] and Wankel[61] returned $\delta^{15}N$ values with the opposite trend: summer maximums and winter minimums. Rainwater collected in Bermuda was found to have higher $\delta^{15}N$ values (-2.1‰) during the warm season than samples collected during the cool season (-5.9‰).[60] Aerosol nitrate collected in Eilat,

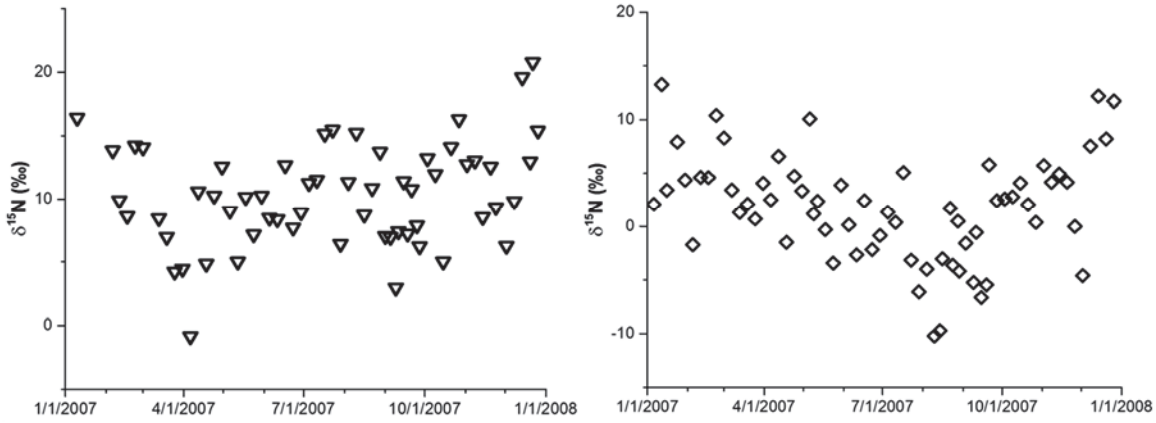

Figure 4.4: $\delta^{15}N_{NO3}$ values as observed in El Cajon (left) and El Centro (right).
are terrestrial systems whereas the latter to are marine systems.

Israel, which lies on the Gulf of Aqaba, recorded $\delta^{15}N$ values with summer maximums (-2.1‰) and winter minimums (-3.7‰).[61] This asynchrony maybe be that the former two

Seasonal variations in $\delta^{15}N$ values were observed at all sites to some extent (Figures 4.3 and 4.4). Overall, $\delta^{15}N_{NO3}$ values were lowest during the summer and highest during the late fall and winter months. The $\delta^{15}N$ seasonal shift in the El Centro nitrate was much more pronounced than observed in El Cajon and Chula Vista. The semi-arid climate of El Centro leads to very little precipitation and produces significant daily and seasonal temperature changes, which effects atmospheric processing and deposition conditions. The Mediterranean climate of El Cajon and Chula Vista may not bring much more precipitation, but proximity to the ocean leads to a small seasonal temperature changes. Additionally, the greater proportion of agricultural activities and lesser proportion of mobile sources enhance the El Centro $\delta^{15}N_{NO3}$ seasonality. However, it is worth noting that the $\delta^{15}N_{NO3}$ values

appear unaffected by wildfire emissions, as the observed $\delta^{15}N_{NO3}$ values do not deviate from the established seasonal trend at any of the sites.

Chula Vista SO_4^{2-} concentrations are low during the winter, but are roughly 2-3 times higher during the spring, summer, and fall. As Chula Vista is a coastal community with relatively warm temperatures year-round, the seasonality of SO_4^{2-} aerosols may be the result of DMS oxidation. Once emitted from the ocean's surface, DMS can deposit onto aerosol surfaces and oxidize into SO_2, and ultimately SO_4^{2-}, which is frequently referred to non-sea salt SO_4^{2-} (nss-SO_4^{2-}). As phytoplankton productivity peaks in the summer, due to increased photolysis, DMS and nss-SO_4^{2-} concentrations also peak in the summer,[62] thus leading to an enhancement in the overall SO_4^{2-} concentrations. Additionally, recent work by Dominguez et al.[23] has found that SO_2 from ship exhaust is also a significant contributor of nss-SO_4^{2-}. Coarse sea salt particles rapidly remove and oxidize SO_2, which can account for 10-44% of the nss-SO_4^{2-} in marine air masses. Cl^- concentration is low for most of the year, indicating that the major Cl^- source, sea salt, varies little throughout the year. Therefore, any seasonality in SO_4^{2-} concentrations would be the result of urban SO_2 (industrial processes) or non-sea salt contributions.

At Chula Vista, daily average O_3 concentrations ranged from 11.1 to 64.8 ppb and peaked in the late spring/early summer (43.2 ppb on average) before falling to winter minimums (24.1 ppb on average). Conversely, daily average CO concentrations peak in the winter (927.7 ppb average) before falling to a minimum in the late summer (434 ppb), and span from 330 to 1790 ppb (Figure 4.5). Daily average NOx concentrations ranged from 5 to 83.1 ppb, with a summer minimum (8.0 ppb on average) and winter maximum (38.5 ppb on average). In the period after heavy wildfire activity, CO and PM

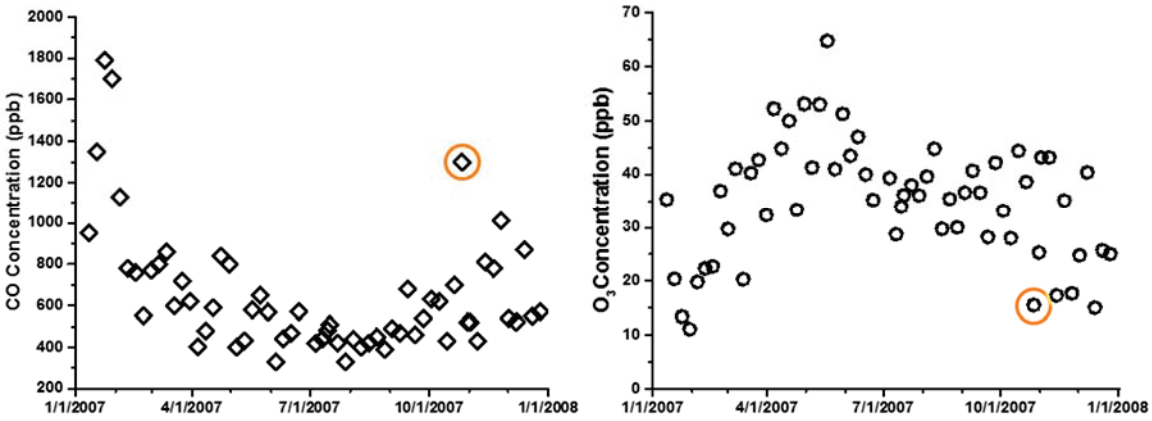

Figure 4.5: CO (left) and O_3 (right) 24-hour average concentrations at Chula Vista, California. Noted wildfire activity during PM_{10} sampling is circled.

concentrations showed a slight increase in daily average concentrations. $PM_{2.5}$ and PM_{10} concentrations, which average 19.7 and 34.3 μg/m^3, respectfully during the fall, nearly doubled in concentration (28.5 and 58 μg/m^3, respectfully) with the addition of wildfire emissions. CO concentrations, which average 650 ppb in the fall, more than doubled in concentration (1300 ppb) as a result of wildfire emissions. Additionally, measured NO_3^- and SO_4^{2-} concentrations at Chula Vista increased after the wildfires, possibly due to dust and ash produced being reintroduced into the atmosphere by the wind. Conversely, daily average O_3 concentration seemed to be unaffected by wildfire emissions, and NOx may show a slight concentration enhancement, but this also falls in line with the shift in seasonal trends.

4.4 Discussion

In order to assess if the seasonality of the $\delta^{15}N_{NO3}$ values was the result of the seasonality of NOx sources[31–33] isotope mass balance was used. Isotope mass balance can be used one of two ways: to calculate an expected $\delta^{15}N_{NO3}$ sample value or to determine the unknown $\delta^{15}N$ value of a source(s). In the first case, source mole fractions (f_i) of each NOx source and the $\delta^{15}N$ values ($\delta^{15}N_i$) of each NOx sources known are summed together to determine the expected $\delta^{15}N_{NO3}$:

$$\delta^{15}N_{NO3} = \sum f_i \delta^{15}N_i \quad \text{(Eq. 1)}$$

In the second instance, the NOx source mole fractions (f) that do not have known $\delta^{15}N$ values ($\delta^{15}N_{unknown}$) are excluded in the summation and the measure NO_3^- $\delta^{15}N$ value is used to determine the $\delta^{15}N$ value of the unknown ($\delta^{15}N_{unknown}$) NOx source(s):

$$\delta^{15}N_{NO3} = f_{unknown}\delta^{15}N_{unknown} + \sum f_i \delta^{15}N_i \quad \text{(Eq. 2)}$$

NOx emission inventories for San Diego and Imperial county were obtained from the CARB[63] and biogenic emissions for each county were obtained using the BEIS3.12 model[64] in the Sparse Matrix Operator Kernel Emissions (SMOKE) modeling system. The emissions data was used to determine monthly mole fractions (f_i) for each NOx source. The emissions data was separated into four EPA categories: stationary sources, area-wide sources, mobile sources, and natural sources (Table 4.3). Stationary NOx sources include Electrical Generating Units (EGUs) and manufacturing plants, as well as smaller sources such as dry cleaners, sewage treatment plants, and landfills. Although approximately 10% of California's power supply comes from coal combustion, neither San Diego nor Imperial County has any coal EGUs. Instead, EGU's in San Diego and Imperial counties (Figure

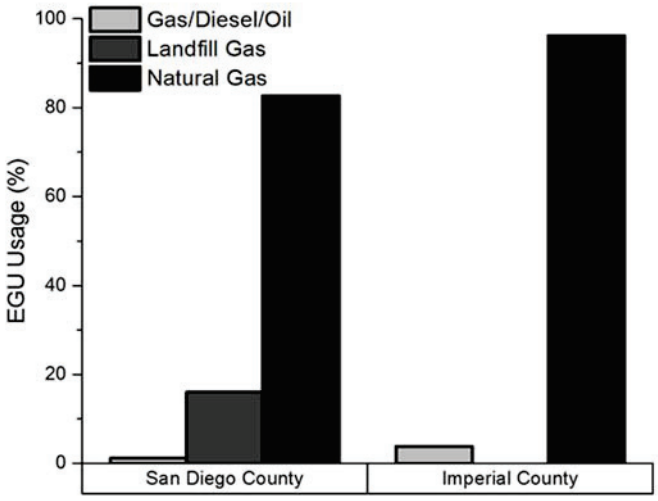

Figure 4.6: EGU fuel usage for San Diego and Imperial Counties, California.

4.6) are mainly fueled by natural gas (83% and 96%, respectfully). Mobile NOx sources include gas and diesel powered cars, trucks, buses, and motorcycles as well as off-road sources such as farm and construction equipment, recreational vehicles, airplanes (small craft and commercial), trains, boats, and ships. Natural NOx sources include biogenic or soil NOx and wildfire emissions, which are highly seasonal. Biogenic emissions often peak in the summer growing season with winter minimums, whereas wildfire season tends to occur in the fall, with little to no contributions made outside this season. Area-wide NOx sources include operations such as pesticides, fertilizers, road dust, residential fires, asphalt paving and roofing, and construction solvents. These NOx sources tend to be small and variable, but may contain some seasonal dependence however the $\delta^{15}N$ values of these sources are unknown.

The $\delta^{15}N$ value of NOx from different sources taken from the literature and are summarized in Table 4.4, and NOx source fractions included in these categories are

summarized in Table 4.3. Overall, the average $\delta^{15}N$ value for each source was chosen to agree with the values used in the isoscape reported in Walters et al.[5] The $\delta^{15}N$ values for gas powered motor vehicles, off-road vehicles, and natural gas power plants were taken from studies conducted by Walters et al.[4,5] For NOx emissions by diesel powered motor vehicles, soils, the mean of the $\delta^{15}N$ value range was used. As $\delta^{15}N_{NOx}$ values for airplanes,

Table 4.3: Proportion of NOx Sources (f) by Category (in bold) and sub-category (italics)

Source	San Diego County	Imperial County
Stationary	**0.043**	**0.180**
EGU	*0.289*	*0.087*
Other NOx Sources	*0.711*	*0.913*
Areawide	**0.016**	**0.016**
Mobile	**0.896**	**0.724**
On-Road Gasoline	*0.364*	*0.202*
On-Road Diesel	*0.385*	*0.480*
Non-road NOx Sources	*0.252*	*0.318*
Natural	**0.045**	**0.080**
Biogenics	*0.890*	*1.000*
Wildfires	*0.110*	*0.000*

Table 4.4: Mass balance source δ^{15}N-NOx values

Source	δ^{15}N range	δ^{15}N used	Reference
Coal Fired Power Plants	+6 to +25.6‰	15‰‡	Walters et al., 2015b; Heaton, 1990; Felix et al., 2012
Natural Gas Power Plants	-18.2 to -14.8‰	-16.5 ± 1.7‰	Walters et al., 2015b
Motor Vehicle - gas	-19.1 to 17‰	-2.6518 ± 1.5‰ (SD) -3.183 ± 1.5‰ (IMP)	Walters et al., 2015a
Motor Vehicle - diesel	-5 to 0‰	-2.5‰‡	Walters et al., 2015b
Off-Road Vehicles - gas	-14.2 to -8.8‰	-11.5 ± 2.7‰‡	
Airplanes	†	0.9‰*	
Ships/Trains	†	-19‰*	
Soils	-48.9 to -19.9‰	34.3‰‡	Walters et al., 2015b; Li & Wang, 2008; Felix & Elliott, 2014
Wildfires	-7 to 12‰	2.5‰‡	Fibiger et al., 2014

† NOx sources not directly measured.
‡ Average based on observation range. High and low end predictions use range end points.
* Value not changed in the high and low end estimates

trains, and ships have not been determined, but the justification given by Walters et al[5] was used for estimating their $\delta^{15}N$ values. The overall isotopic mass balance is calculated as follows:

$$\delta^{15}N_{NO3} = f_{station}\ \delta^{15}N_{station} + f_{area}\ \delta^{15}N_{area} + f_{mobile}\ \delta^{15}N_{mobile} + f_{natural}\ \delta^{15}N_{natural} \quad \text{(Eq. 3)}$$

The $\delta^{15}N$ value for each of the four source categories were further calculated as using follows:

$$\delta^{15}N_{station} = f_{Natural\ Gas}\ \delta^{15}N_{NaturalGas} + f_{other}\ \delta^{15}N_{other} \quad \text{(Eq. 4)}$$

$$\delta^{15}N_{mobile} = f_{on\text{-}road\ gas}\ \delta^{15}N_{on\text{-}road\ gas} + f_{on\text{-}road\ diesel}\ \delta^{15}N_{on\text{-}road\ diesel} + f_{off\text{-}road}\ \delta^{15}N_{off\text{-}road} \quad \text{(Eq. 5)}$$

$$\delta^{15}N_{natural} = f_{biogenic}\delta^{15}N_{biogenic} + f_{wildfire}\delta^{15}N_{wildfire} \quad \text{(Eq. 6)}$$

Using monthly net power generation data obtained from the U.S. Energy Information Administration and annual emission data, monthly EGU emissions were determined in order to account for seasonal power consumption shifts. Monthly biogenic emissions were determined using the EPA's Biogenic Emission Inventory System (BEIS3.12).[64] In order to account for wildfire seasonality, annual wildfire emissions were split between months with documented wildfire activity (July – November). Motor vehicle traffic does vary slightly month to month, approximated using the number of vehicle miles traveled (VMT) each month.[65]

By applying measured $\delta^{15}N_{NO3}$ values, the NOx emission inventory, and the known $\delta^{15}N_{NOx}$ source values from Chula Vista, California, Equation 1 simplifies to (using the Chula Vista $\delta^{15}N_{NO3}$ annual average):

$$7.8‰ = -5.9‰ + \left(0.049\right)\delta^{15}N_{unknown} \quad \text{(Eq. 7)}$$

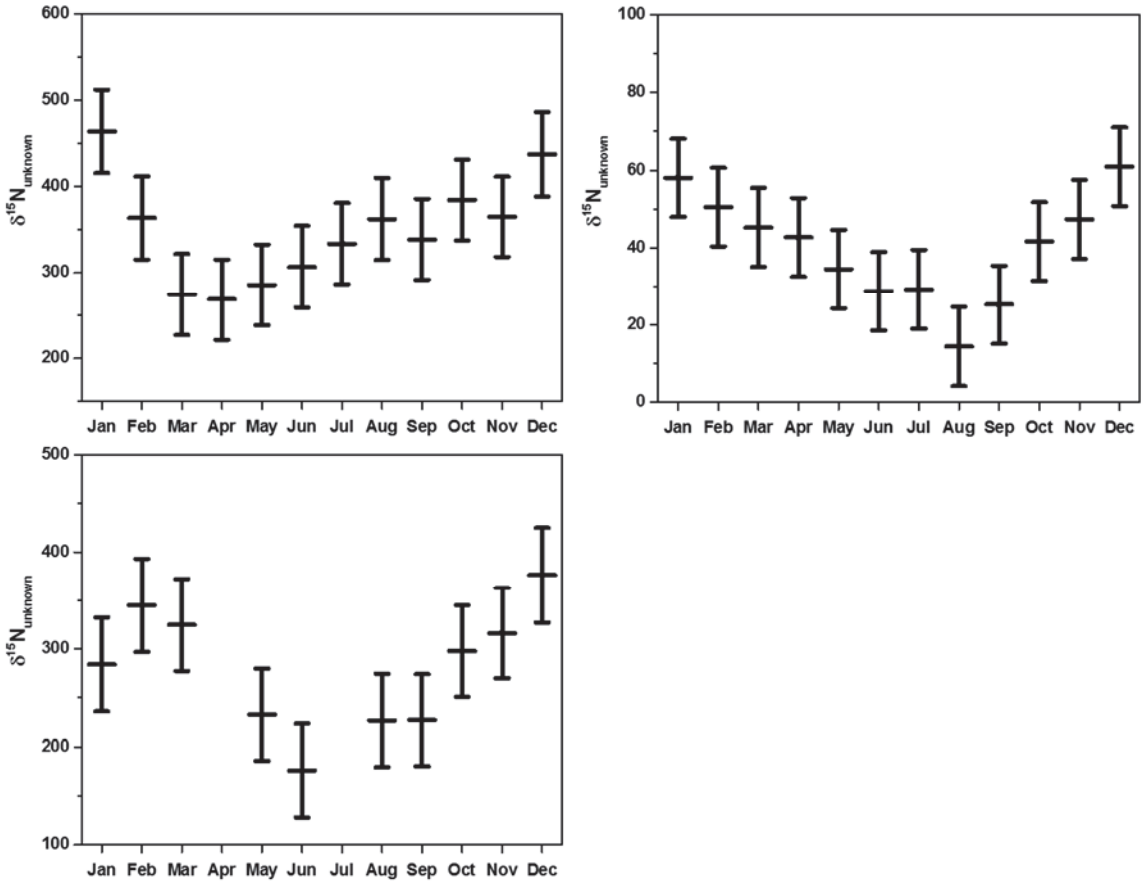

Figure 4.7: Seasonality of unknown $\delta^{15}N$ source for El Centro (top left), El Cajon (top right) and Chula Vista (bottom), California.

where the $0.049 \cdot \delta^{15}N_{unknown}$ represents the NOx sources categorized as area-wide and stationary which have not been characterized for their $\delta^{15}N$ values (i.e. construction/demolition and landfill gas). Ignoring these small NOx contributions (~5%), the isotope mass balance would predict that the $\delta^{15}N$ value of NO_3^- in Chula Vista to be approximately -5.9 ± 0.1‰, and would vary little throughout the year. However, measured $\delta^{15}N_{NO3}$ values are approximately 13‰ more enriched than predicted by NOx sources and exhibit a clear seasonal trend. As a result, given that known NOx sources possess primarily

negative $\delta^{15}N$ values (-5.9‰) and that the unknown NOx source fraction is very small, a highly positive (~280‰, Figure 4.7) NOx source would be required order to predict the $\delta^{15}N_{NO3}$ values observed. Considering the fact that majority of NOx sources $\delta^{15}N$ values have been observed to be negative and the above calculated $\delta^{15}N$ value for unmeasured NOx sources seems highly unlikely, would lend support to the chemistry hypothesis as the controlling factor in the $\delta^{15}N$ of NO_3^- aerosols at this location.

Freyer[66] investigated seasonality of $\delta^{15}N_{NO3}$ values, and suggested that seasonal and diurnal variations in $\delta^{15}N_{NO3}$ values are a combination of seasonal changes in source emissions, a shift in reaction mechanisms, and/or isotopic exchange equilibrium. Further work by Freyer et al.[9] suggested that isotope exchange equilibrium may be the main isotope effect.

$$^{15}NO + {}^{14}NO_2 \leftrightarrow {}^{14}NO + {}^{15}NO_2 \qquad \text{(R11)}$$

The partitioning of isotopes in this equilibrium is quantified using a fractionation factor, $\alpha_{NO2\text{-}NO}$

$$\alpha_{NO2\text{-}NO} = \frac{R_{NO_2}}{R_{NO}} \qquad \text{(Eq. 8)}$$

where R refers to the atomic ratio of the heavy isotopologue to the light isotopologue (e.g. $^{15}NO/^{14}NO$). To further investigate this effect, Freyer et al[9] measured $\delta^{15}N_{NOx}$, $\delta^{15}N_{NO2}$, and the NO_2 mole ratio (χ_{NO2}), and found that $\delta^{15}N_{NO2}$ became more enriched as χ_{NO2} decreased, with $\delta^{15}N_{NOx} = \delta^{15}N_{NO2}$ when $\chi_{NO2} = 1$. The observed[9,35] net effect of the above equilibrium is that ^{15}N accumulates in the more oxidized oxinitrogen species, suggesting that $\delta^{15}N_{NO3}$ values would be similarly enriched.

Although nitrogen exchange between NO and NO_2 has been both modeled and observed, there still existed discrepancies between theoretical calculation and experimental observations. Walters et al.[37] addressed this discrepancy two ways. The authors measured $\alpha_{NO2/NO}$ at 278, 298, 310K and compared the results to a modified form of the Bigeleisen-Mayer equation, recalculated to account for more precise zero point energies. The modified equation was able to more accurately reproduce the observed results. Furthermore, simulating diurnal and seasonal changes, assuming N isotope equilibrium was reached, revealed significant diurnal and seasonal variations in $\delta^{15}N_{NO2}$. This trend is important because without factoring in shifting sources of NO_x, the $\delta^{15}N_{NO2}$ reflected the trends often observed in $\delta^{15}N_{NO3}$ thus strongly supporting the chemistry hypothesis.

Utilizing hourly NO and NO_2 concentrations measured at Chula Vista, hourly $\delta^{15}N_{NO2}$ values were calculated, following the methods of Walters et al,[37] and were aggregated as a 24-point (hour) moving average. Although some observed $\delta^{15}N_{NO3}$ values (Figure 4.8), agree closely with the calculated $\delta^{15}N_{NO2}$ values, large departures from the moving average are noted (nearly 10‰ in some cases), indicating that isotope exchange (R9) is not the only reaction impacting nitrogen isotope composition. This deviation could be due to two possible reasons: a shift in contributions from the isotope exchange equilibrium or isotope effects during the oxidation of NO_2 to NO_3^-/HNO_3. The our calculated $\delta^{15}N_{NO2}$ values assume that this exchange is always occurring, but this exchange requires both NO and NO_2 to be present. However, due to the lack of photolysis at night NO is rapidly oxidized to NO_2, preventing this exchange. This effect also explains why larger deviations are observed in the winter, when days are short.

Comparing observed $\delta^{15}N_{NO3}$ values to calculated $\delta^{15}N_{NO2}$ trends assumes that $\delta^{15}N$ is conserved as NO_2 is oxidized to NO_3^-/HNO_3. However, the fractionation factors for these reactions have yet to be determined, and therefore cannot be ruled out. Additionally, NO_3^-

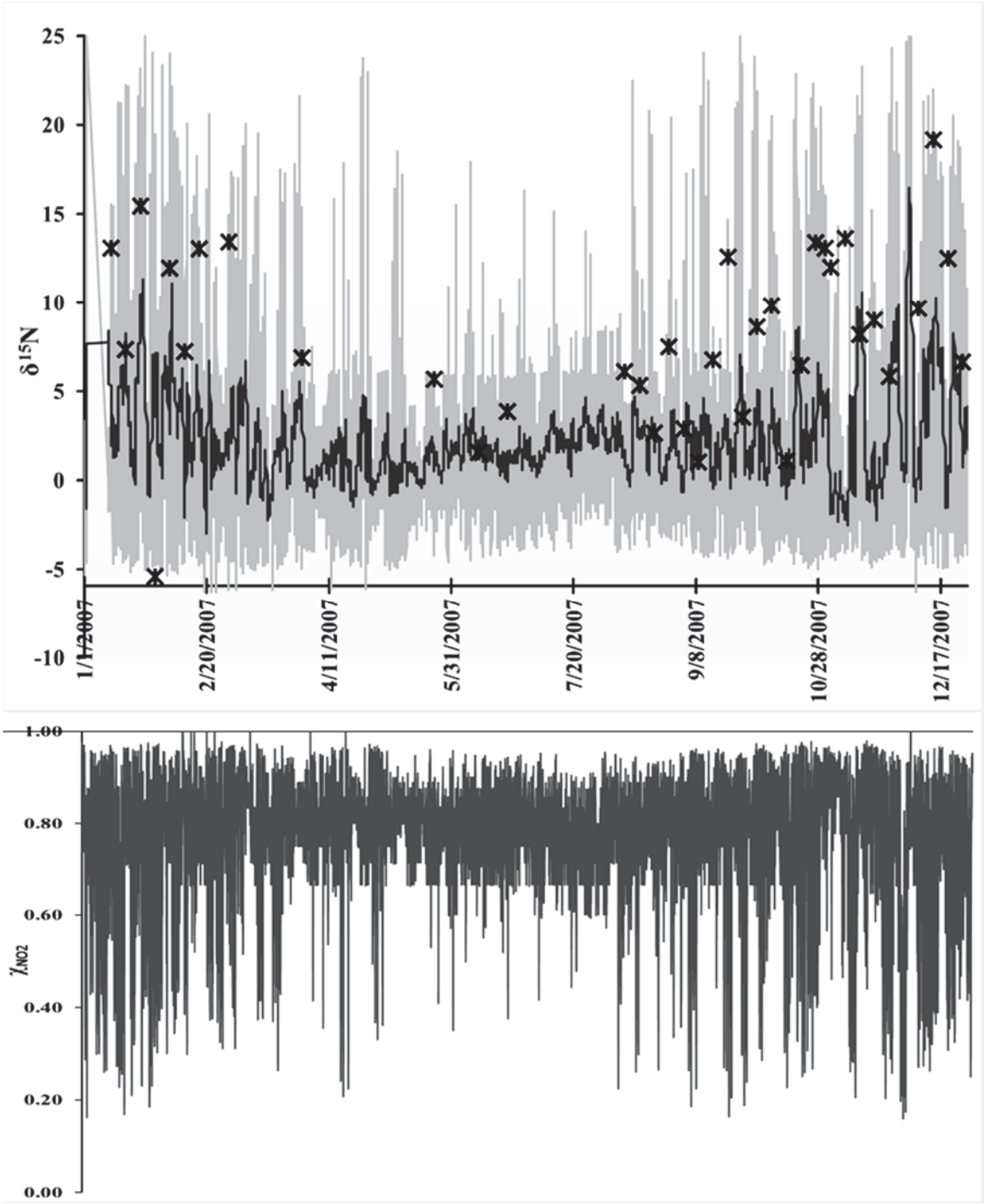

Figure 4.8: Hourly $\delta^{15}N_{NO2}$ (top) and NO_2 mole ratio (bottom) for Chula Vista, CA. In the top figure, trace represents a 24-point moving average. Stars represent observed aerosol NO_3^- $\delta^{15}N$ values.

is produced by numerous chemical reactions, and thus isotope composition of NO_3^- in particulate matter is determined by the mix of reactions contributing NO_3^-. NO_3^- is produced by three main pathways: OH radical oxidation (R4), N_2O_5 (R8), VOC hydrogen abstraction (R6). The OH radical pathway is highly dependent on solar radiation, whereas the N_2O_5 pathway is active only at night. This dependence on solar radiation leads to a diurnal and seasonal variations, which impacts the extent each of these reactions contribute to the NO_3^- concentration. In the summer, where days are long, the OH radical pathway contributes a larger proportion than the N_2O_5 pathway. Each of these pathways possesses its own unique isotope effect, and the overall $\delta^{15}N_{NO3}$ depends on the proportion each reaction contributes to the total NO_3^- concentration in addition to isotope exchange processes. $\delta^{15}N_{NO3}$ values associated with OH radical oxidation is controlled by the HNO_3 - NO_2 exchange equilibrium, where ^{15}N tends to accumulate in HNO_3 ($\alpha_{HNO3\text{-}NO2} = 1.038$, where $\alpha_{HNO3\text{-}NO2} = R_{HNO3}/R_{NO2}$). The $\delta^{15}N_{NO3}$ values associated with the N_2O_5 pathway are governed by the NO_2 – NO_3 exchange equilibrium, which shows ^{15}N accumulating in NO_3^- ($\alpha_{NO3\text{-}NO2} = 0.9819$). VOC hydrogen abstraction does not involve the N atom, thus any isotope effect resulting from this reaction is small. Therefore, $\delta^{15}N_{NO3}$ deviations from the calculated $\delta^{15}N_{NO2}$ trend are likely the result of changes in reaction pathway contributions and/or fractionations associated with the oxidation of NO_2 to NO_3^-/HNO_3.

Aerosol filters collected in Chula Vista, El Cajon, El Centro, and Brawley at the end of October 2007 were impacted by the wildfire emissions, as noted by the monitoring agency's field notes (Table 4.5). At Chula Vista, PM increases as the result of the fire were observed in both the fine ($PM_{2.5}$) and coarse (PM_{10}) fractions (Figure 4.9) due to the

Table 4.5: List of sampling days impacted by wildfires, as recorded in the CARB sampling notes at each sampling site.

Sampling Site	Wildfire Days
Chula Vista	October 21, October 27
El Cajon	October 21, October 27, November 2
Brawley	October 27, November 2
El Centro	October 27, November 2

production of trace gases (CO, NOx, O_3), VOCs, and coarse PM (ash, soot, smoke particles). CO concentrations were also slightly elevated relative to seasonal trends, consistent with previous studies that show a major source of CO is wildfires.[26–28] Although wildfires produce substantial concentrations of CO, urban CO emissions dampen this contribution, as fossil fuel combustion (motor vehicles, industrial processes, power generation) dominates CO concentrations.[27] NOx concentrations at Chula Vista during the fire siege were nearly double (50.4 ppb) the fall average (29 ppb, Figure 4.10), although it is not clear whether this increase is due to shifting seasonal trends or wildfire emissions. However, NO concentrations showed a slight increase and NO_2 nearly doubled its seasonal concentration. In studying the 2008 California wildfire season, Cai et al.[26] noted that increases in NOx concentration was only significant in the immediate area of the fire. However, these monitoring sites were not in the immediate area of the fires, but rather downwind (Figure 4.1). Therefore, although wildfire emissions would contribute NOx emissions, overall concentrations were still dominated by local motor vehicle and industrial emissions.[27] However, NO_2 concentrations are dependent on photolysis (1a and b), which would likely have been decreased as the result of ambient soot and smoke from the fire, leading to increased NO_2 concentrations.[27] O_3 concentration immediately after the wildfire

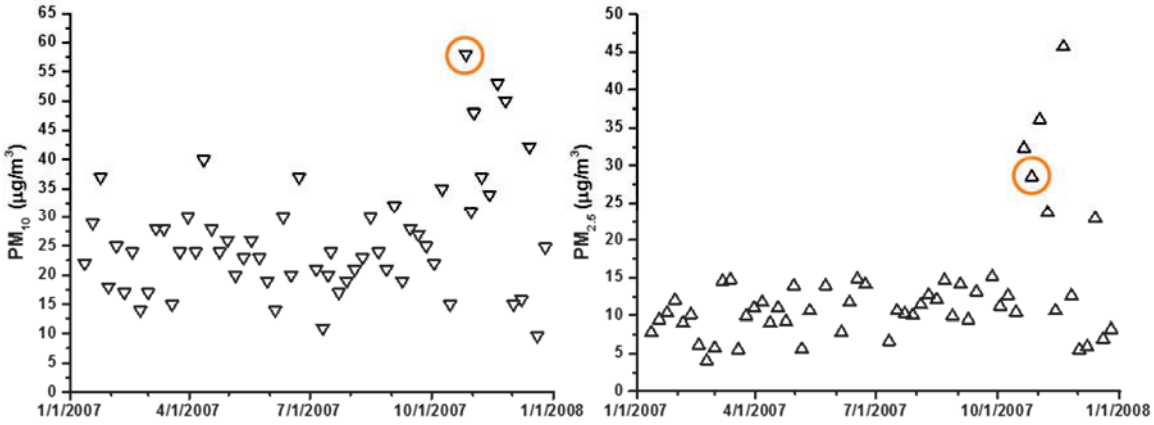

Figure 4.9: PM_{10} (left) and $PM_{2.5}$ (right) concentrations in Chula Vista, California in 2007. Noted wildfire activity during PM_{10} sampling is circled.

decreased, although concentrations did increase in the week post-fire. This O_3 decrease may be due to O_3 reactions on aerosol surfaces. As with NO_2, O_3 concentrations are also photosensitive, which would suggest that concentrations would decrease during and immediately following fire event, when the ambient air reduces photolysis.[27] However, as wildfire emission contain numerous O_3 precursors, O_3 concentrations increase as the smoke clears and photolysis returns to normal levels.

Despite significant differences in the aerosol and trace gas concentrations during the fire event, no deviation in observed $\delta^{15}N_{NO3}$ values is initially apparent at Chula Vista. Fall $\delta^{15}N_{NO3}$ values range from 1.1 to 13.6‰ (8.0‰ on average), with the $\delta^{15}N_{NO3}$ values impacted by wildfire emissions (13.4‰) falling in the same range. However, the observed value for wildfire impacted days may have been impacted by isotope fractionation due to noted loss of NO_3^- during storage. The CARB anion analysis in 2007 showed elevated NO_3^- concentrations in the samples collected post-wildfire, but our re-analysis in 2015 revealed lower NO_3^- concentrations during the fires indicating NO_3^- loss during storage.

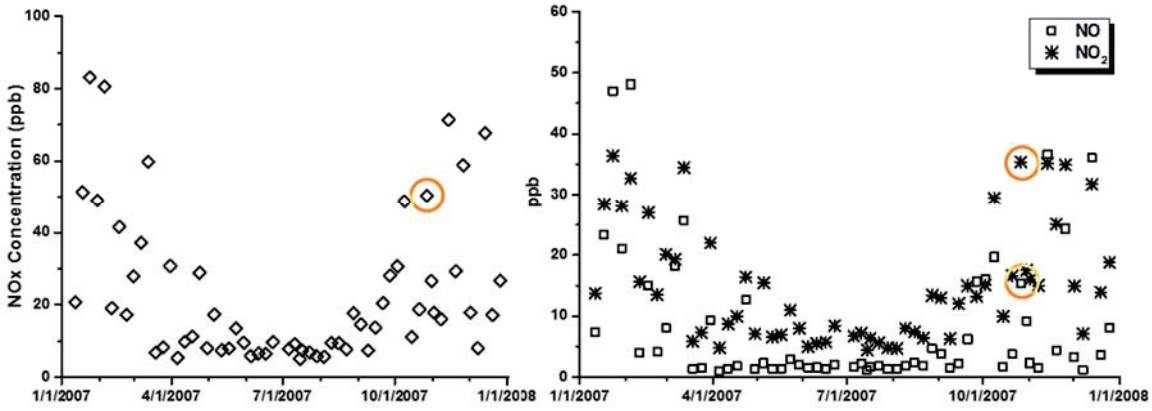

Figure 4.10: NOx (left), NO, and NO_2 (right) concentrations as observed in Chula Vista, California during the year of 2007. Noted wildfire activity during PM_{10} sampling is circled.

The formation of NH_4NO_3 on aerosol filters has been documented, as has its volatilization potential, which increases with increasing temperature.[54,55,59] The volatilization of NH_4NO_3 would lead to isotope fractionation, as the lighter isotope (^{14}N) would volatize first. The degree of fractionation would follow a temperature dependent Rayleigh relationship, as the volatilized NH_4NO_3 would be removed from the system. A previous study by Heaton et al.[67] measured the enrichment factor (ε) for the volatilization of NH_4NO_3 to be -20.6‰. Using this enrichment value, the measured $\delta^{15}N_{NO3}$ value, and the fraction of NO_3^- remaining on the filter, the pre-volatilization $\delta^{15}N_{NO3}$ value can be calculated using the Rayleigh equation:

$$\delta_{initial} = \delta_{final} - \varepsilon \times \ln f_{remain} \qquad \text{(Eq. 8)}$$

For the four sampling days impacted by NH_4NO_3, the $\delta^{15}N_{NO3}$ prior to volatilization (δ_{inital}) were all found to be drastically depleted (-45 to +3.7‰, depending on the amount lost) compared to the rest of the season and year. Therefore, Rayleigh fractionation predicts that wildfire emissions would actually deplete $\delta^{15}N_{NO3}$ values rather than enriching them, as

suggested in previous work.[29,68,69] However, fractionation arising from volatilization is likely masked by the enrichment in NH_4NO_3 from the equilibrium exchange, resulting in $\delta^{15}N_{NO3}$ values that appear uninfluenced by wildfire emissions.[59]

Although wildfire emissions do not have a significant direct effect on NOx concentrations, components of wildfire emissions have a significant impact on OH radical and O_3 concetrations[6,27,28,70], the two main atmospheric oxidants. VOCs are known to react with NO to form NO_2 without the destruction of an O_3 molecule, essentially catalyzing O_3 production.[1,6] VOCs are also known to react with OH radicals to form various organic peroxy radicals,[6] which can also oxidate NO without destroying O_3. While these alternative reaction pathways do not seem to influence NOx concentrations drastically, wildfire emissions have significant influence on the oxidation capacity of the atmosphere, as well as air quality in general.

Although isotopic data indicates the influence of chemistry on $\delta^{15}N$, the extent of this influence has yet to be determined. Although fractionation associated with the isotope exchange equilibrium of NO and NO_2 has been calculated, other fractionation factors still need to be determined. Fractionation factors associated with NO_3^- forming reacions need to be established. Additionally, how these factors vary with temperature, amounts of solar radiation, and in the presence of varying levels of other trace gases. Additionally, the $\delta^{15}N$ values of NOx sources need to be better quantified. Current measured $\delta^{15}N$ values of sources span a large range of values, often with significant overlap. In some cases, the NOx $\delta^{15}N$ value hasn't been measured at all. In order to better predict $\delta^{15}N_{NO3}$ values, the quantification of NOx source $\delta^{15}N$ values and fractionations associated with NOx oxidation pathways will be required. These unknowns should be the focus of future isotopic studies.

4.5 Conclusion

The 2007 wildfire season in Southern California was particularly explosive due to the influence of the Santa Ana winds. Analysis of PM collected at four sampling sites during this period has revealed the influence wildfire emissions had on local atmospheric chemistry. $PM_{2.5}$, PM_{10}, and CO concentrations all showed increases, whereas O_3 concentrations decreased. Daily average concentrations of NO and NO_2 both increased, but by different degrees, suggesting that wildfire emissions impacted NOx cycling.

Although $\delta^{15}N$ is frequently employed as an environmental tracer, the manner by which it is utilized is not agreed upon. Isotopic analysis of collected NO_3^- has suggested that source $\delta^{15}N$ values are likely not conserved as NOx is oxidized into NO_3^-. Given known source contributions and known $\delta^{15}N$ values of NOx sources, isotope mass balance predicts that a NOx source with highly positive $\delta^{15}N$ value must exist for the source hypothesis to be valid. Furthermore, isotopic analysis has also suggested that wildfire emissions may produce a depleted $\delta^{15}N$, disagreeing with previously predicted $\delta^{15}N$ values.[29,68,69] While this data set indicates the need for the consideration of chemistry, additional work must focus on how reactions, atmospheric processing, and post-deposition effects influence $\delta^{15}N_{NO3}$ values.

4.6 References

(1) Hastings, M. G. *IOP Conf. Ser. Earth Environ. Sci.* **2010**, *9*, 012002.

(2) Logan, J. A. *J. Geophys. Res.* **1983**, *88*, 10785.

(3) Logan, J. A.; Prather, M. J.; Wofsy, S. C.; McElroy, M. B. *J. Geophys. Res.* **1981**, *86*, 7210.

(4) Walters, W. W.; Goodwin, S. R.; Michalski, G. *Environ. Sci. Technol.* **2015**, *49*, 2278–2285.

(5) Walters, W. W.; Tharp, B. D.; Fang, H.; Kozak, B. J.; Michalski, G. *Environ. Sci. Technol.* **2015**, *49*, 11363–11371.

(6) Seinfeld, J. H.; Pandis, S. N. *Atmospheric Chemistry and Physics: From Air Pollution to Climate Change, 2nd Edition* -; 2nd ed.; 2006.

(7) James N. Galloway, E. B. C. *Ambio* **2002**, *31*, 64–71.

(8) Galloway, J. N.; Dentener, F. J.; Capone, D. G.; Boyer, E. W.; Howarth, R. W.; Seitzinger, S. P.; Asner, G. P.; Cleveland, C. C.; Green, P. A.; Holland, E. A.; Karl, D. M.; Michaels, A. F.; Porter, J. H.; Townsend, A. R.; V�osmarty, C. J. *Biogeochemistry* **2004**, *70*, 153–226.

(9) Freyer, H. D.; Kley, D.; Volz-Thomas, A.; Kobel, K. *J. Geophys. Res.* **1993**, *98*, 14791.

(10) Sillman, S. *Atmos. Environ.* **1999**, *33*, 1821–1845.

(11) Benkovitz, C. M.; Scholtz, M. T.; Pacyna, J.; Tarrason, L.; Dignon, J.; Voldner, E. C.; Spiro, P. A.; Logan, J. A.; Graedel, T. E. *J. Geophys. Res.* **1996**, *101*, 29239–29253.

(12) Elliott, E. M.; Kendall, C.; Wankel, S. D.; Burns, D. A.; Boyer, E. W.; Harlin, K.; Bain, D. J.; Butler, T. J. *Environ. Sci. Technol.* **2007**, *41*, 7661–7667.

(13) Walters, W. W.; Michalski, G. *Geochim. Cosmochim. Acta* **2015**, *164*, 284–297.

(14) Gobel, A. R.; Altieri, K. E.; Peters, A. J.; Hastings, M. G.; Sigman, D. M. *Geophys. Res. Lett.* **2013**.

(15) Ayers, G. P.; Cainey, J. M. *Environ. Chem.* **2007**, *4*, 366–374.

(16) Charlson, R. J.; Lovelock, J. E.; Andreae, M. O.; Warren, S. G. *Nature* **1987**, *326*, 655–661.

(17) Sievering, H.; Cainey, J.; Harvey, M.; McGregor, J.; Nichol, S.; Quinn, P. *J. Geophys. Res.* **2004**, *109*.

(18) Williams, J.; Keßel, S. U.; Nölscher, A. C.; Yang, Y.; Lee, Y.; Yáñez-Serrano, A. M.; Wolff, S.; Kesselmeier, J.; Klüpfel, T.; Lelieveld, J.; Shao, M. *Atmos. Environ.* **2016**, *125*, 112–118.

(19) Monks, P. S.; Granier, C.; Fuzzi, S.; Stohl, A.; Williams, M. L.; Akimoto, H.; Amann, M.; Baklanov, A.; Baltensperger, U.; Bey, I.; Blake, N.; Blake, R. S.; Carslaw, K.; Cooper, O. R.; Dentener, F.; Fowler, D.; Fragkou, E.; Frost, G. J.; Generoso, S.; Ginoux, P.; Grewe, V.; Guenther, A.; Hansson, H. C.; Henne, S.; Hjorth, J.; Hofzumahaus, A.; Huntrieser, H.; Isaksen, I. S. A.; Jenkin, M. E.; Kaiser, J.; Kanakidou, M.; Klimont, Z.; Kulmala, M.; Laj, P.; Lawrence, M. G.; Lee, J. D.; Liousse, C.; Maione, M.; McFiggans, G.; Metzger, A.; Mieville, A.; Moussiopoulos, N.; Orlando, J. J.; O'Dowd, C. D.; Palmer, P. I.; Parrish, D. D.; Petzold, A.; Platt, U.; Pöschl, U.; Prévôt, A. S. H.; Reeves, C. E.; Reimann, S.; Rudich, Y.; Sellegri, K.; Steinbrecher, R.; Simpson, D.; ten Brink, H.; Theloke, J.; van der Werf, G. R.; Vautard, R.; Vestreng, V.; Vlachokostas, C.; von Glasow, R. *Atmos. Environ.* **2009**, *43*, 5268–5350.

(20) FENN, M. E.; HAEUBER, R.; TONNESEN, G. S.; BARON, J. S.; GROSSMAN-CLARKE, S.; HOPE, D.; JAFFE, D. A.; COPELAND, S.; GEISER, L.; RUETH, H. M.; SICKMAN, J. O. *Bioscience* **2003**, *53*, 391.

(21) Andreae, M. O.; Crutzen, P. J. *Science (80-.).* **1997**, *276*.

(22) Neumann, D.; Matthias, V.; Bieser, J.; Aulinger, A.; Quante, M. *Atmos. Chem. Phys.* **2016**, *16*, 2921–2942.

(23) Dominguez, G.; Jackson, T.; Brothers, L.; Barnett, B.; Nguyen, B.; Thiemens, M. H. *Proc. Natl. Acad. Sci. U. S. A.* **2008**.

(24) Liu, X.-H.; Zhang, Y. *Atmos. Environ.* **2013**, *74*, 259–276.

(25) Zatko, M.; Geng, L.; Alexander, B.; Sofen, E.; Klein, K. *Atmos. Chem. Phys* **2016**, *16*, 2819–2842.

(26) Cai, C.; Kulkarni, S.; Zhao, Z.; Kaduwela, A. P.; Avise, J. C.; DaMassa, J. A.; Singh, H. B.; Weinheimer, A. J.; Cohen, R. C.; Diskin, G. S.; Wennberg, P.; Dibb, J. E.; Huey, G.; Wisthaler, A.; Jimenez, J. L.; Cubison, M. J. *Atmos. Environ.* **2016**, *128*, 28–44.

(27) Phuleria, H. C. *J. Geophys. Res.* **2005**, *110*, D07S20.

(28) Val Martín, M.; Honrath, R. E.; Owen, R. C.; Pfister, G.; Fialho, P.; Barata, F. *J. Geophys. Res. Atmos.* **2006**, *111*, n/a – n/a.

(29) Hastings, M. G.; Jarvis, J. C.; Steig, E. J. *Science* **2009**, *324*, 1288.

(30) Morin, S.; Savarino, J.; Frey, M. M.; Yan, N.; Bekki, S.; Bottenheim, J. W.; Martins, J. M. F. *Science (80-.).* **2008**, *322*, 730–732.

(31) Elliott, E. M.; Kendall, C.; Boyer, E. W.; Burns, D. A.; Lear, G. G.; Golden, H. E.; Harlin, K.; Bytnerowicz, A.; Butler, T. J.; Glatz, R. *J. Geophys. Res.* **2009**, *114*, G04020.

(32) Hastings, M. G. *J. Geophys. Res.* **2004**, *109*, D20306.

(33) Hastings, M. G.; Sigman, D. M.; Lipschultz, F. *J. Geophys. Res. Atmos.* **2003**, *108*, n/a – n/a.

(34) Hoefs, J. *Stable Isotope Geochemistry*; Springer International Publishing: Cham, 2015.

(35) Begun, G. M.; Fletcher, W. H. *J. Chem. Phys.* **1960**, *33*, 1083.

(36) Savarino, J.; Bhattacharya, S. K.; Morin, S.; Baroni, M.; Doussin, J.-F. *J. Chem. Phys.* **2008**, *128*, 194303.

(37) Walters, W. W.; Simonini, D. S.; Michalski, G. *Geophys. Res. Lett.* **2016**, *43*, 440–448.

(38) NASA. NASA Images of California Wildfires http://www.nasa.gov/vision/earth/lookingatearth/socal_wildfires_oct07.html (accessed May 31, 2016).

(39) Marquez, J.; Knapp, T. Freight Planning Fact Sheet: Unified Port of San Diego, 2014.

(40) Valenzuela, C. L.; Evans, L. S.; Ross, K. *Imperial County Agricultural Crop & Livestock Report*; 2014.

(41) Maan, A. A. *Fertilizing Materials: Tonnage Report*; 2012.

(42) *Monthly Climate Summaries*; 2016.

(43) Imperial Irrigation District: Water http://www.iid.com/water.

(44) Dang, H.; Moore, M.; Ross, K.; Carr, C.; Taylor, J.; Hammond, B. *2014 County of San Diego Crop Statistics & Annual Report*; 2014.

(45) San Diego County Water Authority. FAQ and Key Facts http://www.sdcwa.org/frequently-asked-questions-and-key-facts#t7n654.

(46) California Power Plants, 2015.

(47) 2007 Southern California Fire Seige http://interwork.sdsu.edu/fire/resources/2007_fires.html.

(48) Grijalva, R.; Moore, R.; Renteria, H. *California Fire Siege 2007: An Overview*.

(49) California Air Resources Board. Particulate Matter Monitoring as of January 27, 2011 http://www.arb.ca.gov/aaqm/am_tables/partic.htm (accessed Jun 14, 2016).

(50) *Meteorology Data Query Tool*; 2011.

(51) K. L. Casciotti M. Galanter Hastings, J. K. Bo1 hlke, and A. Hilkert, D. M. S. *Anal. Chem.* **2002**, 4905–4912.

(52) D. M. Sigman K. L. Casciotti, M. Andreani, C. Barford,M. Galanter, and J. K. Bolhlke. *Anal. Chem.* **2001**, 4145–4153.

(53) Kaiser, J.; Hastings, M. G.; Houlton, B. Z.; Röckmann, T.; Sigman, D. M. *Anal. Chem.* **2007**, *79*, 599–607.

(54) Achtelik, G. H.; Omand, J. EFFECTS OF ENVIRONMENTAL CONDITIONS ON PARTICULATE NITRATE STABILITY DURING POST SAMPLING PHASE, 1998.

(55) Ashbaughm, L.; Eldred, R.; Hering, S. *Loss of Particulate Nitrate from Teflon Sampling Filters: Effects on Measured Gravimetric Mass*; Davis, CA, 1998.

(56) Riha, K. M. The Use of Stable Isotopes to Constrain the Nitrogent Cycle, Purdue University, 2013.

(57) King, M. Evaluating NOx Sources And Oxidation Pathways Impacting Aerosol Production On The Southern Ute Indian Reservation And Navajo Nation Using Geochemical Isotopic Analysis, Purdue University, 2013.

(58) Wang, H.; Shooter, D. *Atmos. Environ.* **2001**, *35*, 6031–6040.

(59) Freyer, H. D. *Tellus* **1991**, 30–44.

(60) Hastings, M. G.; Sigman, D. M.; Lipschultz, F. *J. Geophys. Res. Atmos.* **2003**, *108*, n/a – n/a.

(61) Wankel, S. D.; Chen, Y.; Kendall, C.; Post, A. F. *Mar. Chem.* **2010**, *120*, 90–99.

(62) Bates, T. S.; Cline, J. D.; Gammon, R. H.; Kelly-Hansen, S. R. *J. Geophys. Res.* **1987**, *92*, 2930.

(63) *Air Quality Data Query Tool*; 2014.

(64) US EPA, O. Biogenic Emission Inventory System (BEIS).

(65) *Traffic Census Program*; 2016.

(66) Freyer, H. D. Seasonal trends of NH + 4 and NO - 3 nitrogen isotope composition in rain collected at Jülich, Germany. *Tellus A*, 1978, *30*.

(67) Heaton, T. H. E.; Spiro, B.; Robertson, S. M. C. *Oecologia* **1997**, 600–607.

(68) Felix, J. D.; Elliott, E. M.; Shaw, S. L. *Environ. Sci. Technol.* **2012**, *46*, 3528–3535.

(69) Agnihotri, R.; Karapurkar, S. G.; Sarma, V. V. S. S.; Yadav, K.; Kumar, M. D.; Sharma, C.; Prasad, M. V. S. N. *Aerosol Air Qual. Res.* **2015**, *15*, 888–900.

(70) Finlayson-Pitts, B. J.; Pitts, J. N.; Jr. *Chemistry of the Upper and Lower Atmosphere: Theory, Experiments, and Applications*; Academic Press, 1999; Vol. 17.

CHAPTER 5: SEASONAL VARIATIONS IN PARTICULATE MATTER AT A COASTAL URBAN CENTER

5.1 Introduction

Particulate matter (PM) is a serious air pollutant, affecting human health more than any other air pollutant.[1] PM_{10} (particulate matter with diameters of 10μm or less) and $PM_{2.5}$ (particulate matter with diameter of 2.5μm or less) have been linked to serious health effects such as cardiovascular and respiratory illnesses and even lung cancer.[1–8] It is for these reasons that the World Health Organization (WHO) has established Air Quality Guidelines[1] and governments worldwide have established standards to limit PM emissions. In New Zealand, the National Environmental Standard for Air Quality (NES) sets a 24-hour average concentration limit at 50μg/m^3 for PM_{10}.[4,9] Additionally, the Ministry for the Environment established ambient air quality guidelines (NZAAQG), which includes a 24-hour average concentration limit for $PM_{2.5}$ of 25μg/m^3.[9] Both the NES and NZAAQG guidelines agrees with the guidelines set forth by the WHO.[1] Monitoring programs, set up and controlled by regional councils, are used to ensure adherence to these and other standards.

The chemical composition of PM is highly dependent on local sources, atmospheric processing, and prevailing meteorology.[3,10] These chemical compositions regionally and seasonally vary, as sources, meteorology, and atmospheric processes are all interdependent. In urban areas, PM is primarily influence by motor vehicle and industrial

combustion emissions, where as remote ocean and continental areas are influenced by natural emissions, such as sea spray or wind-blown dust. Dimethyl sulfide (DMS), produced by marine phytoplankton, is a greater contributor to marine PM during the summer relative to winter, when DMS production is at a minimum. This may influence PM in coastal communities predisposed to marine air masses. Seasonal shifts in temperature and solar radiation can influence atmospheric conditions and alter chemical reaction rates that generate particulate matter, irrespective of gaseous precursors, and must also be considered when assessing causes of changing PM concentrations. Analysis of the chemical composition of PM provides insight into PM sources, which is important for gauging air quality, identifying emission issues and creating mitigation strategies. In this study, PM samples collected in Whangarei, New Zealand were analyzed for chemical and isotopic compositions and utilized to evaluate local PM sources and decipher local and regional atmospheric influences that lead to the formation of PM.

5.2 Sampling Site

The Whangarei District is located near the top of the north island of New Zealand (Figure 5.1). The district has population of 85,900[11] sprawled over 2,852 km^2.[12] The city of Whangarei is the largest city in the district containing 57% of district's population. Whangarei has a sub-tropical climate, with an average annual temperature of approximately 15°C (59°F). Summers are hot and humid summers, with occasional summer cyclones, and winters are mild. The district is positioned at one of the narrowest

Figure 5.1: Location of the Whangarei, New Zealand sampling site

points on New Zealand with only 53 km separating the Tasman Sea from Bream Bay. The interior of the region is hill country, with scoria cone volcanoes scattered across the Northland region, although no elevations in the region exceed 800 m.[13] Whangarei sits between two hilly regions to the northeast and northwest with the Whangarei Harbor forming the southeastern border.

Sampling was conducted on the roof of the Northland Regional Council Building on Water Street in Whangarei. Land use north, south, and southwest of the sampling location is primarily residential and has several main roads (State Highways 1 and 14). An industrial park occupies areas to the southeast and east of the sampler, and the Whangarei Airport is 6 km to the east-southeast of the sampler. A shopping district and marina lie to

the northeast and Whangarei Harbor lies to the southeast of the sampling site. Smaller residential areas lie to the northwest and west, which back up to the distant hills and the Coronation Scenic Reserve and Pukenui Forest.

5.2.1 Materials and Sampling Conditions

A high volume sampler with a PM_{10} inlet was installed on the roof of the Northland Regional Council Building in September 2004. Aerosol samples were collected for 24 hours on a 1-in-6-day basis using glass fiber filters and a flow rate of 70 m^3/hr. Following sampling, PM_{10} mass was determined using gravimetric analysis by the Northland Regional Council. Filters were weighed pre- and post-sampling to determine the amount of PM collected, and evaluated for compliance with NES. Sampling was conducted from late September 2004 through early January 2012, but this work will focus analysis on samples collected throughout 2010 and 2011.

5.3 Analysis Methods

5.3.1 Black Carbon

Black carbon (BC) concentrations were determined by GNS Science using M43D Digital Smoke Stain Reflectometer. Filters are placed over light source, and the amount of light absorbed by the BC on the filter is measured. The amount of light absorbed is proportional to the amount of BC on the filter. Samples are measured with respect to

standards, which were created by collecting acetylene soot on the filters, with standard BC mass determined gravimetrically.

5.3.2 Ion Chromatography

Five 47 mm filter punches were cut out of each filter and dissolved in 14 mL of deionized water in 15 mL centrifuge tubes. Solids were removed from the aerosol solution using a Durapore® Membrane Filter (0.22 μm pore size, EMD Millipore). A ½ mL of the filtered aerosol solution was diluted to 10 mL for anion analysis. Anion concentrations (Cl^-, NO_3^-, and SO_4^{2-}) were determined by ion chromatography, using 5 mL of diluted aerosol solution, a Dionex IonPac AG11 guard column, a Dionex IonPac AS11 analytical column, and 2.0 mM $NaHCO_3/Na_2CO3$ eluent. A self-regenerating suppressor (Dionex ASRS 300) reduces the conductivity of the eluent prior to analysis by the conductivity detector (Dionex CD20). Standards of known NO_3^-, SO_4^{2-}, and Cl^- concentrations were used to calibrate the IC and determine sample concentrations.

5.3.3 X-ray Fluorescence

Elemental analysis was conducted using X-Ray Fluorescence (XRF; Panalytical Epsilon 5) at GNS Science. Analysis was conducted using EPA Method IO-3.3 (June 1999). The XRF at GNS Science uses a 100 kV Sc/W X-Ray tube, allowing for the analysis of elements from Na to U. Emitted x-rays are detected using a high performance Ge detector. Calibration standards for each element of interest were used to determine concentrations, and a NIST reference standard was utilized to verify results.

5.3.4 Stable Isotope Analysis

Another 5-mL portion of the aerosol solution was analyzed to determine the nitrate isotope composition ($\delta^{15}N$ and $\Delta^{17}O$). Samples were injected into a 12 mL vial containing a denitrifying strain of bacteria (*P. Aureofaciens*),[14–16] which converts nitrate in the sample into nitrous oxide (N_2O). N_2O is then extracted from the headspace, purified, and analyzed for the $\delta^{15}N$ and $\delta^{18}O$ values using a Thermo Delta V Isotope Ratio Mass Spectrometer.[14–16] Isotope values are reported in parts per thousand (or per mil, ‰) relative to an isotope standard (air N_2 for $\delta^{15}N$ and Vienna Standard Mean Ocean Water (VSMOW) for $\delta^{17}O$, $\delta^{18}O$, and $\Delta^{17}O$) as follows:

$$\delta(‰) = \left(\frac{R_{sample}}{R_{standard}} - 1 \right) \times 1000 \qquad \text{(Eq. 1)}$$

Working lab standards, of known isotopic composition, were used to account for isotopic fractionation during bacteria denitrification and N_2O purification. The working standards had an average standard deviation of 0.5‰ and 1.0‰ for $\delta^{15}N$ and $\Delta^{17}O$, respectfully.

Meteorological data was obtained from The National Climate Database, a database that provides raw data from climate stations in New Zealand.[17] CliFlo, the web system that provides access to The National Climate Database, is maintained by New Zealand's National Institute of Water and Atmospheric Research (NIWA).

5.4 Results and Discussion

PM concentrations (Figure 5.2) are highly seasonal, with highs in the winter (June, July, and August) and lows during the summer (December, January, and February), opposite the trend observed in the daily average temperature. This same trend is also

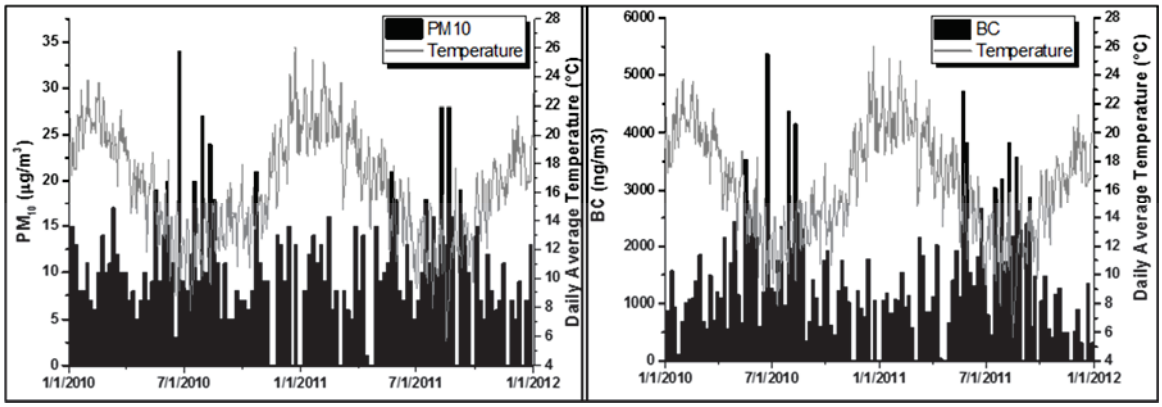

Figure 5.2: PM_{10} (left) and BC (right) concentrations and daily average temperatures for Whangarei, New Zealand

observed in the BC concentration (Figure 5.2). It is also worth noting that BC makes up a large portion of the PM mass, and so the overall PM trend is heavily dependent on the BC trend. BC is produced as consequence of combustion processes, such as motor vehicles, industrial activities, motor vehicle usage, wildfires, and residential heating using wood burning stoves. As motor vehicle and industrial emissions do not vary significantly throughout the year, the increase in BC in the winter is due to an increase in residential heating activities. This is consistent with increases in PM that have been observed in other biomass burning studies.[4,18,19]

Changes in the concentrations of PM and trace gases are also dependent changes on the boundary layer height (BLH), which impacts the effectiveness of vertical mixing and transport of atmospheric gases and pollutants. BLH varies diurnally and seasonally due to changes in solar radiation, humidity, and temperature, leading to lower heights in the winter and at night.[20] The lower the height, the less space for pollutants and trace gases to diffuse through, thus influencing mixing, chemistry, and deposition rates.[21] In the summer, a higher boundary layer (approximately 430 m on average) would allow emissions to mix

further from their sources, effectively diluting concentrations measured at the surface. Conversely, in the winter when the boundary layer is low (approximately 170 m on average), source emissions are held closer to the surface resulting in the observed increase in concentrations.

Boundary layer height has very little effect on the concentrations of particles transported to the region, such as sea salt aerosol. Sea salt aerosols are emitted from the surface of the ocean and then carried with the marine air mass. Unlike local emissions, the concentration of transported species is determined by how far the air mass has traveled, how much removal has occurred, and conditions that influence emission, such as wind speed. Chloride, the primary component of seawater (55.04% by weight), showed no clear seasonal trend during the sampling campaign. This is to be expected, as Whangarei is a coastal city on a narrow portion of the North Island and heavily influenced by the marine air masses. However, variations in Cl^- ion concentration are likely due to the trajectory of the air masses arriving at the sampling site. Air masses arriving from the north and west have traveled across the island, allowing time for deposition to remove Cl^- from the air mass.[22] Conversely, air masses arriving from the south and east are of oceanic origins, thus lacking the time for removal of sea salt aerosols from the air mass.

K^+ ion concentration (Figure 5.3) also shows a slight seasonal trend, with concentrations peaking slightly in the winter before falling to summer lows. However, this seasonal trend is much less pronounced than BC and PM_{10}. K is commonly applied as a secondary tracer of biomass burning, and specifically wood burning.[4] However, sea salt and soil emissions also contribute to K^+ ion concentration, as K is a significant component

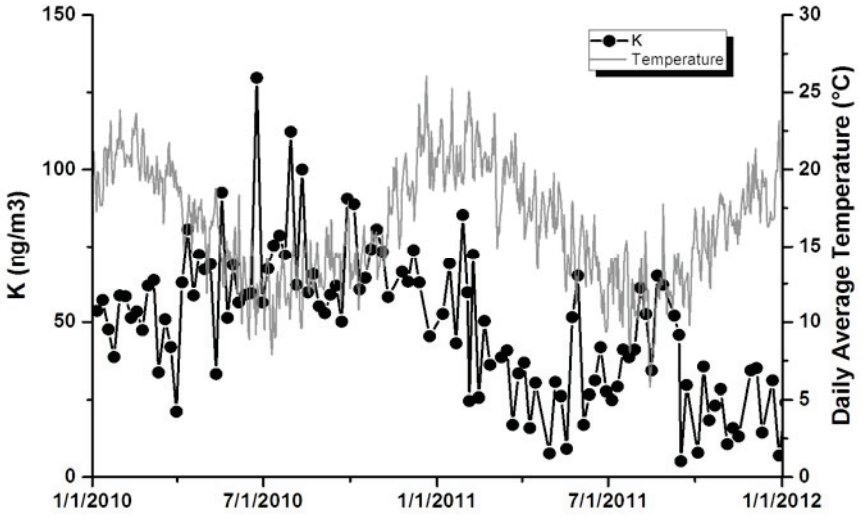

Figure 5.3: Daily average K^+ concentration and temperature for Whangarei, New Zealand

of crustal matter (2.95% by mass) and sea water (1.1% by weight).[10] As Whangarei is a coastal community, sea salt input should vary little throughout the year, and soil contributions are variable and low in concentration.[4] Although the K^+ trend is muted, it does lend support towards residential heating activities and their influence on winter PM_{10}, due to the lack of seasonality in crustal and sea salt emissions.

Chlorine, the primary component of seawater (55.04% by weight), showed no clear seasonal trend. This is to be expected as Whangarei is a coastal city on a narrow portion of the North Island and heavily influenced by the marine air masses. However, when comparing Cl^- ion concentration to S concentration (Figure 5.4), as SO_4^{2-} is another significant component of seawater, it becomes apparent that despite the shared source, the trends do not correlate. Despite a few "event days" (days of unusually high concentration), S concentrations show a seasonal trend, with summer highs and winter lows. The

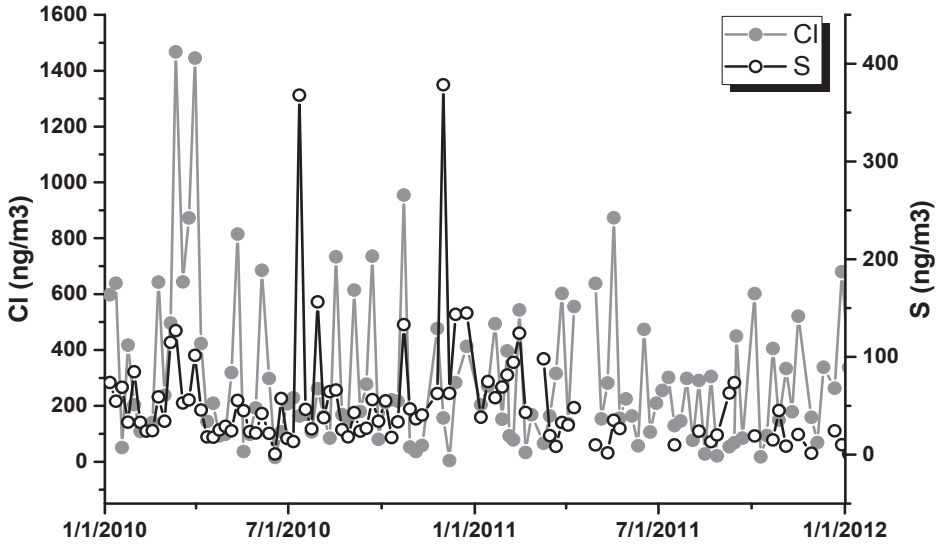

Figure 5.4: Cl and S concentrations for Whangarei, New Zealand.

consistency of Cl^- indicates that sea salt input is constant, but the seasonality of S suggests a non-sea salt input as well. Although marine aerosols are heavily influenced by sea salt aerosols, SO_2, formed as a byproduct of shipping emissions[23] or by oxidation of DMS emitted from phytoplankton,[24,25] is also a significant contributor of S to marine aerosols. SO_4^{2-} resulting for sources other than sea salt, or non-sea salt SO_4^{2-}, can be highly seasonal, as DMS emissions tend to peak in the summer with minimal productivity observed in the winter. Additionally, recent work by Dominguez et al.[23] has reveal that SO_2 emitted from ship exhaust may be rapidly removed from the atmosphere by coarse sea salt aerosols, which undergo deposition quicker than fine aerosols. Whangarei ports account for 28% of New Zealand imports, and is the largest port by volume. Therefore, shipping SO_2 is likely a significant contributor of non-sea salt SO_4^{2-} (nss-SO_4^{2-}), and likely responsible for two S event days during the sampling period.

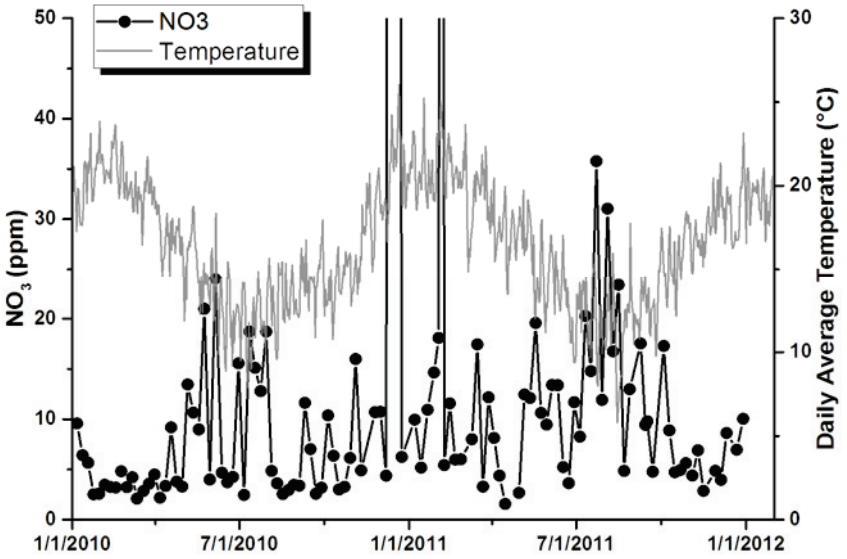

Figure 5.5: Nitrate concentrations and daily average temperatures for Whangarei, New Zealand.

Nitrate concentrations (Figure 5.5) during the sampling period show a similar trend to PM_{10} and BC, with winter maximums and summer minimums. The lower winter temperatures favor the particulate phase over the vapor phase, leading to an increase in NO_3^- concentrations.[10] The boundary layer height is also lower in the winter, which prevents vertical mixing of NOx and its subsequent oxidation resulting in higher NO_3^- concentrations. Additionally, winter residential heating activities (wood burning) may also contribute additional NOx emissions,[26] further enhancing NO_3^- concentrations. NO_3^- is the final product of NOx oxidation, which is a byproduct of combustion processes. Nitrate formation can occur via several different reactions in the atmosphere, depending on the oxidants, surfaces, and amount of solar radiation available.

$$NO + O_3 \rightarrow NO_2 + O_2 \quad \text{(R1)}$$

$$NO_2 + OH + M \rightarrow HNO_3 + M \quad \text{(R2)}$$

$$NO_2 + O_3 \rightarrow NO_3 + O_2 \quad \text{(R3)}$$

$$NO + RO_2 \xrightarrow{[O_2]} NO_2 + RO \quad \text{(R4)}$$

$$NO_2 + NO_3 \leftrightarrow N_2O_5 \quad \text{(R5)}$$

$$N_2O_5 + H_2O + surface \rightarrow 2HNO_3 \quad \text{(R6)}$$

$$NO_3 + VOC \rightarrow HNO_3 + R \quad \text{(R7)}$$

The N_2O_5 pathway is of greater importance to NO_3^- formation at night and in the winter, when temperatures and the amount of sunlight is as at a minimum, thus making N_2O_5 more stable and likely to hydrolyze on aerosol surfaces.[27,28] Oxidation of NO_2 by the OH radical is of greater importance during the summer, when days are long and temperatures are higher, which favors vapor phase reactions. Hydrogen abstraction from VOCs is a minor pathway, but can be regionally important in areas with high VOC concentrations.[29]

Analysis of the nitrate isotopes ($\delta^{15}N$ and $\Delta^{17}O$) was conducted to further understand the Whangarei NOx chemistry (Figure 5.6). Stable isotopes of N and O are commonly employed as tracers of source emissions and chemical reactions that occur in the environment. Although oxygen isotopes ($\delta^{17}O$, $\delta^{18}O$, and $\Delta^{17}O$) are accepted as tracers of oxidations pathways,[30] the use of N isotopes as a tracer is less unanimous, with parties being split between its use as a tracer of sources[31–35] and a tracer of chemistry[30,36,37]. Advocates of the source hypothesis argue that once emitted, the N atom is conserved

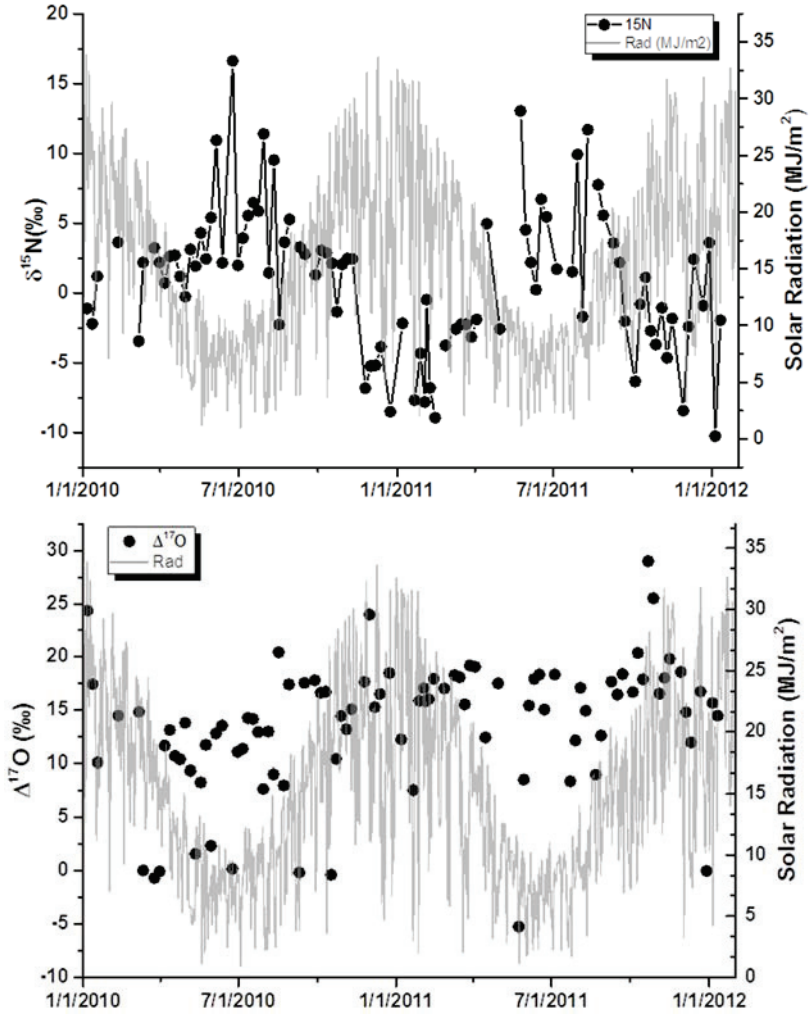

Figure 5.6: $\delta^{15}N$ (top) and $\Delta^{17}O$ (bottom) for NO_3^- collected in Whangarei, New Zealand

regardless of any physical process or chemical reaction.[31,35,38] Therefore, the $\delta^{15}N$ value of the source NOx would also be the $\delta^{15}N$ value of the NO_3^-. The chemistry hypothesis argues that $\delta^{15}N$ values are a combination of source $\delta^{15}N$ values, atmospheric transformations or reactions, and post-deposition effects (chemical reactions, biological processing).[30,36,37] Despite the controversy, isotopes of NO_3^- do provide important details about local atmospheric chemistry.

The $\delta^{15}N$ values of NO_3^- (hereafter referred to as $\delta^{15}N_{NO3}$) showed a seasonal trend, with enrichment peaking in the winter when solar radiation is at a minimum. Recent work on NOx equilibrium exchange has found that the $\delta^{15}N$ value of NO_2 (hereafter referred to as $\delta^{15}N_{NO2}$) shows enrichment during the winter, when temperatures and the amount of incoming solar radiation are low and the mole fraction of NO_2 (f_{NO2} = mole fraction of NOx as NO_2) is also low.[39] During the daytime, the Leighton Cycle controls the NO and NO_2 concentrations:

$$NO + O_3 \rightarrow NO_2 + O_2 \qquad \text{(R8)}$$

$$NO_2 + h\upsilon \rightarrow NO + O(^3P) \qquad \text{(R9)}$$

$$O(^3P) + O_2 + M \rightarrow O_3 + M \qquad \text{(R10)}$$

In general, f_{NO2} decreases with increasing amount of solar radiation, leading to larger fractions at night and in the winter. The $\delta^{15}N_{NO2}$ values are determined by f_{NO2} and an isotope exchange equilibrium first suggested by Freyer:[36]

$$^{15}NO + {}^{14}NO_2 \leftrightarrow {}^{14}NO + {}^{15}NO_2 \qquad \text{(R11)}$$

At night, photolysis and the isotope exchange cease, all NOx exists in the form of NO_2 ($f_{NO2} = 1$), and $\delta^{15}N_{NO2}$ equals the $\delta^{15}N$ value of the NOx source. During the day, NO and NO_2 undergo isotope exchange equilibrium, with ^{15}N accumulating in the more oxidized form (NO_2).[36,37] As NO_2 is ultimately oxidized to NO_3^- and the $\delta^{15}N_{NO3}$ seasonal trend tends to correlate with seasonal variations in temperature and solar radiation, this equilibrium would contribute to the seasonal $\delta^{15}N_{NO3}$ trend, lending support to the chemistry tracer hypothesis.

Analysis of the oxygen isotopes ($\Delta^{17}O$) also revealed significant non-zero values. Majority of the samples had $\Delta^{17}O$ values of 10-15‰, with no clear seasonal trend apparent. However, there were a handful of sampling days during this two-year period that had much lower $\Delta^{17}O$ values, in the 0-5% range. As oxygen isotopes reflect the oxidation pathway(s) used, it can be concluded that O_3 plays a prominent role in oxidation chemistry in this area. Previous studies[25,40–42] have noted that sea salt particles, particularly those originating from the Southern Ocean, contain alkalinity in excess of bulk seawater. Heterogeneous oxidation pathways are pH dependent, and this excess acts to buffer the aerosol at a pH > 6, thus promoting O_3 oxidation. The low $\Delta^{17}O$ values were likely the result of contributions from air masses lacking the necessary buffering for O_3 oxidation, thus promoting gas phase oxidation by OH radicals, or heterogeneous oxidation by H_2O_2. The dominance of O_3 oxidation throughout the year further emphasizes the impact that marine air masses have on local chemistry.

5.5 Conclusions

Particulate matter is influenced by both natural and anthropogenic sources, as well as local atmospheric chemistry and meteorological conditions. Due to its coastal location, Whangarei Cl^- concentrations varied very little throughout the year, indicating that sea salt input was influenced by the trajectory of the marine air masses arriving at the site. Sulfur concentrations, however, did reveal a seasonal trend, with concentrations peaking during the summer months. This indicates the presence of a significant non-sea salt S source, likely DMS produced by marine phytoplankton or a greater contribution of SO_2 from shipping emissions. Potassium shows a slight seasonal trend, which is likely dampened due

to a mixing of sources (natural sea salt and anthropogenic combustion sources). Black carbon shows as seasonal trend, with concentrations peaking in the winter months, due to residential heating applications. BC was also found to contribute the greatest proportion to the overall PM_{10} mass, therefore the PM_{10} seasonal trend echoes that of BC.

Nitrate concentrations also showed seasonality, peaking in the winter when the boundary layer height is at a minimum. NO_3^- concentrations were also found to be pathway dependent, as NOx sources (motor vehicles, industrial processes) vary very little throughout the year. Additionally, the lower temperatures and lesser amounts of solar radiation during the winter promotes NO_3^- formation via N_2O_5. Nitrate isotope analysis revealed a seasonal trend in $\delta^{15}N$ values, with higher $\delta^{15}N$ values during the winter when solar radiation is at a minimum. $\Delta^{17}O$ values were found to be primarily in the 10-15‰ range, indicating that O_3 oxidation is important in this area. Only a handful of samples were found to have low $\Delta^{17}O$ values (0-5‰), which was likely the result of a shift in oxidation pathway, likely brought about by an "event" (precipitation, wind shift).

5.6 References

(1) *Ambient (outdoor) air quality and health*; World Health Organization, 2014.

(2) Dockery, D. W.; Pope, C. A.; Xu, X.; Spengler, J. D.; Ware, J. H.; Fay, M. E.; Ferris, B. G.; Speizer, F. E. *N. Engl. J. Med.* **1993**, *329*, 1753–1759.

(3) Katzman, T. L.; Rutter, A. P.; Schauer, J. J.; Lough, G. C.; Kolb, C. J.; Van Klooster, S. *Aerosol Air Qual. Res.* **2010**, *10*, 140–U13.

(4) Ancelet, T.; Davy, P. K.; Mitchell, T.; Trompetter, W. J.; Markwitz, A.; Weatherburn, D. C. *Environ. Sci. Technol.* **2012**, *46*, 4767–4774.

(5) Pope, C. A.; Rodermund, D. L.; Gee, M. M. *Environ. Health Perspect.* **2007**, *115*, 679–683.

(6) Pope, C. A. *Inhal. Toxicol.* **2007**, *19 Suppl 1*, 33–38.

(7) Nel, A.; Dockery, D. W.; Samet, J. M.; Brook, R. D.; Donaldson, K.; Tran, C. L.; Oberdörster, G.; Utell, M. J.; Nel, A. E.; Ghio, A. J.; Devlin, R. B.; Muranaka, M.; Gurgueira, S. A.; Lim, H. B.; Xiao, G. G.; Li, N.; Silbajoris, R.; Li, N.; Gilliland, F. D.; Nemmar, A. *Science* **2005**, *308*, 804–806.

(8) Russell, A. G.; Brunekreef, B. *Environ. Sci. Technol.* **2009**, *43*, 4620–4625.

(9) Davy, P. K.; Ancelet, T. *Air Particulate Matter Composition, Sources, and Trends in the Whangarei Airshed*; 2014.

(10) Seinfeld, J. H.; Pandis, S. N. *Atmospheric Chemistry and Physics: From Air Pollution to Climate Change, 2nd Edition* -; 2nd ed.; 2006.

(11) *Subnational population estimates (RC, constituency), by age and sex, at 30 June 2013-15 (2015 boundaries)*.

(12) District Council, W. **2013**.

(13) About Whangarei http://whangareinz.com/about.

(14) K. L. Casciotti M. Galanter Hastings, J. K. Bo1 hlke, and A. Hilkert, D. M. S. *Anal. Chem.* **2002**, 4905–4912.

(15) D. M. Sigman K. L. Casciotti, M. Andreani, C. Barford,M. Galanter, and J. K. Bolhlke. *Anal. Chem.* **2001**, 4145–4153.

(16) Kaiser, J.; Hastings, M. G.; Houlton, B. Z.; Röckmann, T.; Sigman, D. M. *Anal. Chem.* **2007**, *79*, 599–607.

(17) The National Climate Database.

(18) Grange, S. K. K.; Salmond, J. A. A.; Trompetter, W. J. J.; Davy, P. K. K.; Ancelet, T. *Atmos. Environ.* **2013**, *70*, 28–38.

(19) Trompetter, W. J. J.; Grange, S. K. K.; Davy, P. K. K.; Ancelet, T. *Atmos. Environ.* **2013**, *75*, 179–187.

(20) Coulter, R. L. *J. Appl. Meteorol.* **1979**, *18*, 1495–1499.

(21) Sillman, S. *Atmos. Environ.* **1999**, *33*, 1821–1845.

(22) Wang, H.; Shooter, D. *Atmos. Environ.* **2001**, *35*, 6031–6040.

(23) Dominguez, G.; Jackson, T.; Brothers, L.; Barnett, B.; Nguyen, B.; Thiemens, M. H. *Proc. Natl. Acad. Sci. U. S. A.* **2008**.

(24) Charlson, R. J.; Lovelock, J. E.; Andreae, M. O.; Warren, S. G. *Nature* **1987**, *326*, 655–661.

(25) Sievering, H.; Cainey, J.; Harvey, M.; McGregor, J.; Nichol, S.; Quinn, P. *J. Geophys. Res.* **2004**, *109*.

(26) Cai, C.; Kulkarni, S.; Zhao, Z.; Kaduwela, A. P.; Avise, J. C.; DaMassa, J. A.; Singh, H. B.; Weinheimer, A. J.; Cohen, R. C.; Diskin, G. S.; Wennberg, P.; Dibb, J. E.; Huey, G.; Wisthaler, A.; Jimenez, J. L.; Cubison, M. J. *Atmos. Environ.* **2016**, *128*, 28–44.

(27) Geyer, A.; Ackermann, R.; Dubois, R.; Lohrmann, B.; Müller, T.; Platt, U. *Atmos. Environ.* **2001**, *35*, 3619–3631.

(28) Riemer, N. *J. Geophys. Res.* **2003**, *108*, 4144.

(29) Gobel, A. R.; Altieri, K. E.; Peters, A. J.; Hastings, M. G.; Sigman, D. M. *Geophys. Res. Lett.* **2013**.

(30) Hastings, M. G. *IOP Conf. Ser. Earth Environ. Sci.* **2010**, *9*, 012002.

(31) Elliott, E. M.; Kendall, C.; Wankel, S. D.; Burns, D. A.; Boyer, E. W.; Harlin, K.; Bain, D. J.; Butler, T. J. *Environ. Sci. Technol.* **2007**, *41*, 7661–7667.

(32) Felix, J. D.; Elliott, E. M.; Shaw, S. L. *Environ. Sci. Technol.* **2012**, *46*, 3528–3535.

(33) Hastings, M. G. *J. Geophys. Res.* **2004**, *109*, D20306.

(34) Hastings, M. G.; Sigman, D. M.; Lipschultz, F. *J. Geophys. Res. Atmos.* **2003**, *108*, n/a – n/a.

(35) Morin, S.; Savarino, J.; Frey, M. M.; Yan, N.; Bekki, S.; Bottenheim, J. W.; Martins, J. M. F. *Science (80-.).* **2008**, *322*, 730–732.

(36) Freyer, H. D. *Tellus* **1991**, 30–44.

(37) Freyer, H. D.; Kley, D.; Volz-Thomas, A.; Kobel, K. *J. Geophys. Res.* **1993**, *98*, 14791.

(38) Elliott, E. M.; Kendall, C.; Boyer, E. W.; Burns, D. A.; Lear, G. G.; Golden, H. E.; Harlin, K.; Bytnerowicz, A.; Butler, T. J.; Glatz, R. *J. Geophys. Res.* **2009**, *114*, G04020.

(39) Walters, W. W.; Simonini, D. S.; Michalski, G. *Geophys. Res. Lett.* **2016**, *43*, 440–448.

(40) Alexander, B.; Park, R. J.; Jacob, D. J.; Li, Q. B.; Yantosca, R. M.; Savarino, J.; Lee, C. C. W.; Thiemens, M. H. *J. Geophys. Res.* **2005**, *110*.

(41) Gurciullo, C.; Lerner, B.; Sievering, H.; Pandis, S. N. *J. Geophys. Res.* **1999**, *104*, 21719–21731.

(42) Sievering, H.; Lerner, B.; Slavich, J.; Anderson, J.; Posfai, M.; Cainey, J. *J. Geophys. Res.* **1999**, *104*, 21707–21717.

CHAPTER 6: CONCLUSIONS

The research laid out in this dissertation focused how reactions, particularly those occurring in the atmosphere, influence the isotope composition of nitrogen and oxygen. Isotope of oxygen were utilized in order to decipher the $2NO + O_2$ reaction mechanism, which has been suggested to proceed through three possible mechanisms: a termolecular collision, formation of a NO_2 dimer, and the formation of a NO_3 intermediate. Laboratory studies found that the residual O_2 became depleted as a result of this reaction, indicating that the heavy oxygen isotopes are preferentially incorporated by the NO_2 produced, also known as an inverse isotope effect. The presence of the inverse isotope effect indicated that the mechanism proceeds through two steps, eliminating the termolecular mechanism. The fractionation observed in the O isotopes also eliminated the NO_2 dimer possibility, as O_2 does not participate in the equilibrium step. The NO_3 intermediates have been proposed: nitrogen trioxide and peroxynitrate. Since laboratory studies revealed that the O_2 was depleted in a mass dependent manner, the intermediate was determined to be peroxynitrate, due to its asymmetrical nature. This result is significantly different from previous studies, which tend to favor the more energetically stable nitrogen trioxide form.

The nitrogen stable isotope composition ($\delta^{15}N$) is frequently used as a tracer, but the manner is a subject of debate. Proponents of the source hypothesis argue that $\delta^{15}N$ reflects source contributions which is conserved during subsequent chemical and physical

reactions (oxidation, phase changes). Conversely, supporters of the chemistry hypothesis contend that $\delta^{15}N$ values are impacted by both source contributions and fractionation arising during chemical or physical processing. $\delta^{15}N$ values of NO_3^- ($\delta^{15}N_{NO3}$) collected in Chula Vista, CA during 2007 and Whangarei, NZ during 2010- 2011, were found to be highly seasonal, peaking in the winters before falling to summer lows. The source hypothesis explains this seasonality as the result in seasonal shifts in source emissions, whereas the chemistry hypothesis attributes this to shifts in reaction pathway contributions caused by changes in temperature, photolysis, the amount of precipitation, and/or the availability of trace gases and particles.

The plausibility of the source hypothesis was evaluated using isotope mass balance, source emissions data, previously determined $\delta^{15}N$ values of NOx sources ($\delta^{15}N_{NOx}$), and $\delta^{15}N_{NO3}$ values observed in Chula Vista, CA. Based on source hypothesis claims, isotope mass balance would be able to replicate observed $\delta^{15}N_{NO3}$ values using source inputs and their associated $\delta^{15}N_{NOx}$ values. However, isotope mass balance was not able to replicated observed values, requiring the remaining unknown fraction (~5%) to contribute a highly positive $\delta^{15}N_{NOx}$ value (~280‰) in order to do so. As known sources are primarily negative (-5.9‰), this discrepancy firmly disputes the assumptions held by the source hypothesis and suggests that future work focus on how chemistry impacts $\delta^{15}N$.

At Whangarei, NZ the $\delta^{15}N_{NO3}$ value was found to be inversely related to the amount of available solar radiation. The amount of incoming solar radiation is low in the winter when days are short, and peaks during the summer. Conversely, $\delta^{15}N_{NO3}$ values are peak in the winter and with summer lows. As numerous NOx reaction pathways are dependent on photolysis, this inverse relationship is attributed to increased contributions

of these pathways in the summer months. Using hourly NOx concentration measurements and $\delta^{15}N_{NOx}$ values from Chula Vista, NO_2 $\delta^{15}N$ values ($\delta^{15}N_{NO2}$) were calculated to quantify how the isotope exchange equilibrium between NO and NO_2 impacts observed $\delta^{15}N_{NO3}$ values. This exchange was found to produce the same seasonal trend observed in NO_3^-, and even explained many observed $\delta^{15}N_{NO3}$ values. However, discrepancies between predicted $\delta^{15}N_{NO2}$ values and observed $\delta^{15}N_{NO3}$ values, particularly in the winter months. These discrepancies are due to two reasons: shifts in the contribution of this exchange (only important when both NO and NO_2 are present) and contributions from other reaction pathways (oxidation, removal). Since the concentration of NO is dependent on photolysis, isotope exchange equilibrium is only significant during daylight hours, and thus contributes less during the winter when days are short. Contributions from other reaction pathways can further enrich or deplete $\delta^{15}N$ values of the NO_3^- produced. NOx removal processes, NO_2 + OH and the formation of N_2O_5 in particular have both been shown to enrich the NO_3^- produced.

As NOx sources essentially set a base $\delta^{15}N$, further studies should address unknown NOx sources. Additionally, although isotope effects associated with several reactions in the NOx cycle have been determined, many still need to be determined. Previous studies into isotope effects in the NO_x cycle have focused on the major reactions (OH and O_3 oxidation, Leighton cycle), but reactions influenced by VOCs still need to be studied. Future work needs to address uncharacterized reactions, particularly those influenced by VOCs, as well as any additional exchange processes that may occur in the atmosphere.

APPENDICES

Appendix A: Investigating Sulfur Sources And Oxidation Chemistry In Sulfate Aerosol Production In The Southern Ocean And New Zealand Mainland

This appendix summarizes on-going sampling work, to be completed Summer 2016. This appendix presents the project background, sampling plan, and proposed analyses. This work is part of a collaboration with New Zealand's GNS Science and NIWA.

A.1 Introduction

Sulfate aerosols are a critical part of climate change, the hydrologic cycle, and have significant human health impacts,[1–5] yet we do not completely understand the sources of S,[5,6] nor how it is oxidized into sulfate in the atmosphere.[2,7,8] I propose to assess the sources of atmospheric sulfur emitted from the Southern Ocean and New Zealand, and evaluate the oxidation pathways that convert it into sulfate. This was accomplished by collecting size segregated aerosols at Baring Head, NZ which were analyzed using stable isotopes ($\Delta^{17}O$ and $\delta^{34}S$), elemental (XRF), gravimetric analysis, and geochemistry. This study compliments my current research on the origin of sulfate aerosols collected at Whangarei, New Zealand, a collaborative project with the Institute of Geological and Nuclear Science (GNS) of New Zealand. Since many Baring Head aerosols are of pristine marine origin and Whangarei aerosols are influenced by urban emissions, shipping, and volcanism, a comparison of the two sites will give insight into the relative importance of S sources (e.g.

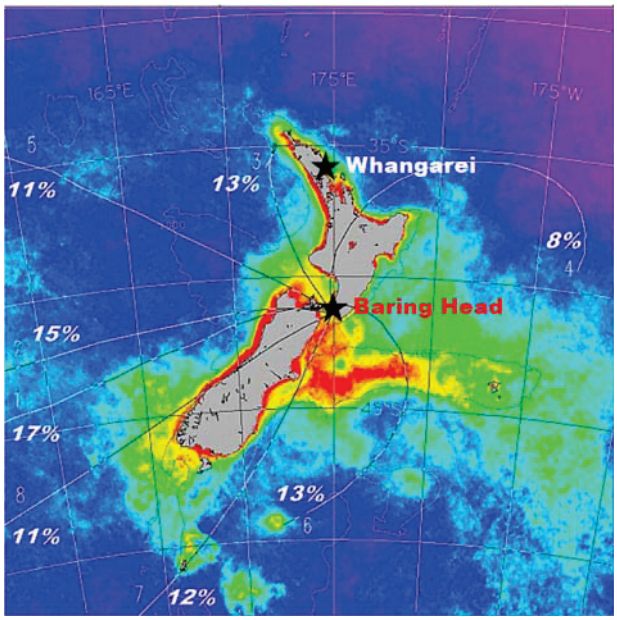

Figure A.1: New Zealand aerosol sampling locations. Warmer colors indicate areas of high biological productivity and DMS fluxes. The 8 most common back trajectories from Baring Head (% occurrences) indicate shifts in terrestrial and oceanic SO_4^{2-} loading. Modified from Sievering et al., 2004.

DMS at Baring Head; anthropogenic SO_2 at Whangarei) and oxidation pathways (e.g. aqueous oxidation at Baring Head; gas phase at Whangarei). The unique sampling location and analytical capability of GNS makes New Zealand an ideal location for studying S cycling.

Globally, 70% of S emissions are anthropogenic and the remainder is biogenic, which are spatially and temporally variable.[5,9] In contrast to the northern hemisphere, where ~90% of S is anthropogenic, biogenic emissions dominate (>50%) in the southern hemisphere.[9,10] Over half of this is thought to be dimethyl sulfide (DMS)[10] but there are considerable uncertainties in DMS fluxes due to highly variable environmental conditions such as wind speed and sea surface temperature.[5,6,11–13] While DMS is the main sulfur source over the entire southern hemisphere, anthropogenic and volcanic S can be regionally

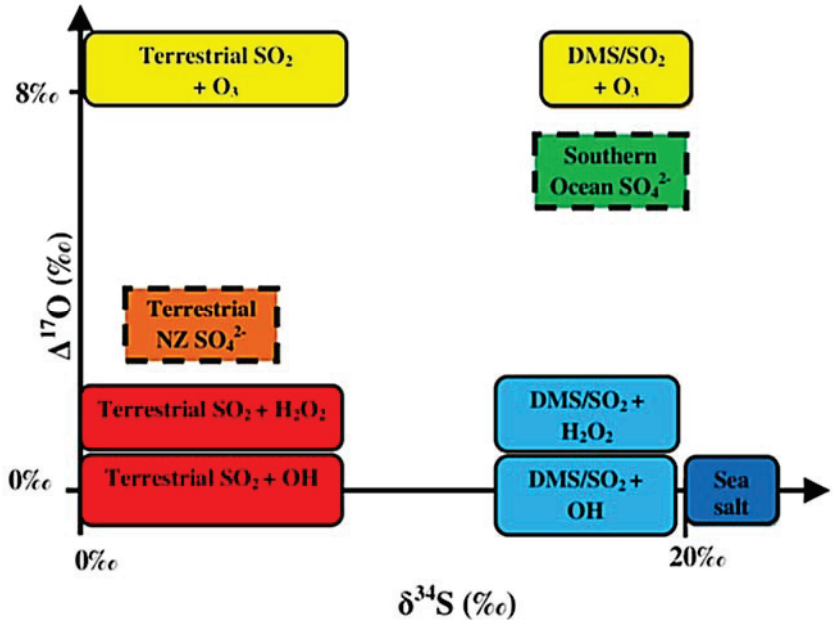

Figure A.2: $\Delta^{17}O$ vs. $\delta^{34}S$ in sulfate from different sources and oxidation pathways. Mass dependent fractionation follow $\delta^{17}O = 0.52 \times \delta^{18}O$ and produce $\Delta^{17}O \approx 0‰$. Mass independent fractionation follows $\Delta^{17}O = \delta^{17}O - 0.52 \times \delta^{18}O$, where $\Delta^{17}O > 0‰$. Terrestrial SO_4^{2-} should be isotopically distinct from Southern Ocean SO_4^{2-}. My working hypothesis suggests these two isotopic "end-members" (dashed boxes) will be found in aerosols with different air mass trajectories and in different aerosol sizes, or as mixture between the two end-members.

significant.[1,10] For example, in New Zealand annual terrestrial S emissions are estimated to be 350 kg S/km^2 and are comprised mainly of volcanism (20%), coal burning (41%) and petroleum sources (31%)[9] while average oceanic DMS fluxes are approximately 35kg S/km^2 but can be 3 times higher in high productivity regions (Figure A.1).[14] In order to understand regional sulfate aerosol production, one must be able to delineate between oceanic (sea salt), biologic (DMS), and terrestrial S sources, which is often complex.[15] Therefore, I propose to use stable sulfur isotope systematics to isolate the relevant proportion of DMS derived sulfate in aerosols collected along the New Zealand coast to better understand regional sulfur cycling in the southern hemisphere.

Stable sulfur isotopes are an elegant way of distinguishing between S sources in the biosphere (Figure A.2). Terrestrial sources, anthropogenic and natural, have low $\delta^{34}S$ typically between 0 and 10‰[16] and New Zealand volcanism varies between 2 and 4‰.[17] In contrast, oceanic sources have elevated $\delta^{34}S$; sea salt at 21‰ and DMS 15-18‰.[16,18] Therefore, it is possible to use S isotopes to evaluate non-sea salt S sources that form sulfate aerosols. Thus, I propose to measure $\delta^{34}S$ in size segregated sulfate aerosols collected at Baring Head and PM_{10} collected at Whangarei using the analytical capabilities at GNS (where sulfur isotope analysis was pioneered). The Whangarei analysis will be completed during EAPSI project period and submitted as a peer reviewed research paper exploring hemisphere variations in DMS emission and S cycling.

Sulfur emitted to the atmosphere is ultimately oxidized into SO_4^{2-}, but there are still uncertainties in the relative importance of various oxidation pathways.[10] Reduced S (i.e. DMS, MSA, and H_2S) is first oxidized into SO_2, then into SO_4^{2-}. In oceanic environments this non sea salt secondary SO_4^{2-} (nss-SO_4^{2-}) is distinguished from SO_4^{2-} in sea water (ss-SO_4^{2-}). The $SO_2 \rightarrow SO_4^{2-}$ step occurs via three major pathways: OH radicals in the gas phase and by H_2O_2 and O_3 in the aqueous phase. There are uncertainties in the importance of aqueous oxidation of SO_2 in coastal regions because the oxidation pathways are pH dependent[2,8,14] (Figure A.3) and alkalinity of sea salt aerosols is spatially variable.[2] Atmospheric models often use an average aerosol pH and this oxidation uncertainty may lead to an over/under prediction of sulfate production relative to the real atmosphere.[2] The pH dependence of sulfate production can be evaluated at Baring Head, where upwelling generates more alkaline aerosols[14] and may enhance aqueous O_3 oxidation of SO_2. Such an enhancement can be tested using oxygen isotopes in SO_4^{2-} aerosols.

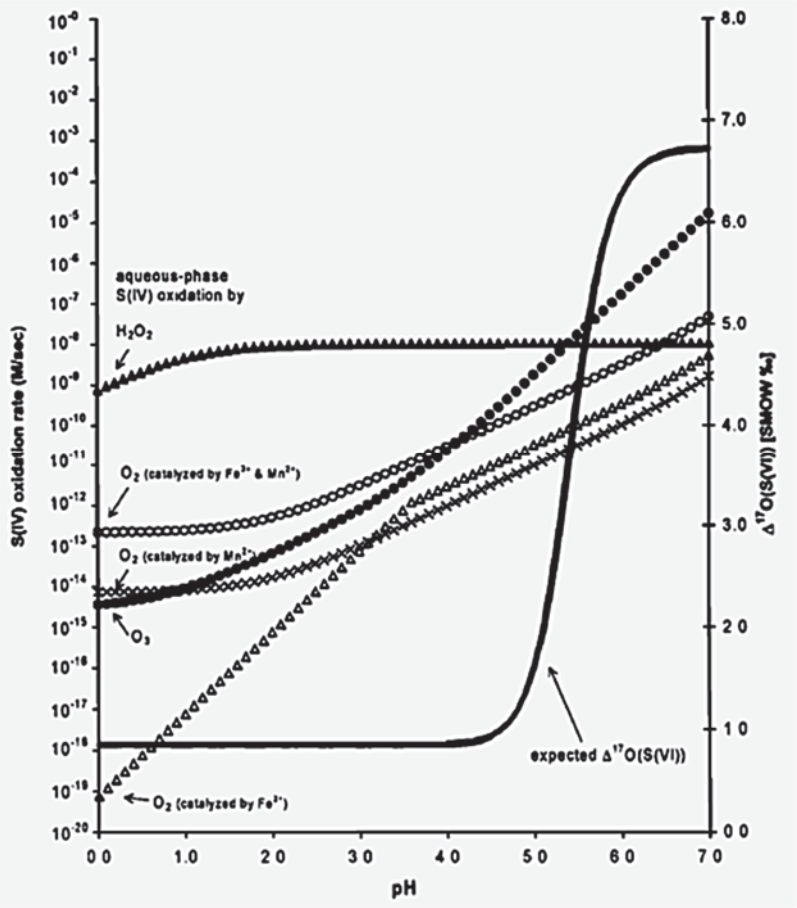

Figure A.3: pH dependent of SO_2 oxidation and its impact on the product SO_4^{2-} and $\Delta^{17}O$ value.[19]

Stable oxygen isotope analysis has the potential to provide insight into the oxidation pathways of the S cycle (Figure A.2). Oxygen has three stable isotopes (^{16}O, ^{17}O, and ^{18}O) which fractionate via mass dependent processes or via mass independent processes.[2,8,20,21] The only known oxidants to possess $\Delta^{17}O > 0‰$ are H_2O_2 (1.7‰) and O_3 (35‰) and these produce sulfate with positive $\Delta^{17}O$. In contrast, gas phase oxidation of SO_2 by OH produces SO_4^{2-} with $\Delta^{17}O = 0‰$. Additionally, SO_4^{2-} is incredibly stable and will resist isotopic exchange with water once formed.[18] Therefore, $\Delta^{17}O$ has been shown to be an effective

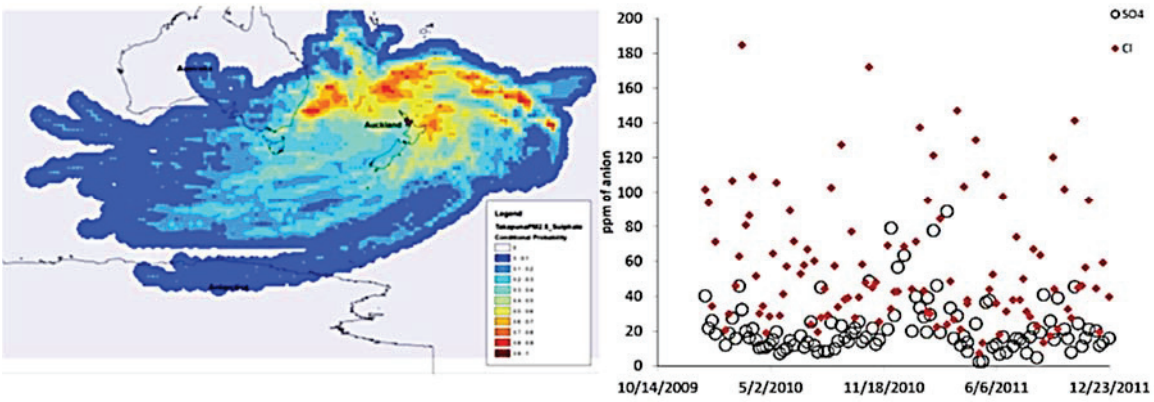

Figure A.4: Whangarei SO_4^{2-} concentrations (circles, right) peak in the summer, whereas Cl^- (red diamond) does not, indicating a large DMS flux rather than an increase in sea salt. Statistical analysis of HySplit back trajectories suggests secondary SO_4^{2-} in Whangarei (left) originates in the Tasman Sea or the western Pacific. Baring Head secondary SO_4^{2-} originates in the Southern Ocean, and allows for the comparison of regional S cycles (Subtropics vs. Southern Ocean).

tracer of aqueous phase oxidation of SO_2, in particular evaluating the importance of O_3 oxidation. I propose to measure $\Delta^{17}O$ in size segregated sulfate aerosols collected at Baring Head in order to evaluate how aerosol alkalinity impacts O_3 oxidation of SO_2 near New Zealand. This will be carried out post-EAPSI in the Purdue Stable Isotope Lab.

My working hypothesis is that S source and oxidation chemistry will uniquely manifest itself in different sized aerosols collected at Baring Head. Course aerosol particles (0.9-16 μm diameter) at Baring Head are 50% seas salt including excess biologic $CaCO_3$ making them alkaline.[14] The enhanced alkalinity would promote O_3 oxidation generating larger $\Delta^{17}O$ in course mode nss- SO_4^{2-} (course [nss- SO_4^{2-}] can be determined by using Mg^{2+} or Na^+). Conversely, in very fine particles (< 0.4 μm diameter) sea salt accounts for only 5% thus lacking sufficient buffering for O_3 oxidation and thus H_2O_2 or OH oxidation would be evident by a low nss-SO_4^{2-} $\Delta^{17}O$ values (Figure A.2). Sulfate in air masses

derived from pristine regions of the Southern Ocean (southeast) are hypothesized to be predominately a mixture of sea salt SO_4^{2-} and DMS derived SO_4^{2-}, which could be verified by elevated $\delta^{34}S$ values (Figure A.2). Further, summer DMS blooms should be observable in both nss-SO_4^{2-} and $\delta^{34}S$ values (Figure A.4). In contrast, 10% of air masses (north) arriving at Baring head will pass over NZ volcanic zones and urban centers and I hypothesize that terrestrial SO_2 will be the main sources of SO_4^{2-} during those periods, which would be verified by low $\delta^{34}S$ values. Since both sea salt aerosol and DMS flux increase with increasing wind speed I can further hypothesize that SO_4^{2-} and $\Delta^{17}O$ of nss-SO_4^{2-} will be positively correlated. Aerosols will be collected for twice a week for an entire year (based on collaborative support-pending), therefore I anticipate having a sufficient number of samples to assess the statistical significance of my hypothesis. This year long sampling will also allow me to assess both how the DMS contribution to the S budget and oxidation pathways vary with season (Figure A.4).

A.2 Site Description

Baring Head, NZ is a unique place to conduct this research for several reasons. First, the Baring Head Clean Air Monitoring Station has been in operation for more than 40 years, measuring greenhouse gases, other trace gases and related species in air that is representative of the mid latitude southern hemisphere. The air arriving at this site from the south has origins in the Southern Ocean and lacks anthropogenic influence.[14] Secondly, the site is a 20-minute drive from the GNS labs in Lower Hutt, NZ making it convenient for instrument set up, filter retrieval, and training of staff to do filter collection after I depart

Figure A.5: Baring Head Atmospheric Research Station at Baring Head Lighthouse.

from NZ. Finally, it is distant enough from my Whangarei site that contrast and compare analysis can be conducted. Specifically, air mass out of the northeast at Whangarei will reflect equatorial Pacific (Figure A.4), which is largely unperturbed by anthropogenic emissions, and when combined with the Baring Head data will likely yield powerful information about S cycling in the Southern Hemisphere. A high volume air sampler with a 6 stage size segregating impactor (slotted filters collecting 10-7.2 µm, 7.2-3.0 µm, 3.0-1.5 µm, 1.5-0.95 µm, 0.95-0.49 µm, and an 8x10" sheet filter collecting 0.49-0.05 µm) will be installed at Baring Head. The impactor will collect for 15-20 hours and filters will be changed based on air mass forecasting to isolate remote marine and terrestrial air masses.

A.3 Sampling Plan

The objective of this project is to collect size segregated aerosols at Baring Head in order to assess S sources and evaluate SO_4^{2-} oxidation pathways using stable isotope

Figure A.6: The 15 m tower located at Baring Head (left) will have one sampler at the top and one at the bottom. A previously installed Lear Siegler sampler with PM10 inlet at the top of the tower will sample only southerly events. A second sampler, installed at the base of the tower (right) during EAPSI, will continuously sample all air masses.

geochemistry ($\Delta^{17}O$ and $\delta^{34}S$). Two samplers were utilized, with one sampler set at the top of a 15 m tower for marine air mass sampling and the second set at the base to continuously sample all air masses. This year-long sampling campaign will illustrate seasonal shifts in sulfur sources and oxidation pathway changes. Additionally, this sampling program will create a robust data set that will provide new insight into the Southern Hemisphere S cycling, compliment modeling studies, and enhance our understanding of the impact sulfate aerosols have on climate change, the hydrological cycle, and human health.

A.4 Methods and Materials

Two Lear Siegler air samplers (PM_{10}) will be fitted with Tisch Environmental Inc. Cascade Impactors (TE-235) to collect size segregated aerosols. The impactor collection utilized the first and fourth plates of the impactor (0.95-10 μm and 0.49-0.95 μm) as well as the 8" x 10" back filter collecting ultra-fine aerosols fraction (0.05-0.49). A yearlong sampling period was used in order to measure seasonal variances in sources and oxidation pathways.

The second Lear Siegler sampler (PM_{10}) was installed at the base of the 15 m tower at Baring Head, to compliment the current Lear Siegler sampler and impactor installed by NIWA at the top of the tower. It should be noted that the both the sampler and impactor are of the same model. The sampler was fitted with previously weighed cellulose filters; slotted for stages 1 and 4 and an 8" x 10" for the ultra-fine. The filters for this sampler will collect for a week regardless of wind direction or air mass origin.

The sampler installed at the top of a 15 m tower sampled remote ocean derived air masses. The marine sampler only collected when southerly air flows were detected, and filters will be changed as necessary (dependent on season and exposure time) with date and filter designation logged. As with the continuous sampler, the sampler will be fitted with previously weighed cellulose filters; slotted for stages 1 and 4 and an 8" x 10" for ultra-fine. Each sample will contain approximately 40 hours of southerly events, which will likely contain multiple events due to low remote ocean S concentrations.

The sampler's flow rate was calibrated prior to use and a field blank was collected every 2 months. Lab blanks were collected at the beginning of the sampling period. Prior

to portioning or analysis, exposed filters were weighed to determine the mass of PM_{10} collected.

Sampling at Baring Head began in July 2015, and concluded in July 2016, with analysis to follow. Cellulose filters were selected to allow for isotope analysis of samples, as glass fiber filters are known to introduce a positive sulfate artifact.[22] Once collected, the filters were portioned for multiple analyses: NO_3^- isotopes ($\Delta^{17}O$ and $\delta^{15}N$) by IRMS, SO_4^{2-} isotopes ($\delta^{34}S$ and $\Delta\delta^{17}O$) by EA-IRMS, anion concentrations by ion chromatography, elemental analysis by XRF, and black carbon content. Determination of cation (ICP-OES) and ammonia (discrete analysis) concentrations and particle morphology (SEM) may also be conducted.

A.5 References

(1) Charlson, R. J.; Lovelock, J. E.; Andreae, M. O.; Warren, S. G. *Nature* **1987**, *326*, 655–661.

(2) Alexander, B.; Allman, D. J.; Amos, H. M.; Fairlie, T. D.; Dachs, J.; Hegg, D. A.; Sletten, R. S. *J. Geophys. Res.* **2012**, *117*.

(3) Calhoun, J. A.; Bates, T. S.; Charlson, R. J. *Geophys. Res. Lett.* **1991**, *18*, 1877–1880.

(4) Gray, B. A.; Wang, Y. H.; Gu, D. S.; Bandy, A.; Mauldin, L.; Clarke, A.; Alexander, B.; Davis, D. D. *J. Atmos. Chem.* **2011**, *68*, 27–53.

(5) Lana, A.; Bell, T. G.; Simo, R.; Vallina, S. M.; Ballabrera-Poy, J.; Kettle, A. J.; Dachs, J.; Bopp, L.; Saltzman, E. S.; Stefels, J.; Johnson, J. E.; Liss, P. S. *Global Biogeochem. Cycles* **2011**, *25*.

(6) Faloona, I. *Atmos. Environ.* **2009**, *43*, 2841–2854.

(7) Alexander, B.; Park, R. J.; Jacob, D. J.; Gong, S. L. *J. Geophys. Res.* **2009**, *114*.

(8) Alexander, B.; Park, R. J.; Jacob, D. J.; Li, Q. B.; Yantosca, R. M.; Savarino, J.; Lee, C. C. W.; Thiemens, M. H. *J. Geophys. Res.* **2005**, *110*.

(9) Spiro, P. A.; Jacob, D. J.; Logan, J. A. *J. Geophys. Res.* **1992**, *97*, 6023–6036.

(10) Barnes, I.; Hjorth, J.; Mihalopoulos, N. *Chem. Rev.* **2006**, *106*, 940–975.

(11) Marandino, C. A.; Tegtmeier, S.; Krueger, K.; Zindler, C.; Atlas, E. L.; Moore, F.; Bange, H. W. *Atmos. Chem. Phys.* **2013**, *13*, 8427–8437.

(12) Yang, M.; Huebert, B. J.; Blomquist, B. W.; Howell, S. G.; Shank, L. M.; McNaughton, C. S.; Clarke, A. D.; Hawkins, L. N.; Russell, L. M.; Covert, D. S.; Coffman, D. J.; Bates, T. S.; Quinn, P. K.; Zagorac, N.; Bandy, A. R.; de Szoeke, S. P.; Zuidema, P. D.; Tucker, S. C.; Brewer, W. A.; Benedict, K. B.; Collett, J. L. *Atmos. Chem. Phys.* **2011**, *11*, 5079–5097.

(13) O'Dowd, C. D.; Lowe, J. A.; Clegg, N.; Smith, M. H.; Clegg, S. L. *J. Geophys. Res.* **2000**, *105*, 7143–7160.

(14) Sievering, H.; Cainey, J.; Harvey, M.; McGregor, J.; Nichol, S.; Quinn, P. *J. Geophys. Res.* **2004**, *109*.

(15) Hill-Falkenthal, J.; Priyadarshi, A.; Thiemens, M. *J. Geophys. Res.* **2012**, *117*.

(16) Said-Ahmad, W.; Amrani, A. *Rapid Commun. Mass Spectrom.* **2013**, *27*, 2789–2796.

(17) Browne, P.; Coulter, G.; Grant, M.; Grindley, G.; Lawless, J.; Lyon, G.; MacDonald, W.; Robinson, R.; Sheppard, D.; Skinner, D. *The Ngawha Geothermal Area*; Wellington, 1981.

(18) Programme Scientific Committee on Problems in the Environment (SCOPE). *Stable Isotopes: Natural and Anthropogenic Sulphur in the Envirionment*; Krouse, H. R.; Grinenko, V. A., Eds.; John Wiley & Sons, Ltd, 1991.

(19) Savarino, J.; Lee, C. C. W.; Thiemens, M. H. *J. Geophys. Res.* **2000**, *105*, 29079–29088.

(20) Savarino, J.; Thiemens, M. H. *Atmos. Environ.* **1999**, *33*, 3683–3690.

(21) Savarino, J.; Alexander, B.; Darmohusodo, V.; Thiemens, M. H. *Anal. Chem.* **2001**, *73*, 4457–4462.

(22) Coutant, R. W. *Environ. Sci. Technol.* **1977**, *4*, 873–878.

Appendix B: Laser Decomposition Isotope Interface (LADII)

B.1 Introduction

One of the huge disadvantages of off-line sample preparation is the sample size requirement. A dual inlet system, which is often used with offline processes, requires 10-100 micromoles of sample. A continuous flow system can handle 1-500 nanomoles of sample, and can be integrated easily into on-line sample preparations. The Laser Decomposition Isotope Interface (LADII) will take advantage of the continuous flow system and allow for online sample preparation of samples with small concentrations, which are common in stable isotope research. In addition, this interface will utilize a laser and an autosampler, which will allow for nearly instantaneous decomposition of the solid sample and a fully automated method. Both of these characteristics will allow for a large amount of samples to be analyzed in a relatively short amount of time.

B.2 Method

The schematic for LADII is shown in Figure B.2. The system operates in two modes: Mode A: Load, where the sample is decomposed and trapped, and Mode B: Inject, where the sample is sent to the IRMS. The method sequence starts by flushing the autosampler with He gas, which will serve as the carrier gas for the system. The 3-port

valve controls the addition of He from He #1. When flushing the autosampler, the 10-port valve is in Mode B (allows Port 1 to connect to Port 10) and the 3-port valve connects Port 1 on the 10-port valve to He #1. When flushing is complete, the 3-port connects Port 1 to Port 2 on the 10-port valve, and the 10-port returns to Mode A.

B.2.1 Mode A: Load

The laser (Synrad Firestar Series V40; Mukilteo, Washington) is positioned directly above the autosampler's viewing window, and when on, will decompose the sample.

$$Ag_2SO_4(s) \rightarrow 2Ag(s) + SO_2(g) + O_2(g) \qquad (R1)$$

When in Mode A, the resultant gas is carried through the SO_2 trap, which is submerged in liquid nitrogen, to the O_2 sample trap, which is also submerged in liquid nitrogen. The sample trap contains Washed 5A Molecular Sieve powder, which traps O_2 at liquid nitrogen temperatures. When in Mode A, both traps are submerged in liquid nitrogen and He purges the two GC columns.

B.2.2 Mode B: Inject

Once the sample has been trapped, the system switches to Mode B and the traps are removed from the liquid nitrogen to thaw. The sample gas is then sent to the 30 m Molecular Sieve 5A GC Column (Agilent Technologies, Santa Clara, CA). From the column, the gas is carried to the Open Split, a continuous flow gas inlet system, which injects the sample into the IRMS for isotope analysis.

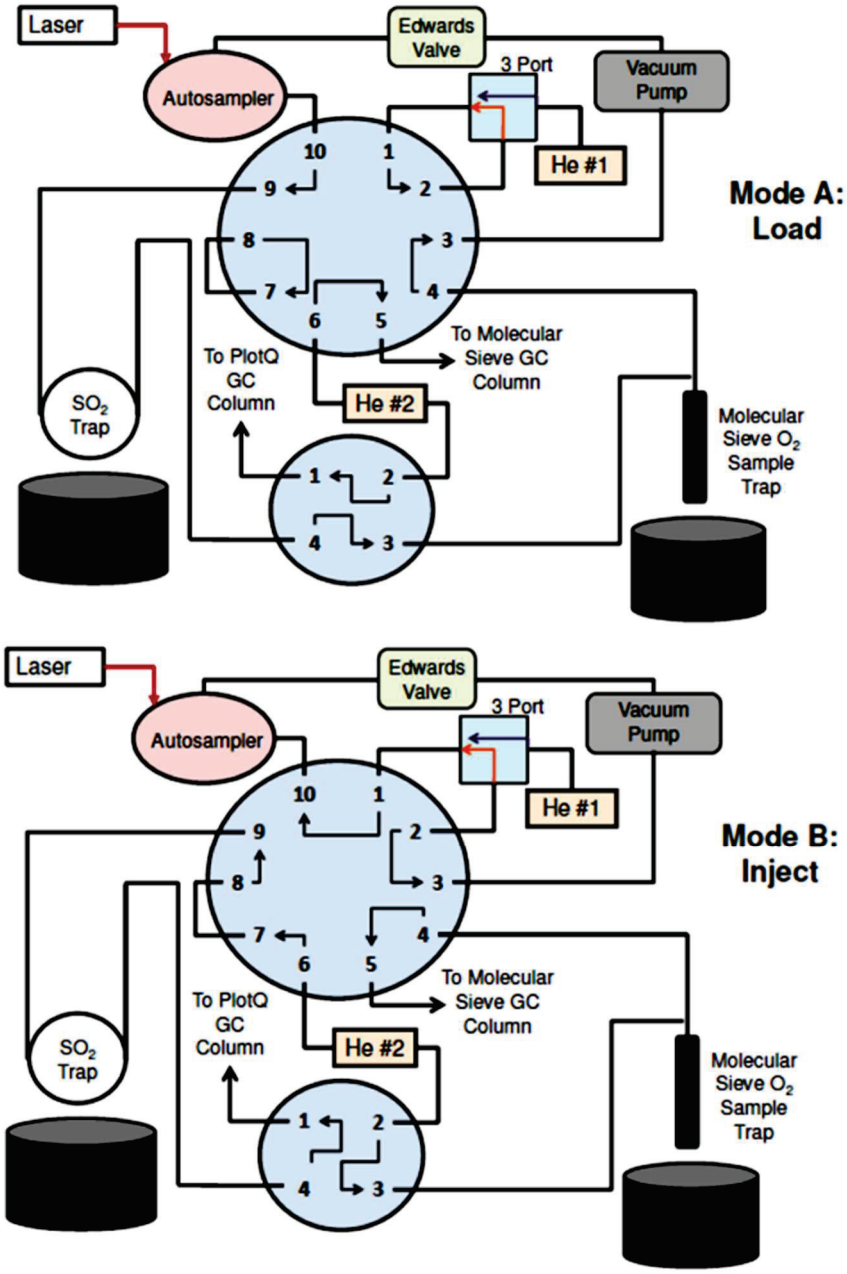

Figure B.1: Laser Decomposition Isotope Interface (LADII) Mode A (top) and Mode B (bottom). The 3-Port valve has 2 functions: connecting to He #1 (purple arrow) and bypassing He #1 (orange arrow).

Table B.1: Isodat Control Code Settings for LADII

Control Code	Relay Connection or LHS Connection	Valve
0	Relay J5	no connection
1	Relay J2	3-Port
2	Relay J4	4-Port
3	Relay J3	10-Port
4	LHS Pin 4	Edwards
5	LHS Pin 5	O_2 Trap
6	LHS Pin 6	SO_2 Trap
7	LHS Pin 7	Laser

B.3 Future Work

The system has been programmed and linked to the IRMS, but the laser and autosampler are currently unattached. In order to automate LADII, all of the valves needed to be controlled by the IRMS's operating program, Isodat. The computer communicates with the system through a Plug and Measure Adapter. For full automation, Isodat must be able to control the laser, the autosampler, the 2 traps (each controlled by a pneumatic valve), the 3, 4, and 10-Port valves, and an Edwards valve (which isolates the autosampler from the vacuum pump). When programming the solenoid valves, it was discovered that there were double solenoid valves. This was an issue since triggering both functions would require two control codes and operating the system in this manner would exceed the number available on the adapter (8 control codes per adapter). To work around this, I worked with the Jonathan Amy Facility for Chemical Instrumentation to develop a relay board to trigger both solenoids with one control code. Isodat control codes as they pertain to the relay board and LADII are summarized in Table B.2.

The current run time is just under 18 minutes, however, the sample seems to elude in two peaks, one sharper and one very long and broad. I believe this may be related to how the sample trap thaws. The sample that thaws quickly would produce the sharper peak, and the slower thawing sample would produce a long and broad peak. The current setup has been tested using a fan, a small homemade heater (heating coil wrapped around a thin metal tube), and a small tub of hot water, all of which produced conflicting results. In addition, the GC may or may not be dampening the sample signal (again, quite a few conflicting results). Baking the GC column has shown some potential to cure this problem, but this has not consistently worked. Future work needs to concentrate on these issues.

VITA

VITA

Tanya Katzman was born in Monroe, Wisconsin on March 2, 1988, but grew up in Burlington, Wisconsin. She grew up on a dairy farm, and participated in both 4-H and FFA, feeding her love of science. Between her junior and senior years of high school, she took as many science and agriculture courses as she could, and was awarded the 2006 Outstanding Senior in Science during graduation.

In the Fall of 2006, she began college at The University of Wisconsin-Madison, majoring in Chemistry. While at UW-Madison, Tanya worked for two years with Dr. Andrew Rutter, a post-doctoral fellow working in the Environmental Chemistry and Technology Program (EC&T) within the College of Engineering. Her research at EC&T primarily focused on deposition and uptake of elemental mercury in the environment, which included collection of rain water and particulate matter at a ranger station in Devil's Lake State Park. In addition to her mercury work, she conducted data analysis on particulate matter samples collected in early 2006, which led to the publication of a first author manuscript. In addition to majoring in Chemistry, she also participated in the Criminal Justice Program, which led to an internship with Captain Jim Wheeler at the Madison Police Department. Tanya graduated from UW-Madison with a B.S in Chemistry in May 2011.

Tanya began her graduate career during the Summer of 2011 as a bridging summer student in Dr. Greg Michalski's lab before officially joining the lab in Fall 2011. During Summer 2015, she participated in NSF's East Asia and Pacific Summer Institute (EAPSI), which allowed her to visit her New Zealand collaborators at GNS Science. During EAPSI, she expanded her collaboration to include the National Institute of Water and Atmospheric Research (NIWA) and set up a sampling campaign at NIWA's Baring Head Research Station, which will conclude during Summer 2016. In August 2016, Tanya earned her Ph.D. in Chemistry after 5 years of atmospheric chemistry research.

PUBLICATION

PUBLICATION

To be submitted for publication

2007 CALIFORNIA AEROSOL STUDY: EVALUATION OF $\delta^{15}N$ AS A TRACER

T. L. Katzman[1,3], and G. Michalski[1-3]

[1]Department of Chemistry, Purdue University, West Lafayette, Indiana, United States

[2]Department of Earth, Atmosphere, and Planetary Sciences, Purdue University, West Lafayette, Indiana, United States

[3]Purdue Climate Change Research Center, Purdue University, West Lafayette, Indiana, United States

Corresponding author: Greg Michalski (gmichals@purdue.edu)

Key Points:

- Source inputs could not justify observed $\delta^{15}N_{NO3}$ values
- NOx from wildfires may be depleted of ^{15}N
- Use of $\delta^{15}N$ as a tracer must account for fractionations associated with chemical or physical processing

Abstract

Stable isotope ratios are typically applied as tracers of sources and local chemistry, which is extremely useful for deciphering PM. As the main NOx sink, the stable isotope composition of NO_3^- reflects NOx sources contributions, oxidation pathways, and other processes that effect the isotope distribution (e.g. equilibrium exchange). Oxygen isotopes ($\delta^{17}O$, $\delta^{18}O$, $\Delta^{17}O$) are known to act as tracers of oxidation pathways. However, the use of N isotopes ($\delta^{15}N$) as a tracer is usually split between two schools of thought: the source hypothesis and the chemistry hypothesis. The source hypothesis claims that the NO_3^- $\delta^{15}N$ value is solely determined by NOx source $\delta^{15}N$ values. The chemistry hypothesis agrees that source $\delta^{15}N$ values do contribute to the NO_3^- $\delta^{15}N$ value, but chemical reactions also contribute to the isotopic composition. This work uses elemental and stable isotope analysis to evaluate local atmospheric chemistry at four sites in Southern California (Chula Vista, El Cajon, El Centro, and Brawley) PM from each site revealed seasonal trends, but also how emissions from the 2007 wildfire season impacted local chemistry. Additionally, stable isotope analysis of these sites strongly supported the chemistry hypothesis, as source contributions failed to explain observed nitrate $\delta^{15}N$ values.

1 Introduction

Nitrogen oxides (NOx = NO + NO_2) are extremely important trace gases in the atmosphere. They play a role in regulating the oxidative capacity of the atmosphere[*Logan et al.*, 1981; *Logan*, 1983; *Hastings*, 2010] and determining the chemical composition of the atmosphere by participating in chemical reactions such as the photochemical production of O_3.[*Logan et al.*, 1981; *Logan*, 1983; *Seinfeld and Pandis*, 2006; *Walters et al.*, 2015a, 2015c] As a result, NOx influences the formation of particulate matter, impacting regional air quality and the Earth's radiative balance. The modern NOx cycle is dominated by anthropogenic emissions,[*James N. Galloway*, 2002; *Galloway et al.*, 2004; *Hastings*, 2010; *Walters et al.*, 2015a, 2015c] although natural NOx sources do contribute regionally.[*Seinfeld and Pandis*, 2006; *Hastings*, 2010; *Walters et al.*, 2015a] The strength of these sources varies regionally and seasonally, producing significant differences in air quality between urban and rural environments on an annual basis. The relatively short lifetime of NOx (few days at most[*Freyer et al.*, 1993; *Hastings*, 2010]) in addition to the regional variability of NO_x emissions also means that NOx mixing ratios are globally highly variable.[*Logan et al.*, 1981; *Freyer et al.*, 1993] For this reason, chemical transport models are utilized to decipher NOx cycling and its impact on the environment, often using local NO_3^- or O_3 measurements to evaluate the model.[*Logan et al.*, 1981; *Benkovitz et al.*, 1996; *Sillman*, 1999]

NOx has four major source categories: fossil fuel combustion, biomass burning, soil emissions, and lightning.[*Walters et al.*, 2015a] Fossil fuel combustion dominates the current NOx budget and is the primary source in urban areas, where as rural areas are often a mixture of combustion sources and soil emissions. Once emitted, NOx cycles back and forth between its two forms via the Leighton Cycle during the day.[*Freyer et al.*, 1993; *Seinfeld and Pandis*, 2006; *Elliott et al.*, 2007]

$$NO + O_3 \rightarrow NO_2 + O_2 \quad (1a)$$

$$NO_2 + h\upsilon \rightarrow NO + O\left(^3P\right) \quad (1b)$$

$$O\left(^3P\right) + O_2 \rightarrow O_3 \quad (1c)$$

The above reactions, and NO oxidation by oxygenated radicals, establish steady state mixing ratios of NO, NO_2 and O_3.[*Freyer et al.*, 1993; *Seinfeld and Pandis*, 2006] Volatile organic compounds (VOCs) react with OH radicals during the day to produce organic peroxy radicals:

$$VOC + OH \xrightarrow{\left[O_2\right]} RO_2 + H_2O \quad (2)$$

Organic peroxy radicals further react to oxidize NO to NO_2:

$$NO + RO_2 \rightarrow NO_2 + RO \quad (3)$$

VOCs, such as hydroperoxyl radicals (HO_2) and other organic peroxy radicals (ROO), form NO_2 without the participation of O_3. During the day, the VOC-oxidized NO_2 will be added to the Leighton Cycle, where it will photolyze into NO and contribute to the formation of new O_3 molecules. Thus this photochemical cycle involving NOx and volatile organic compounds (VOCs), are responsible for regulating the O_3 concentration in the atmosphere.[*Seinfeld and Pandis*, 2006; *Hastings*, 2010; *Walters and Michalski*, 2015; *Walters et al.*, 2015a, 2015c]

NOx is removed from the atmosphere by conversion to HNO_3 via different chemical pathways during the day and night. During the daytime, NOx is removed from the Leighton cycle by reacting with photochemically produced OH radicals to form HNO_3[*Gobel et al.*, 2013].

$$NO_2 + OH + M \rightarrow HNO_3 + M \quad (4)$$

During the night, NO_2 photolysis and OH production ceases and the OH pathway to HNO_3 shuts down. Any NO present in the troposphere reacts rapidly with O_3 to form NO_2 (Equation 1a) followed by the formation of NO_3 radical

$$NO_2 + O_3 \rightarrow NO_3 + O_2 \quad (5)$$

Reaction 2 is the only significant source of NO_3 radical in the atmosphere. At night, the NO_3 radical acts as the major oxidant thus influencing trace gases in the atmosphere.[*Seinfeld and Pandis*, 2006] VOCs and dimethyl sulfide (DMS) can react with NO_3 radicals to form HNO_3 by hydrogen abstraction.[*Gobel et al.*, 2013]

$$NO_3 + HR \rightarrow HNO_3 + R\cdot \quad (6)$$

This pathway is especially important at night when NO_3 radical concentrations are high. Marine phytoplankton have been shown to produce DMS, which is emitted from the surface of the ocean,[*Charlson et al.*, 1987; *Sievering et al.*, 2004; *Ayers and Cainey*, 2007; *Gobel et al.*, 2013] therefore this reaction is of particular interest in the coastal and marine air masses. Additionally, due to the lack of NO at night, NO_3 radical reacts with NO_2 to form N_2O_5[*Seinfeld and Pandis*, 2006]

$$NO_2 + NO_3 + M \rightarrow N_2O_5 + M \quad (7)$$

with the reverse reaction triggered by thermal decomposition. N_2O_5 can undergo heterogeneous hydrolysis on aerosol surfaces to form HNO_3

$$N_2O_5 + H_2O + \text{surface} \rightarrow 2HNO_3 \quad (8)$$

serving as the major nighttime NOx sink.[*Seinfeld and Pandis*, 2006]

Nitrogen chemistry is highly dependent on local N emissions and meteorology, as well as the presence of other trace gases. These dependencies are largely responsible for regional differences, especially across climates. In urban areas, anthropogenic N emissions overwhelm natural emissions due to a high concentration of motor vehicle traffic, industrial activities, and power generation processes.[*Seinfeld and Pandis*, 2006; *Monks et al.*, 2009; *Williams et al.*, 2016] On the other hand, rural areas experience significant natural emissions, but also a moderate influence of anthropogenic NOx sources, such as motor vehicle traffic.[*Seinfeld and Pandis*, 2006] In agriculture areas, N emissions tend to be in reduced forms (NH_3, NH_4^+), arising from fertilizer application and livestock operations.[*FENN et al.*, 2003] Emissions in remote areas are primarily from natural sources, such as lightening and dust, but transported secondary aerosol products (NO_3^-, SO_4^{2-}) can be present, depending on regional meteorology.

In addition to regional land uses, climate has a significant influence on N chemistry. Temperatures, amount of precipitation, elevation, amount of solar radiation, and other trace gases and particles all impact local chemistry and atmospheric processing. Arid and semi-arid climates receive very little precipitation throughout the year, thus promoting dry deposition processes.[*FENN et al.*, 2003] These areas also tend to have a significant input of mineral dust, which tends to be more alkaline than other particles.[*Andreae and Crutzen*, 1997] This in turn influences oxidation and other chemical pathways, which can be pH dependent. Coastal areas experience a mixture of continental and marine air masses, with chemistry being influenced by the presence of sea salt particles. Sea salt particles provide gases with a surface to condense on, and undergo aqueous phase reactions rather than gas phase reactions.[*Neumann et al.*, 2016] Additionally, as sea salt particles are larger than fine particles, dry deposition occurs much more rapidly and often locally. However, the impact of sea salt on NOx is only significant in urban influenced coastal areas, as the concentration of NOx in the marine boundary layer (MBL) is too low.[*Dominguez et al.*, 2008] Chemistry in areas with high concentrations of VOCs is distinct from areas with low or non-existent VOC concentrations.[*Liu and Zhang*, 2013] Polar chemistry tends to be highly seasonal, due to the lack of photochemistry during the winter and low concentrations year round. However, snowpack photolysis during the arctic spring, recycles reactive N species (NOx, HONO) back into the atmosphere.[*Zatko et al.*, 2016]

This study investigates aerosols collected during 2007 in San Diego, USA which is a coastal urban area influenced by sea salt aerosols, anthropogenic combustion emissions, and seasonal wildfires. Wildfires also have a significant influence on local chemistry and 2007 was notable for being the worst fire season in the San Diego region on record. In addition to NOx emissions, wildfires emit precursors to O_3 formation, such as CO and VOCs,[*Phuleria*, 2005; *Cai et al.*, 2016] which can in turn influence oxidation pathways.[*Val Martín et al.*, 2006; *Monks et al.*, 2009] Wildfires also influences the partitioning between reactive nitrogen species (NOx, HNO_3, HONO, particulate-NO_3^-). Additionally, as atmospheric chemistry varies by location, the effect wildfire NOx emissions have on NO_3^- formation is also of interest. Given the connection between nitrate (as HNO_3 or particulate NO_3^- (p-NO_3)) and NOx, it is readily accepted that the

sources of NOx must influence the isotopic composition of the resulting nitrate. Due to this effect, it has been suggested that nitrogen stable isotopes could be utilized as tracers in order to understand how NOx cycles through the environment,[*Elliott et al.*, 2007; *Morin et al.*, 2008; *Hastings et al.*, 2009; *Hastings*, 2010; *Walters et al.*, 2015a, 2015c] to evaluate chemical models, and to decipher the historical climate record.

Although stable isotopes of N are commonly used as a source tracer, how this tracer is applied is a point of contention. One hypothesis argues that the $\delta^{15}N$ value of NO_3^- reflects the $\delta^{15}N$ value of NOx source inputs into the environment, and any variation is the result of difference in source contributions. Proponents of this hypothesis argue that the $\delta^{15}N$ value of the resultant NO_3^- reflects the $\delta^{15}N$ value of the original NOx source, as the N atom is conserved during the oxidation process.[*Hastings et al.*, 2003a; *Hastings*, 2004; *Elliott et al.*, 2009] Therefore, the observed variations in NO_3^- $\delta^{15}N$ values are the result of changes in source emissions due to seasonal changes or regional influences. Any potential physical or chemical processing after emission is ignored or assumed to have negligible effect on $\delta^{15}N$ values.[*Morin et al.*, 2008] The second hypothesis argues that N isotopes are influenced by chemical reactions, atmospheric or biologic processing, and post-depositional effects.[*Hastings*, 2010] As mass differences are most pronounced for the lightest elements (H, C, N, O, S),[*Hoefs*, 2015] N is often subject to kinetic and equilibrium isotope fractionation effects,[*Freyer et al.*, 1993; *Walters et al.*, 2015a] which vary based on temperature. In the case of equilibrium exchange between nitrogen oxide forms, equilibrium favors ^{15}N enrichment in the more oxidized form.[*Begun and Fletcher*, 1960; *Freyer et al.*, 1993] Kinetic fractionations are also predicted to vary by season, due to shifts in reaction pathways and equilibrium systems (summer dominance of NO_2 + OH pathway vs winter $NO_2/NO_3^-/N_2O_5$ equilibrium).[*Freyer et al.*, 1993] Previous studies often apply the source hypothesis, writing off the chemistry hypothesis as "minor,"[*Savarino et al.*, 2008; *Hastings et al.*, 2009] but few do support acknowledge the impact chemistry has on $\delta^{15}N$ values[*Freyer et al.*, 1993; *Hastings*, 2010; *Walters et al.*, 2015b].

Stable isotope studies in regions with consistent NOx sources throughout the year could be used to settle this debate, as each hypothesis would produce different behavior. The source hypothesis would predict that a simple source mixing model and isotope mass balance would explain observed $\delta^{15}N$ values in nitrate samples. Since anthropogenic emissions are monitored and regulated by the U.S. Environmental Protection Agency (EPA), local and regional emissions can be used to quantify and calculate expected $\delta^{15}N$ values for local NO_3^- sample, due to the conservation of source $\delta^{15}N$ values. Since NO_3^- results from the oxidation of a mixture of contributing NOx sources, the observed $\delta^{15}N$ value of NO_3^- (henceforth referred to as $\delta^{15}N_{NO3}$) would be a result of mixing NOx sources based on the source's contributing fraction. The chemistry hypothesis would predict that reactions or processes would shift the $\delta^{15}N$ values from their original source $\delta^{15}N$ values, with the magnitude of the shift dependent on atmospheric and/or meteorological conditions and the energetics of the reaction or process.

Given the known complications, this work seeks to assess the use of stable isotopes as tracers, specifically, the assumption that the $\delta^{15}N$ value is a tracer of source alone without significant influence from chemical reactions. Using source emission data and known source $\delta^{15}N$ values, isotope mass balance should be able to approximate

measured $\delta^{15}N_{NO3}$ values and determine the $\delta^{15}N$ value associated with wildfire derived NOx, which is currently unknown. Significant deviations from observed values would support the significance of isotope effects associated with chemical reaction and processing in the atmosphere. Aerosols collected in Southern California, emission data, and isotopic analysis were utilized to determine the utility of a $\delta^{15}N$ tracer.

2 Methods

2.1 Site Description

The study area was the Southern California region near San Diego and the Mexican border during 2007. Particulate matter less than 10 μm and other air quality data was collected by the San Diego and Imperial County Air Pollution Control Districts and the California Air Resources Board (CARB). Four monitoring locations from two different counties (Figure 1) were chosen for this study: Chula Vista and El Cajon in San Diego County and Brawley and El Centro in Imperial County. Imperial County locations are located between the Salton Sea and the US-Mexico Border in the Imperial Valley and the Colorado Desert. Despite the desert climate, irrigation has made land-use in this region highly agricultural; thus, soil NO emissions may be important in the Valley. These valley locations are also less populated than San Diego locations, with a combined population of 179,091. San Diego County locations are part of the greater San Diego metropolitan area, much closer to the Pacific coast (~7.5 km and 29.5 km from the Chula Vista and El Cajon sampling sites, respectfully), and experience a Mediterranean climate.

Table 1: Site Demographics as recorded by the US Census Bureau and California Air Resources Board.

	Chula Vista	El Cajon	Brawley	El Centro
Latitude	32.63123	32.7912	32.97831	32.79215
Longitude	-117.05905	-116.9421	-115.53904	-115.56299
Elevation (m)	55	144	-15	9
Population	260988	103091	25820	43763
Area (sq mi)	49.63	14.43	7.68	11.08
Distance from Pacific Ocean (km)*	7.5	29.5	162	158
Air Basin	San Diego	San Diego	Salton Sea	Salton Sea
County	San Diego	San Diego	Imperial	Imperial
Climate	Mediterranean	Mediterranean/ Semi-arid	Low Desert	Desert
Land Use	Residential/ Metropolitan	Residential/ Metropolitan	Residential/ Agriculture	Residential/ Agriculture
ARB Site	80 E. J St.	1155 Redwood Ave	220 Main St.	150 9th St
Monitoring Site Maintained by:	San Diego Air Pollution Control District	San Diego Air Pollution Control District	Imperial County Air Pollution Control District	Imperial County Air Pollution Control District
* Estimated using Google Earth				

These areas are also much more densely populated, with a metropolitan population of approximately 3.3 million and local NOx emissions are dominated by residential and metropolitan sources. Seasonal and daily shifts in temperature and NOx emissions are more apparent in the Imperial County locations, due to the coastal influence on the San Diego County sites. Additionally, the Port of San Diego has two cargo terminals, one cruise terminal, two ship repair yards, the West Coast's only shipyard, and serves as the base for the largest naval complex in the world. In 2013, the Port recorded 556 arriving vessels.[*Marquez and Knapp*, 2014] Table 1 further summarizes site demographics.

Imperial County has 489,137 acres of agricultural, with over 95% of this acreage lying in the Imperial Valley. Alfalfa, onions, head lettuce, and broccoli dominate field and vegetable crops, and cattle dominates livestock operations although sheep operations are also significant. The valley's climate allows for multiple harvests per year for some planted crops.[*Valenzuela et al.*, 2014] Agricultural operations and other non-farm applications used 271,239 tons of fertilizer in 2012.[*Maan*, 2012] As the county receives very little precipitation throughout the year (2.61" annually),[*Anon*, 2016b] the region depends heavily on irrigation from the Colorado River.[*Anon*, 2016a] San Diego County also has significant agriculture industry, with 268,592 acres of planted crops (80.6%), vegetables (1.7%), fruit and nut trees and shrubs (13.0%), and nursery and cut flowers (4.7%), with avocados utilizing the most acreage. In 2012, San Diego County used 163,785 tons of fertilizer, which included agricultural uses as well as non-farm uses (gardening, landscaping).[*Maan*, 2012] Cattle operations are also prevalent in San Diego County, with hog operations also significant.[*Dang et al.*, 2014] Although the county receives more precipitation than Imperial County (10.13" annually), 80% of San Diego County's water is imported from Northern California and the Colorado River.[*San Diego County Water Authority*, 2016]

Although 10% of the California's power is supplied by coal, San Diego and Imperial Counties, which lie along the US-Mexico border, do not rely on coal for power generation. Instead, power plants located in San Diego and Imperial counties use natural gas, wind, water, solar energy, and biomass to produce energy (Table X). A few plants in Imperial County also utilize geothermal energy for power generation.[*Anon*, 2015] However, plants using renewable power generation methods (hydro, wind solar, geothermal) do not use combustion for power generation, and therefore do not emit NOx.

Table 1: Power Plants in San Diego County and Imperial County by fuel/operation type as of 2015[45]

Powered by:	San Diego County	Imperial County
Natural Gas	60	1
Hydro	10	10
Wind	2	1
Solar	29	13
Biomass	0	1
Geothermal	0	20
Digester Gas	3	0
Landfill Gas	8	0

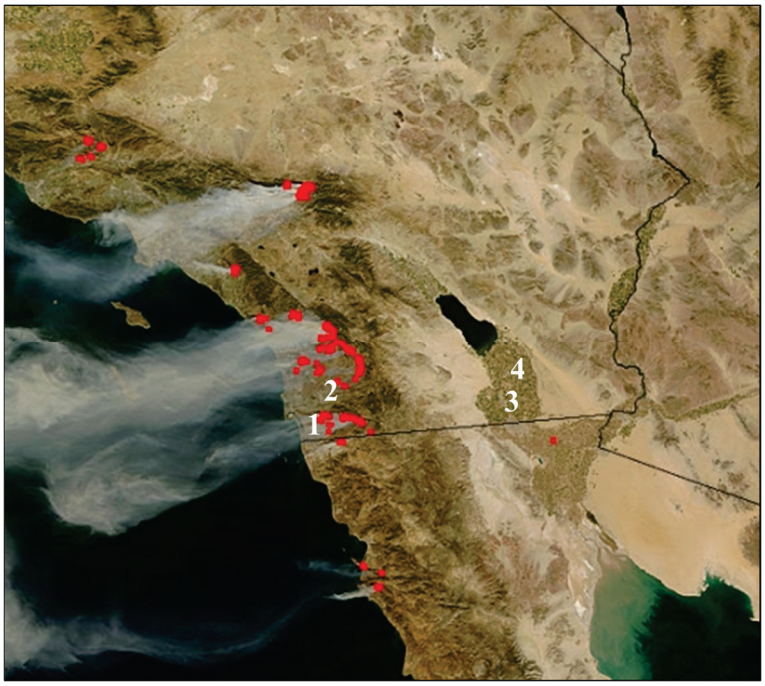

Figure 1: Satellite image of Southern California, taken October 22, 2007. Image show fires burning (red) and presence of strong Santa Ana winds pushing smoke offshore. Sampling sites are numbered as follows: Chula Vista (1), El Cajon (2), El Centro (3), and Brawley (4). Image courtesy of NASA/MODIS Rapid Response)

2.2 2007 California Wildfire Season

Although wildfires are common to the Western United States, 2007 was a particularly explosive season for Southern California. Rainfall and snow pack levels were at historic lows causing to live fuel moistures levels to reach all-time lows. These conditions, along with the larger than normal dead fuel accumulations resulted in the rapid spread of the fires, especially during the month of October.[*Anon*, n.d.; *Grijalva et al.*, n.d.] The first wildfire of the season, the Zaca Fire, began two months early than normal, on July 4, 2007 in Santa Barbara County. The fire burned for two months, scorching 240,207 acres before it was finally contained. The season continued with several small fires throughout September and early October, before Ranch Fire, fed by as strong Santa Ana winds, set off a chain of events that sparked 23 fires in rapid succession.[*Anon*, n.d.] Although some fires continued through early November, the first three days were the most destructive as the Santa Ana Winds were the strongest during this period. These late October fires burned through half a million acres of land, impacting populated areas, wildlife reserves, and watersheds, displacing hundreds of thousands of residents.[*Anon*, n.d.; *Grijalva et al.*, n.d.]

Fires in San Diego County consumed more acres than fires in other counties, with some fires burning in for 10 days prior to containment. Fueled by extremely dry conditions, brought about by below average winter precipitation and very little summer rain, and strong (40-70 mph) Santa Ana winds, wildfires spread rapidly.[*Grijalva et al.*,

n.d.] Harris Fire, located along the U.S. – Mexico border, started October 21, 2007. Pushed west by Santa Ana winds, the fire reached the Chula Vista city limits by October 23. Containment strategies were hampered by strong winds, and it was 6 days before significant containment was obtained. Harris fire was fully contained by October 31, but not before consuming 90,440 acres.[*Grijalva et al.*, n.d.] Witch Fire, located approximately 25 miles NE of El Cajon, CA, also started October 21, 2007. As with Harris Fire, Santa Ana winds grounded air crews and hampered suppression methods. The fire merged with Poomacha Fire, which began October 23 on the La Jolla Indian Reservation, on October 25 before containment was reached on October 31. Witch Fire was the largest of the Fire Seige, consuming 197,990 acres. Poomacha Fire was mostly contained by October 31, but full containment wasn't reached until November 13.[*Grijalva et al.*, n.d.]

2.3 Sample Analysis

Aerosol filters were collected on 8x10" Quartz Microfiber filters using a High Volume PM_{10} Inlet Sampler on a 1-in-6-day basis by the San Diego County and Imperial County Air Pollution Control Districts. Samples were collected for 24 hours at a flow rate of approximately 1.05 m^3/min. Initial analysis was conducted by the CARB, using a quarter of the exposed filter, in order to determine overall PM mass by Electronic Analytical Balance (ARB Analysis Method 016) as well as the nitrate, sulfate, chloride, ammonium, and potassium concentrations by Ion Chromatography (ARB Analysis Methods 007 and 023).[*California Air Resources Board*, 2011] Most collection sites also monitor trace gas concentrations (CO, NO_2, O_3), hydrocarbon concentrations, and meteorological conditions (temperature, wind direction speed, humidity) using standard protocols,[*Anon*, 2011] thus adding data that was useful for interpreting the isotopic results. Post-analysis, filters were sealed and stored in separate folders and boxed away for future use, and were procured by Purdue University from the CARB in 2015.

A secondary ion analysis was conducted in 2015 at Purdue University using standard protocols. Briefly, the filters were soaked in 100mL of Millipore water (EMD Millipore, Fischer Scientific) to dissolve the collected particulates and ions. This extract was split into 6 - 15mL centrifuge tubes (VWR), each portion containing ~13mL. One portion was utilized for anion analysis using Ion Chromatography. Anions (chloride, nitrate, and sulfate) were determined using a Dionex IonPac AS14 analytical column with a Omnifit SPE Sorbant C18 chromatographic column and 3.5mM $NaHCO_3$/1mM Na_2CO_3 eluent. A Dionex AMMS300 suppressor with 50mN H_2SO_4 was used prior to detection with an Alltech Model 650 Conductivity Detector. Standards of known NO_3^-, SO_4^{2-} and Cl^- concentration were used to calibrate the IC and determine the sample concentrations.

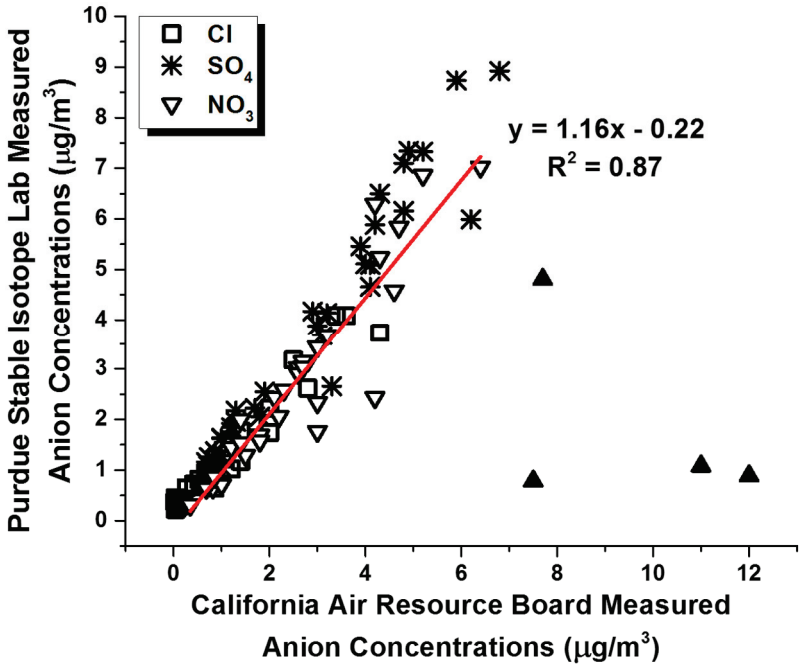

Figure 2: Comparison of anion concentrations as measured by the California Air Resources Board in 2007and the Purdue Stable Isotope Lab in 2015.

Another portion of the filter extract was used for isotopic analysis of N and O. The sample was concentrated using a freeze dryer down to final volume of ~1-2mL. This portion was injected into a 12mL vial containing a denitrifying strain of bacteria (P. Aureofaciens).[*D. M. Sigman K. L. Casciotti, M. Andreani, C. Barford,M. Galanter, and J. K. Bolhlke*, 2001; *K. L. Casciotti M. Galanter Hastings, J. K. Bo1 hlke, and A. Hilkert*, 2002; *Kaiser et al.*, 2007] The bacteria convert nitrate in the sample into nitrous oxide (N_2O). The N_2O is extracted from the headspace, purified, and analyzed for $\delta^{15}N$ and $\delta^{18}O$ values using a Thermo Delta V Isotope Ratio Mass Spectrometer.[*D. M. Sigman K. L. Casciotti, M. Andreani, C. Barford,M. Galanter, and J. K. Bolhlke*, 2001; *K. L. Casciotti M. Galanter Hastings, J. K. Bo1 hlke, and A. Hilkert*, 2002; *Kaiser et al.*, 2007] Working lab standards, calibrated against USGS34 and USGS35, were used to account for isotopic fractionation during bacteria denitrification and N_2O purification. The working standards had an average standard deviation of 1.6‰.

3 Results

In order to verify the aerosol ion composition had not changed while in storage, filters were re-analyzed using Ion Chromatography and compared to the results obtained by CARB in post-sampling (Figure 1). The NO_3^-, Cl^-, and SO_4^{2-} concentrations measured in 2015 agreed with concentrations measured in 2007, but four samples showed significant NO_3^- loss. Two of these samples, collected November 8th and 20th, correspond with a relatively large concentration of NH_4^+, suggesting that the NO_3 loss may have been due to NH_4NO_3 volatilization during storage. Previous studies conducted by the CARB found that filters stored in open containers for over six days experienced

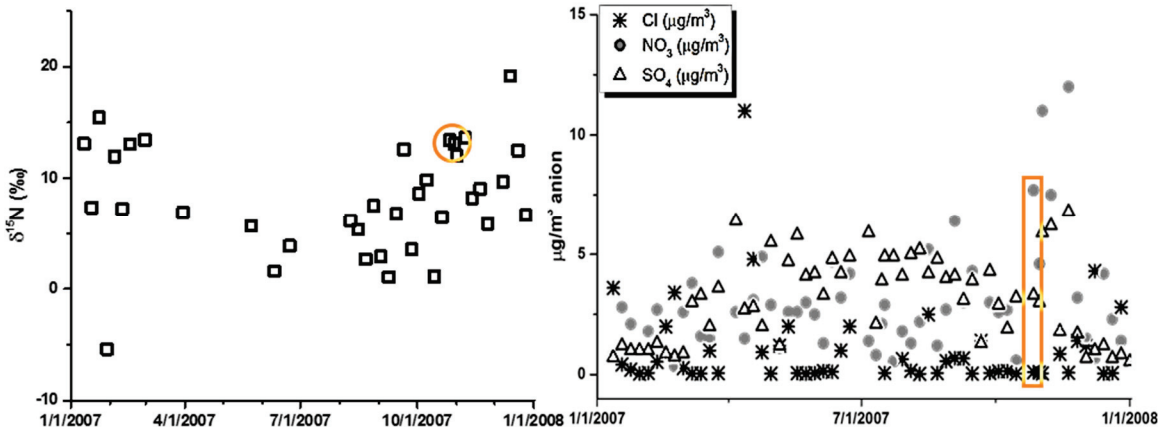

Figure 2: $\delta^{15}N_{NO3}$ (left) and anion concentrations (right) for Chula Vista, California.

significant NO_3^- volatilization. Additionally, the study found that at temperatures elevated above room temperature volatilization occurred in both a sealed and open container.[*Achtelik and Omand*, 1998] The other two samples do not have any (November 2nd) or very little (October 27th) NH_4^+ to explain this loss. Another study prepared for the CARB noted that HNO_3 and NH_4^+ could react with fine organic matter, leading to NH_4NO_3 being associated with organic matter.[*Ashbaughm et al.*, 1998] As organic matter was filtered out of extracted samples, it is possible that associated NH_4NO_3 would also be removed. However, the impact this loss has on the $\delta^{15}N$ value of the remaining NO_3^-, can be accounted for using the Rayleigh distillation equation, and thus will still provide valuable data about wildfire NOx emissions.

Chula Vista NO_3^- concentrations (Figure 3) averaged 3.0 ± 2.3 ppm, and showed no consistent seasonality. However, concentrations in the days after the fire, NO_3^- concentrations increased, reaching concentrations 2-4 times the annual average. In contrast with previous studies,[*Wang and Shooter*, 2001; *Elliott et al.*, 2009; *King*, 2013; *Riha*, 2013] which observed a winter increase in NO_3^- concentrations, NO_3^- concentrations at Chula Vista showed no apparent increase. While it is possible that the wildfire NOx emissions could be obscuring any seasonal NO_3^- concentration shifts. Previous studies[*Wang and Shooter*, 2001; *King*, 2013; *Riha*, 2013] attribute the winter increase in NO_3^- concentrations to a lower boundary layer height, which would trap NOx and oxidants closer to the surface, promoting oxidation.[*Sillman*, 1999] However, the relatively narrow temperature range, which averages 17.6 ± 4.1°C (68.7 ± 39.4°F), likely would not change the boundary layer height significantly, suggesting a seasonal shift in NO_3^- concentrations is likely absent at Chula Vista.

The annual average nitrate $\delta^{15}N$ value in Chula Vista was 8.3 ± 5.0‰, with summer minimums (4.1‰ average) and winter maximums (10.0‰). This seasonal trend echoes a study by Freyer,[*Freyer*, 1991] which observed summer minima and winter maxima in NO_3^- collected
in rain samples (-5% and 0‰, respectfully) and particulate samples (3‰ and 7%, respectfully). Conversely, studies by Hastings[*Hastings et al.*, 2003b] and Wankel[*Wankel et al.*, 2010] returned $\delta^{15}N$ values with the opposite trend: summer maximums and winter minimums. Rainwater collected in Bermuda was found to have

higher $\delta^{15}N$ values (-2.1‰) during the warm season than samples collected during the cool season (-5.9‰).[*Hastings et al.*, 2003b] Aerosol nitrate collected in Eilat, Israel, which lies on the Gulf of Aqaba, recorded $\delta^{15}N$ values with summer maximums (-2.1‰) and winter minimums (-3.7‰).[*Wankel et al.*, 2010]

Seasonal variations in $\delta^{15}N$ values were observed at all sites to some extent (Figure X). Overall, $\delta^{15}N_{NO3}$ values were lowest during the summer and highest during the late fall and winter months. The $\delta^{15}N$ seasonal shift in the El Centro nitrate was much more pronounced than observed in El Cajon and Chula Vista. The semi-arid climate of El Centro leads to very little precipitation and produces significant daily and seasonal temperature changes, which effects atmospheric processing and deposition conditions. The Mediterranean climate of El Cajon and Chula Vista may not bring much more precipitation, but proximity to the ocean leads to a small seasonal temperature changes. Additionally, the greater proportion of agricultural activities and lesser proportion of mobile sources enhance the El Centro $\delta^{15}N_{NO3}$ seasonality. However, it is worth noting that the $\delta^{15}N_{NO3}$ values appear unaffected by wildfire emissions, as the observed $\delta^{15}N_{NO3}$ values do not deviate from the established seasonal trend at any of the sites.

Chula Vista SO_4^{2-} concentrations are low during the winter, but are roughly 2-3 times higher during the spring, summer, and fall. As Chula Vista is a coastal community with relatively warm temperatures year round, the seasonality of SO_4^{2-} aerosols may be the result of DMS oxidation. Once emitted from the ocean's surface, DMS can deposit onto aerosol surfaces and oxidize into SO_2, and ultimately SO_4^{2-}, which is frequently referred to non-sea salt SO_4^{2-} (nss-SO_4^{2-}). As phytoplankton productivity peaks in the summer, due to increased photolysis, DMS and nss-SO_4^{2-} concentrations also peak in the summer,[*Bates et al.*, 1987] thus leading to an enhancement in the overall SO_4^{2-} concentrations. Additionally, recent work by Dominguez et al.[*Dominguez et al.*, 2008] has found that SO_2 from ship exhaust is also a significant contributor of nss-SO_4^{2-}. Coarse sea salt particles rapidly remove and oxidize SO_2, which can account for 10-44% of the nss-SO_4^{2-} in marine air masses. Cl^- concentration is low for most of the year, indicating that the major Cl^- source, sea salt, varies very little throughout the year. Therefore, any

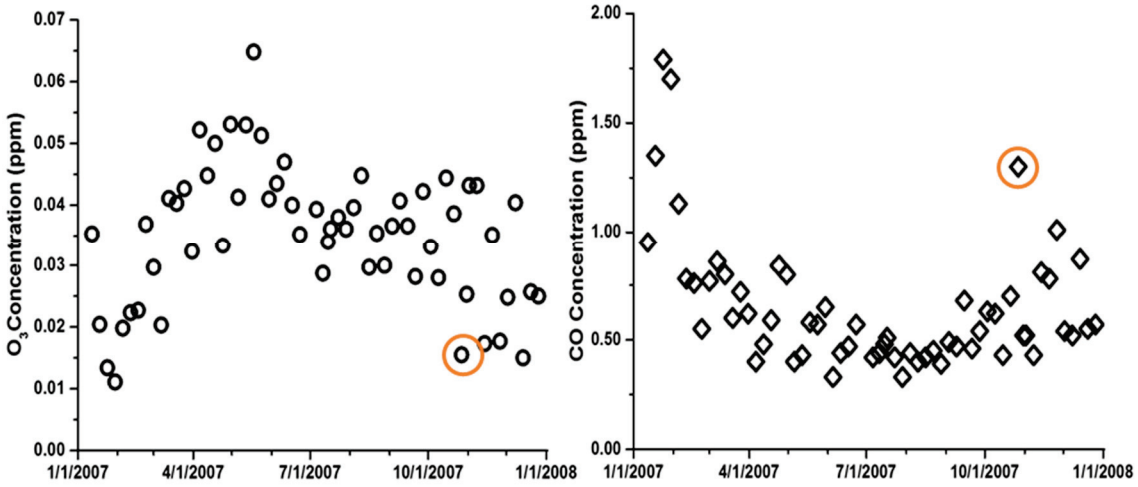

Figure 4: O_3 (top) and CO (bottom) 24-hour average concentrations at Chula Vista, California

seasonality in SO_4^{2-} concentrations would be the result of urban SO_2 (industrial processes) or non-sea salt contributions.

Trace gas concentration measurements were also collected at the sites. At Chula Vista, daily average O_3 concentrations ranged from 64.8 to 11.1 ppb and peaked in the late spring/early summer (37 ppb on average) before falling to winter minimums (24 ppb on average). Conversely, daily average CO concentrations peak in the winter (928 ppb average) before falling to a minimum in the late summer (434 ppb), and span from 330 ppb to 1.79 ppm. Daily average NOx concentrations ranged from 50 to 83 ppb, with a summer minimum (80 ppb average) and winter maximum (38 ppb). Daily average SO_2 concentrations were very low year round (2.6 ppb on average), with concentrations ranging from 2 to 4.2 ppb. Although the shift was very small, a small increase in daily average SO_2 concentrations was observed in the fall (from 2.4 to 3.2 ppb), and concentrations remained elevated into December 2007. In the period after heavy wildfire activity, CO and PM concentrations showed a slight increase in daily average concentrations. $PM_{2.5}$ and PM_{10} concentrations, which average 19.7 and 34.3 ppm, respectfully, nearly doubled in concentration (28.5 and 58 ppm, respectfully) with the addition of wildfire emissions. CO concentrations, which average 650 ppb in the fall, more than doubled in concentration (1.3 ppm) as a result of wildfire emissions. Additionally, measured NO_3^- and SO_4^{2-} concentrations at Chula Vista increased after the wildfires. Conversely, daily average O_3 concentration seemed to be unaffected by wildfire emissions, and NOx may show a slight concentration enhancement, but this also falls in line with the shift in seasonal trends.

4 Discussion

In order to assess if the seasonality of the $\delta^{15}N_{NO3}$ values was the result of the seasonality of NOx sources[*Hastings et al.*, 2003a; *Hastings*, 2004; *Elliott et al.*, 2009] isotope mass balance was used. Isotope mass balance can be used one of two ways: to calculate an expected $\delta^{15}N_{NO3}$ sample value or to determine the unknown $\delta^{15}N$ value of a source(s). In the first case, source mole fractions (f_i) of each NOx source and the $\delta^{15}N$ values ($\delta^{15}N_i$) of each NOx sources is known are summed together to determine the expected $\delta^{15}N_{NO3}$:

$$\delta^{15}N_{NO3} = \sum f_i \delta^{15}N_i \tag{9}$$

In the second instance, the NOx source mole fractions (f) that do not have known $\delta^{15}N$ values ($\delta^{15}N_{unknown}$) are excluded in the summation and the measure NO_3^- $\delta^{15}N$ value is used to determine the $\delta^{15}N$ value of the unknown ($\delta^{15}N_{unknown}$) NOx source(s):.

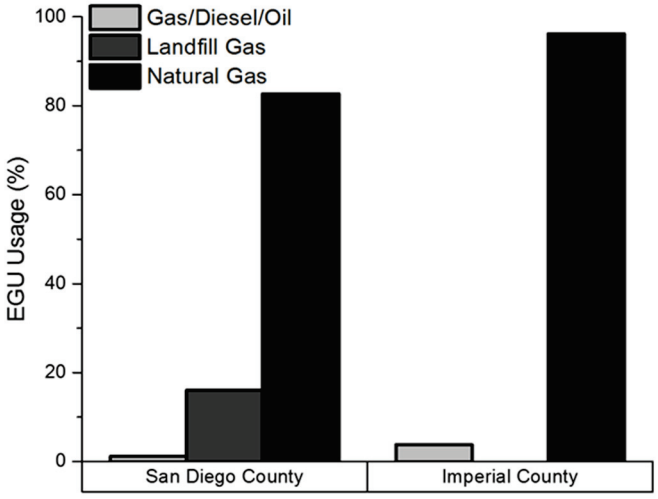

Figure 3: EGU fuel usage by county

$$\delta^{15}N_{NO3} = f_{unknown}\delta^{15}N_{unknown} + \sum f_i \delta^{15}N_i \quad (10)$$

NOx emission inventories for San Diego and Imperial county were obtained from the CARB[*Anon*, 2014] and biogenic emissions for each county were obtained using the BEIS3.12 model[*US EPA*, n.d.] in the Sparse Matrix Operator Kernel Emissions (SMOKE) modeling system. The emissions data was used to determine monthly mole fractions (f_i) for each NOx source. The emissions data was separated into four categories: stationary sources, area-wide sources, mobile sources, and natural sources

Table 3: Mass balance source δ^{15}N-NOx values

Source	δ^{15}N range	δ^{15}N used	Reference
Coal Fired Power Plants	+6 to +25.6‰	15‰‡	Walters et al., 2015b; Heaton, 1990; Felix et al., 2012
Natural Gas Power Plants	-18.2 to -14.8‰	-16.5 ± 1.7‰	Walters et al., 2015b
Motor Vehicle - gas	-19.1 to 17‰	-2.6518 ± 1.5‰ (SD) -3.183 ± 1.5‰ (IMP)	Walters et al., 2015a
Motor Vehicle - diesel	-5 to 0‰	-2.5‰‡	Walters et al., 2015b
Off-Road Vehicles - gas	-14.2 to -8.8‰	-11.5 ± 2.7‰‡	
Airplanes	†	0.9‰*	
Ships/Trains	†	-19‰*	
Soils	-48.9 to -19.9‰	34.3‰‡	Walters et al., 2015b; Li & Wang, 2008; Felix & Elliott, 2014
Wildfires	-7 to 12‰	2.5‰‡	Fibiger et al., 2014

† NOx sources not directly measured.
‡ Average based on observation range. High and low end predictions use range end points.
* Value not changed in the high and low end estimates

(Table 3). Stationary NOx sources include Electrical Generating Units (EGUs) and manufacturing plants, as well as smaller sources such as dry cleaners, sewage treatment plants, and landfills. Although approximately 10% of California's power supply comes from coal combustion, neither San Diego nor Imperial County has any coal EGUs. Instead, EGU's in San Diego and Imperial counties are mainly fueled by natural gas (83% and 96%, respectfully). Mobile NOx sources include gas and diesel powered cars, trucks, buses, and motorcycles as well as off-road sources such as farm and construction equipment, recreational vehicles, airplanes (small craft and commercial), trains, boats, and ships. Natural NOx sources include biogenic or soil NOx and wildfire emissions, which are highly seasonal. Biogenic emissions often peak in the summer growing season with winter minimums, whereas wildfire season tends to occur in the fall, with little to no contributions made outside this season. Area-wide NOx sources include operations such as pesticides, fertilizers, road dust, residential fires, asphalt paving and roofing, and construction solvents. These NOx sources tend to be small and variable, but may contain some seasonal dependence however the $\delta^{15}N$ values of these sources is unknown.

The $\delta^{15}N$ value of NOx from different sources taken from the literature and are summarized in Table 3, and NOx sources included in these categories are summarized in Table 3. Overall, the average $\delta^{15}N$ value for each source was chosen to agree with the values used in the isoscape reported in Walters et al.[*Walters et al.*, 2015a] The $\delta^{15}N$ values for gas powered motor vehicles, off-road vehicles, and natural gas power plants were taken from studies conducted by Walters et al.[*Walters et al.*, 2015a, 2015c] For diesel powered motor vehicles, soil emissions, coal power plants, and wildfire emissions, the mean of the $\delta^{15}N$ value range was used. As $\delta^{15}N_{NOx}$ values for airplanes, trains, and ships have not been determined, the justification given by Walters et al[*Walters et al.*, 2015a] was used. The overall isotopic mass balance is calculated as follows:

$$\delta^{15}N_{NO3} = f_{station}\,\delta^{15}N_{station} + f_{area}\,\delta^{15}N_{area} + f_{mobile}\,\delta^{15}N_{mobile} + f_{natural}\,\delta^{15}N_{natural} \quad (11)$$

The $\delta^{15}N$ value for each of the four source categories were further calculated as using follows:

Table 4: Proportion of NOx Sources (f) by Category (in bold) and sub-category (italics)

Source	San Diego County	Imperial County
Stationary	**0.043**	**0.180**
EGU	*0.289*	*0.087*
Other NOx Sources	*0.711*	*0.913*
Areawide	**0.016**	**0.016**
Mobile	**0.896**	**0.724**
On-Road Gasoline	*0.364*	*0.202*
On-Road Diesel	*0.385*	*0.480*
Non-road NOx Sources	*0.252*	*0.318*
Natural	**0.045**	**0.080**
Biogenics	*0.890*	*1.000*
Wildfires	*0.110*	*0.000*

$$\delta^{15}N_{station} = f_{Natural\ Gas}\,\delta^{15}N_{NaturalGas} + f_{other}\,\delta^{15}N_{other} \quad (12a)$$

$$\delta^{15}N_{mobile} = f_{on\text{-}road\ gas}\,\delta^{15}N_{on\text{-}road\ gas} + f_{on\text{-}road\ diesel}\,\delta^{15}N_{on\text{-}road\ diesel} + f_{off\text{-}road}\,\delta^{15}N_{off\text{-}road} \quad (12b)$$

$$\delta^{15}N_{natural} = f_{biogenic}\,\delta^{15}N_{biogenic} + f_{wildfire}\,\delta^{15}N_{wildfire} \quad (12c)$$

Using monthly net power generation data obtained from the U.S. Energy Information Administration and annual emission data, monthly EGU emissions were determined in order to account for seasonal power consumption shifts. Monthly biogenic emissions were determined using the EPA's Biogenic Emission Inventory System (BEIS3.12)[*US EPA*, n.d.]. In order to account for wildfire seasonality, annual wildfire

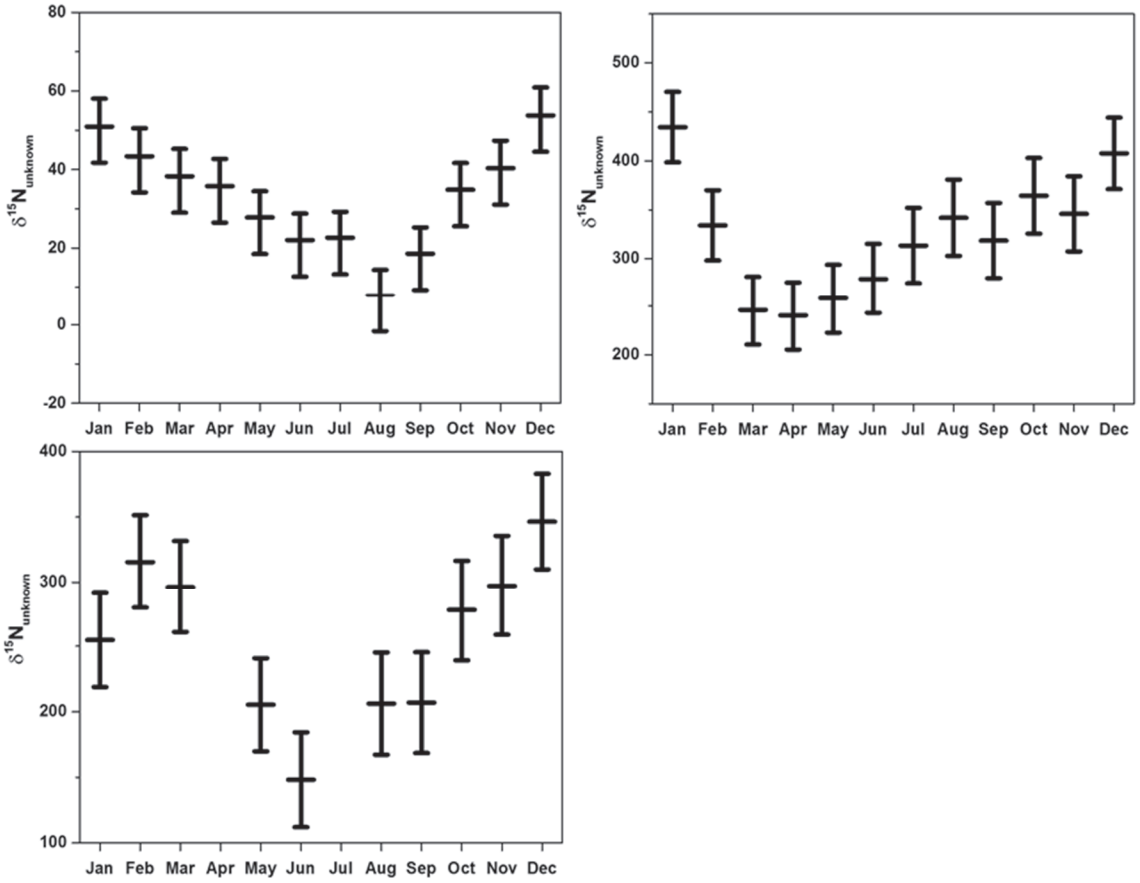

Figure 6: Seasonality of unknown $\delta^{15}N$ source for El Centro (top), El Cajon (middle) and Chula Vista (bottom) California.

emissions were split between months with documented wildfire activity (July – November). Motor vehicle traffic does so some slight difference month to month, and this flux was approximated using the number of vehicle miles traveled (VMT) each month.[*Anon*, 2016c]

By applying measured $\delta^{15}N_{NO3}$ values, the NOx emission inventory, and the known $\delta^{15}N_{NOx}$ source values from Chula Vista, California, Equation 1 simplifies to (using the Chula Vista $\delta^{15}N_{NO3}$ annual average):

$$7.8‰ = -5.9‰ + (0.049)\delta^{15}N_{unknown} \quad (13)$$

where the $0.049 \cdot \delta^{15}N_{unknown}$ represents the NOx sources categorized as area-wide and stationary which have not been characterized for their $\delta^{15}N$ values (i.e. construction/demolition and landfill gas). Ignoring these small NOx contributions, the isotope mass balance would predict that the $\delta^{15}N$ value of NO_3^- in Chula Vista to be approximately -5.9 ± 0.1‰, and varying very little throughout the year. However, measured $\delta^{15}N_{NO3}$ values are approximately 13‰ more enriched than predicted by NOx sources and exhibit a clear seasonal trend. As a result, given that known NOx sources possess primarily negative $\delta^{15}N$ values (-5.9‰) and that the unknown NOx source fraction is very small, a highly positive (~280‰) NOx source would be required order to predict the $\delta^{15}N_{NO3}$ values observed (Figure 5). Yet, considering the fact that majority of NOx sources have been observed to be negative, the above calculated $\delta^{15}N$ value seems

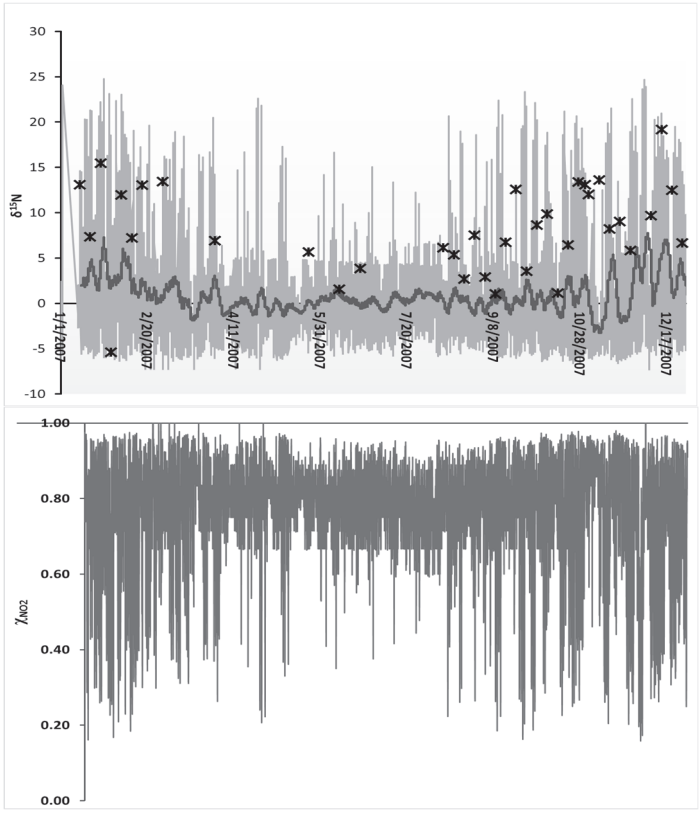

Figure 4:Hourly $\delta^{15}N_{NO2}$ and NO_2 mole ratio for Chula Vista, CA. In the top figure, trace represents a 100-point moving average. Stars represent observed aerosol NO_3 $\delta\delta^{15}N$ values.

highly unlikely, thus lending support to the chemistry hypothesis.

Freyer[*Freyer*, 1978] investigated seasonality of $\delta^{15}N_{NO3}$ values, and suggested that seasonal and diurnal variations in $\delta^{15}N_{NO3}$ values are a combination seasonal changes in source emissions, a shift in reaction mechanisms and/or isotopic exchange equilibrium (14). Further work by Freyer et al.[*Freyer et al.*, 1993] suggested that isotope exchange equilibrium may be the main isotope effect.

$$^{15}NO + {}^{14}NO_2 \leftrightarrow {}^{14}NO + {}^{15}NO_2 \quad (14)$$

To further investigate this effect, Freyer et al[*Freyer et al.*, 1993] measured $\delta^{15}N_{NOx}$, $\delta^{15}N_{NO2}$, and the NO_2 mole ratio (χ_{NO2}), and found that $\delta^{15}N_{NO2}$ became more enriched as χ_{NO2} decreased, with $\delta^{15}N_{NOx} = \delta^{15}N_{NO2}$ when $\chi_{NO2} = 1$. The observed[*Begun and Fletcher*, 1960; *Freyer et al.*, 1993] net effect of the above equilibrium is that ^{15}N accumulates in the more oxidized oxinitrogen species, suggesting that $\delta^{15}N_{NO3}$ values would be similarly enriched. However, as NO_3^- was lost during storage, likely due to volatilization of NH_4NO_3, fractionation resulting from volatilization is likely masked by the enrichment in

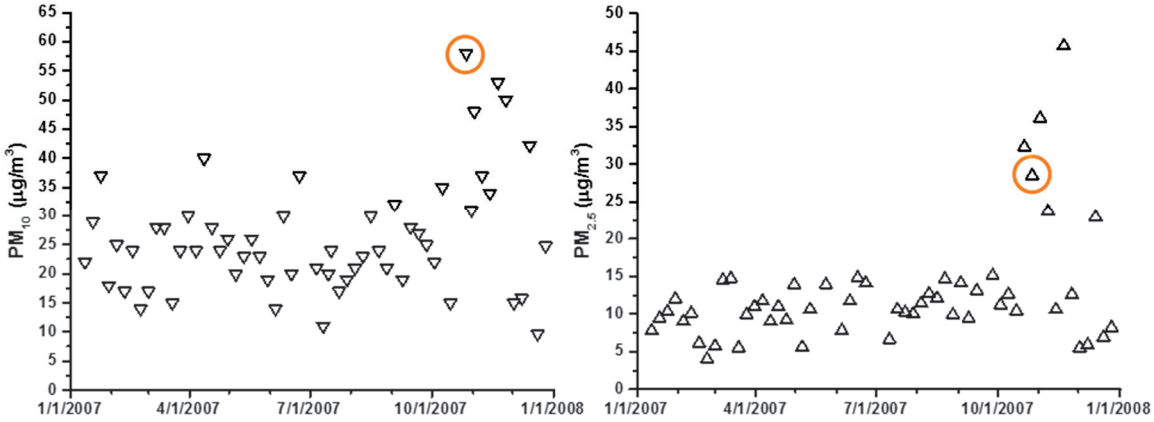

Figure 8: PM concentrations

NH_4NO_3 from the equilibrium exchange.[*Freyer*, 1991]

Although nitrogen exchange between NO and NO_2 has been both modeled and observed, there still existed discrepancies between theoretical calculation and experimental observations. Walters et al.[*Walters et al.*, 2015b] addressed this discrepancy two ways. The authors measured $\alpha_{NO2/NO}$ at 278, 298, 310K and compared the results to a modified form of the Bigeleisen-Mayer equation, recalculated to account for more precise zero point energies. The modified equation was able to more accurately reproduce the observed results. Furthermore, simulating diurnal and seasonal changes, assuming N isotope equilibrium was reached, revealed significant diurnal and seasonal variations in $\delta^{15}N_{NO2}$. This trend is important because without factoring in shifting sources of NO_x, the $\delta^{15}N_{NO2}$ reflected the trends often observed in $\delta^{15}N_{NO3}$ thus strongly supporting the chemistry hypothesis.

Aerosol filters collected in Chula Vista, El Cajon, El Centro, and Brawley at the end of October 2007 were impacted by the wildfire emissions, as noted by the monitoring agency's field notes. PM increases as the result of the fire were observed in both the fine ($PM_{2.5}$) and coarse (PM_{10}) fractions due to the production of trace gases (CO, NOx, O_3), VOCs, and coarse PM (ash, soot, smoke particles). CO concentrations were also slightly elevated relative to seasonal trends, consistent with previous studies that show a major source of CO is wildfires.[*Phuleria*, 2005; *Val Martín et al.*, 2006; *Cai et al.*, 2016] Although wildfires produce substantial concentrations of CO, urban CO emissions dampen this contribution, as fossil fuel combustion (motor vehicles, industrial processes, power generation) dominates CO concentrations.[*Phuleria*, 2005] NOx concentrations

during the fire siege were nearly double (50 ppb) the fall average (29 ppb), although it is not clear whether this increase is due to shifting seasonal trends or wildfire emissions. However, NO concentrations showed a slight increase and NO_2 nearly doubled its seasonal concentration. In studying the 2008 California wildfire season, Cai et al.[*Cai et al.*, 2016] noted that increases in NOx concentration was only significant in the immediate area of the fire. However, these monitoring sites were not in the immediate area of the fires, but rather downwind (Figure 1). Therefore, although wildfire emissions would contribute NOx emissions, overall concentrations were still dominated by local motor vehicle and industrial emissions.[*Phuleria*, 2005] However, NO_2 concentrations are dependent on photolysis (1a and b), which would likely have been decreased as the result of ambient soot and smoke from the fire, leading to increased NO_2 concentrations.[*Phuleria*, 2005] O_3 concentration immediately after the wildfire decreased, although concentrations did increase in the week post-fire. As with NO_2, O_3 concentrations are also photosensitive, which would suggest that concentrations would decrease during and immediately following fire event, when the ambient air reduces photolysis.[*Phuleria*, 2005] However, as wildfire emission contain numerous O_3 precursors, O_3 concentrations increase as the smoke clears and photolysis returns to

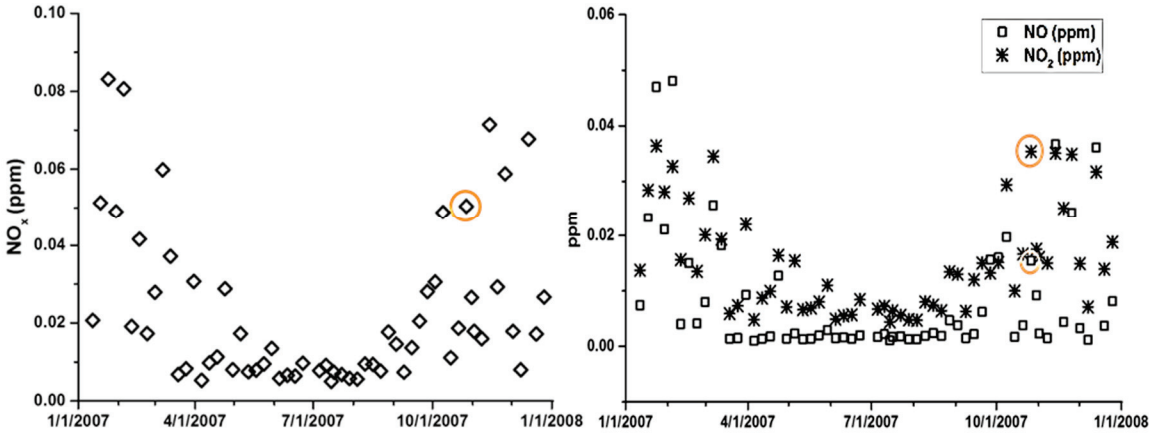

Figure 7: NOx, NO, and NO2 Concentrations

normal levels.

Despite significant differences in the aerosol and trace gas concentrations during the fire event, there no apparent deviation of $\delta^{15}N_{NO3}$ values was observed during the wildfire. Fall $\delta^{15}N_{NO3}$ values range from 1.1 to 13.6‰ (8.0‰ on average), with the $\delta^{15}N_{NO3}$ values impacted by wildfire emissions (13.4‰) falling in the same range. However, the observed value for wildfire impacted days may have been impacted by isotope fractionation due to noted loss of NO_3^- during storage. The CARB anion analysis in 2007 showed elevated NO_3^- concentrations in the samples collected post-wildfire, but our re-analysis in 2015 revealed lower NO_3^- concentrations during the fires indicating NO_3^- loss during storage. The formation of NH_4NO_3 on aerosol filters has been documented, as has its volatilization potential, which increases with increasing temperature.[*Freyer*, 1991; *Achtelik and Omand*, 1998; *Ashbaughm et al.*, 1998] The

volatilization of NH_4NO_3 would lead to isotope fractionation, as the lighter isotope (^{14}N) would volatize first. The degree of fractionation would follow a temperature dependent Rayleigh relationship, as the volatilized NH_4NO_3 would be removed from the system. A previous study by Heaton et al.[*Heaton et al.*, 1997] measured the enrichment factor (ε) for the volatilization of NH_4NO_3 to be -20.6‰. Using this enrichment value, the measured $\delta^{15}N_{NO3}$ value, and the fraction of NO_3^- remaining on the filter, the pre-volatilization $\delta^{15}N_{NO3}$ value can be calculated using the Rayleigh equation:

$$\delta_{initial} = \delta_{final} - \varepsilon \times \ln f_{remain} \quad (15)$$

For the four sampling days impacted by NH_4NO_3, the $\delta^{15}N_{NO3}$ prior to volatilization (δ_{inital}) were all found to be drastically depleted (-45 to +3.7‰, depending on the amount lost) compared to the rest of the season and year. Therefore, Rayleigh fractionation predicts that wildfire emissions would actually deplete $\delta^{15}N_{NO3}$ values rather than enriching them, as suggested in previous work.[*Hastings et al.*, 2009; *Felix et al.*, 2012; *Agnihotri et al.*, 2015]

Although wildfire emissions do not have a significant direct effect on NOx concentrations, components of wildfire emissions have a significant impact on OH radical and O_3 concetrations[*Finlayson-Pitts et al.*, 1999; *Phuleria*, 2005; *Seinfeld and Pandis*, 2006; *Val Martín et al.*, 2006], the two main atmospheric oxidants. VOCs are known to react with NO to form NO_2 without the destruction of an O_3 molecule, essentially catalyzing O_3 production.[*Seinfeld and Pandis*, 2006; *Hastings*, 2010] VOCs are also known to react with OH radicals to form various organic peroxy radicals,[*Seinfeld and Pandis*, 2006] which can also oxidate NO without destroying O_3. While these alternative reaction pathways do not seem to influence NOx concentrations drastically, wildfire emissions have significant influence on the oxidation capacity of the atmosphere, as well as air quality in general.

Although isotopic data indicates the influence of chemistry on $\delta^{15}N$, the extent of this influence has yet to be determined. Although fractionation associated with the isotope exchange equilibrium of NO and NO_2 has been calculated, other fractionation factors still need to be determined. Fractionation factors associated with NO_3^- forming reacions need to be established. Additionally, how these factors vary with temperature, amounts of solar radiation, and in the presence of varying levels of other trace gases. Additionally, the $\delta^{15}N$ values of NOx sources need to be better quantified. Current measured $\delta^{15}N$ values of sources span a large range of values, often with significant overlap. In some cases, the NOx $\delta^{15}N$ value hasn't been measured at all. In order to better predict $\delta^{15}N_{NO3}$ values, the quantification of NOx source $\delta^{15}N$ values and fractionations associated with NOx oxidation pathways will be required. These unknowns should be the focus of future isotopic studies.

5 Conclusions

The 2007 wildfire season in Southern California was particularly explosive due to the influence of the Santa Ana winds. Analysis of PM collected at four sampling sites during this period has revealed the influence wildfire emissions had on local atmospheric chemistry. $PM_{2.5}$, PM_{10}, and CO concentrations all showed increases, whereas O_3

concentrations decreased. Daily average concentrations of NO and NO_2 both increased, but by different degrees, suggesting that wildfire emissions impacted NOx cycling.

Although $\delta^{15}N$ is frequently employed as an environmental tracer, the manner by which it is utilized is not agreed upon. Isotopic analysis of collected NO_3^- has suggested that source $\delta^{15}N$ values are likely not conserved as NOx is oxidized into NO_3^-. Given known source contributions and known $\delta^{15}N$ values of NOx sources, isotope mass balance predicts that a NOx source with highly positive $\delta^{15}N$ value must exist for the source hypothesis to be valid. Furthermore, isotopic analysis has also suggested that wildfire emissions may produce a depleted $\delta^{15}N$, disagreeing with previously predicted $\delta^{15}N$ values.[*Hastings et al.*, 2009; *Felix et al.*, 2012; *Agnihotri et al.*, 2015] While this data set indicates the need for the consideration of chemistry, additional work must focus on how reactions, atmospheric processing, and post-deposition effects influence $\delta^{15}N_{NO3}$ values.

References

Achtelik, G. H., and J. Omand (1998), EFFECTS OF ENVIRONMENTAL CONDITIONS ON PARTICULATE NITRATE STABILITY DURING POST SAMPLING PHASE,

Agnihotri, R., S. G. Karapurkar, V. V. S. S. Sarma, K. Yadav, M. D. Kumar, C. Sharma, and M. V. S. N. Prasad (2015), Stable isotopic and chemical characteristics of bulk aerosols during winter and summer season at a station in Western Coast of India (Goa), *Aerosol Air Qual. Res.*, *15*(3), 888–900, doi:10.4209/aaqr.2014.07.0127.

Andreae, M. O., and P. J. Crutzen (1997), Atmospheric Aerosols: Biogeochemical Sources and Role in Atmospheric Chemistry, *Science (80-.).*, *276*(5315).

Anon (2011), *Meteorology Data Query Tool*.

Anon (2014), *Air Quality Data Query Tool*.

Anon (2015), California Power Plants,

Anon (2016a), Imperial Irrigation District: Water, Available from: http://www.iid.com/water

Anon (2016b), *Monthly Climate Summaries*.

Anon (2016c), *Traffic Census Program*.

Anon (n.d.), 2007 Southern California Fire Seige, *San Diego Wildfires Educ. Proj.* Available from: http://interwork.sdsu.edu/fire/resources/2007_fires.html

Ashbaughm, L., R. Eldred, and S. Hering (1998), *Loss of Particulate Nitrate from Teflon Sampling Filters: Effects on Measured Gravimetric Mass*, Davis, CA.

Ayers, G. P., and J. M. Cainey (2007), The CLAW hypothesis: a review of the major developments, *Environ. Chem.*, *4*(6), 366–374, doi:10.1071/en07080.

Bates, T. S., J. D. Cline, R. H. Gammon, and S. R. Kelly-Hansen (1987), Regional and seasonal variations in the flux of oceanic dimethylsulfide to the atmosphere, *J. Geophys. Res.*, *92*(C3), 2930, doi:10.1029/JC092iC03p02930.

Begun, G. M., and W. H. Fletcher (1960), Partition Function Ratios for Molecules Containing Nitrogen Isotopes, *J. Chem. Phys.*, *33*(4), 1083, doi:10.1063/1.1731338.

Benkovitz, C. M., M. T. Scholtz, J. Pacyna, L. Tarrason, J. Dignon, E. C. Voldner, P. A. Spiro, J. A. Logan, and T. E. Graedel (1996), Global gridded inventories of anthropogenic emissions of sulfur and nitrogen, *J. Geophys. Res.*, *101*(D22), 29239–29253, doi:10.1029/96jd00126.

Cai, C. et al. (2016), Simulating reactive nitrogen, carbon monoxide, and ozone in California during ARCTAS-CARB 2008 with high wildfire activity, *Atmos. Environ.*, *128*, 28–44, doi:10.1016/j.atmosenv.2015.12.031.

California Air Resources Board (2011), Particulate Matter Monitoring as of January 27, 2011, Available from: http://www.arb.ca.gov/aaqm/am_tables/partic.htm (Accessed 14 June 2016)

Charlson, R. J., J. E. Lovelock, M. O. Andreae, and S. G. Warren (1987), OCEANIC PHYTOPLANKTON, ATMOSPHERIC SULFUR, CLOUD ALBEDO AND CLIMATE, *Nature*, *326*(6114), 655–661, doi:10.1038/326655a0.

D. M. Sigman K. L. Casciotti, M. Andreani, C. Barford,M. Galanter, and J. K. Bolhlke (2001), A Bacterial Method for the Nitrogen Isotopic Analysis of Nitrate in Seawater and Freshwater, *Anal. Chem.*, 4145–4153.

Dang, H., M. Moore, K. Ross, C. Carr, J. Taylor, and B. Hammond (2014), *2014 County of San Diego Crop Statistics & Annual Report*.

Dominguez, G., T. Jackson, L. Brothers, B. Barnett, B. Nguyen, and M. H. Thiemens (2008), Discovery and measurement of an isotopically distinct source of sulfate in Earth's atmosphere., *Proc. Natl. Acad. Sci. U. S. A.*, doi:10.1073/pnas.0805255105.

Elliott, E. M., C. Kendall, S. D. Wankel, D. A. Burns, E. W. Boyer, K. Harlin, D. J. Bain, and T. J. Butler (2007), Nitrogen Isotopes as Indicators of NO x Source Contributions to Atmospheric Nitrate Deposition Across the Midwestern and Northeastern United States, *Environ. Sci. Technol.*, *41*(22), 7661–7667, doi:10.1021/es070898t.

Elliott, E. M., C. Kendall, E. W. Boyer, D. A. Burns, G. G. Lear, H. E. Golden, K. Harlin, A. Bytnerowicz, T. J. Butler, and R. Glatz (2009), Dual nitrate isotopes in dry deposition: Utility for partitioning NO x source contributions to landscape nitrogen

deposition, *J. Geophys. Res.*, *114*(G4), G04020, doi:10.1029/2008JG000889.

Felix, J. D., E. M. Elliott, and S. L. Shaw (2012), Nitrogen isotopic composition of coal-fired power plant NOx: influence of emission controls and implications for global emission inventories., *Environ. Sci. Technol.*, *46*(6), 3528–35, doi:10.1021/es203355v.

FENN, M. E. et al. (2003), Nitrogen Emissions, Deposition, and Monitoring in the Western United States, *Bioscience*, *53*(4), 391, doi:10.1641/0006-3568(2003)053[0391:NEDAMI]2.0.CO;2.

Finlayson-Pitts, B. J., J. N. Pitts, and Jr. (1999), *Chemistry of the Upper and Lower Atmosphere: Theory, Experiments, and Applications*, Academic Press.

Freyer, H. D. (1978), Seasonal trends of NH + 4 and NO - 3 nitrogen isotope composition in rain collected at Jülich, Germany, *Tellus A*, *30*(1).

Freyer, H. D. (1991), Seasonal Variation of 15N/14N ratios in Atmospheric Nitrate Species, *Tellus*, (43B), 30–44.

Freyer, H. D., D. Kley, A. Volz-Thomas, and K. Kobel (1993), On the interaction of isotopic exchange processes with photochemical reactions in atmospheric oxides of nitrogen, *J. Geophys. Res.*, *98*(D8), 14791, doi:10.1029/93JD00874.

Galloway, J. N. et al. (2004), Nitrogen Cycles: Past, Present, and Future, *Biogeochemistry*, *70*(2), 153–226, doi:10.1007/s10533-004-0370-0.

Gobel, A. R., K. E. Altieri, A. J. Peters, M. G. Hastings, and D. M. Sigman (2013), Insights into anthropogenic nitrogen deposition to the North Atlantic investigated using the isotopic composition of aerosol and rainwater nitrate, *Geophys. Res. Lett.*, doi:10.1002/2013GL058167.

Grijalva, R., R. Moore, and H. Renteria (n.d.), *California Fire Siege 2007: An Overview*.

Hastings, M. G. (2004), Seasonal variations in N and O isotopes of nitrate in snow at Summit, Greenland: Implications for the study of nitrate in snow and ice cores, *J. Geophys. Res.*, *109*(D20), D20306, doi:10.1029/2004JD004991.

Hastings, M. G. (2010), Evaluating source, chemistry and climate change based upon the isotopic composition of nitrate in ice cores, *IOP Conf. Ser. Earth Environ. Sci.*, *9*, 012002, doi:10.1088/1755-1315/9/1/012002.

Hastings, M. G., D. M. Sigman, and F. Lipschultz (2003a), Isotopic evidence for source changes of nitrate in rain at Bermuda, *J. Geophys. Res. Atmos.*, *108*(D24), n/a–n/a, doi:10.1029/2003JD003789.

Hastings, M. G., D. M. Sigman, and F. Lipschultz (2003b), Isotopic evidence for source

changes of nitrate in rain at Bermuda, *J. Geophys. Res. Atmos.*, *108*(D24), n/a–n/a, doi:10.1029/2003JD003789.

Hastings, M. G., J. C. Jarvis, and E. J. Steig (2009), Anthropogenic impacts on nitrogen isotopes of ice-core nitrate., *Science*, *324*(5932), 1288, doi:10.1126/science.1170510.

Heaton, T. H. E., B. Spiro, and S. M. C. Robertson (1997), Potential canopy in uences on the isotopic composition of nitrogen and sulphur in atmospheric deposition, *Oecologia*, (109), 600–607.

Hoefs, J. (2015), *Stable Isotope Geochemistry*, Springer International Publishing, Cham.

James N. Galloway, E. B. C. (2002), Reactive Nitrogen and the World: 200 Years of Change, *Ambio*, *31*(2), 64–71.

K. L. Casciotti M. Galanter Hastings, J. K. Bo1 hlke, and A. Hilkert, D. M. S. (2002), Measurement of the Oxygen Isotopic Composition of Nitrate in Seawater and Freshwater Using the Denitrifier Method, *Anal. Chem.*, 4905–4912.

Kaiser, J., M. G. Hastings, B. Z. Houlton, T. Röckmann, and D. M. Sigman (2007), Triple oxygen isotope analysis of nitrate using the denitrifier method and thermal decomposition of N2O., *Anal. Chem.*, *79*(2), 599–607, doi:10.1021/ac061022s.

King, M. (2013), Evaluating NOx Sources And Oxidation Pathways Impacting Aerosol Production On The Southern Ute Indian Reservation And Navajo Nation Using Geochemical Isotopic Analysis, Purdue University.

Liu, X.-H., and Y. Zhang (2013), Understanding of the formation mechanisms of ozone and particulate matter at a fine scale over the southeastern U.S.: Process analyses and responses to future-year emissions, *Atmos. Environ.*, *74*, 259–276, doi:10.1016/j.atmosenv.2013.03.057.

Logan, J. A. (1983), Nitrogen oxides in the troposphere: Global and regional budgets, *J. Geophys. Res.*, *88*(C15), 10785, doi:10.1029/JC088iC15p10785.

Logan, J. A., M. J. Prather, S. C. Wofsy, and M. B. McElroy (1981), Tropospheric chemistry: A global perspective, *J. Geophys. Res.*, *86*(C8), 7210, doi:10.1029/JC086iC08p07210.

Maan, A. A. (2012), *Fertilizing Materials: Tonnage Report*.

Marquez, J., and T. Knapp (2014), Freight Planning Fact Sheet: Unified Port of San Diego,

Monks, P. S. et al. (2009), Atmospheric composition change – global and regional air quality, *Atmos. Environ.*, *43*(33), 5268–5350, doi:10.1016/j.atmosenv.2009.08.021.

Morin, S., J. Savarino, M. M. Frey, N. Yan, S. Bekki, J. W. Bottenheim, and J. M. F. Martins (2008), Tracing the Origin and Fate of NOx in the Arctic Atmosphere Using Stable Isotopes in Nitrate, *Science (80-.).*, *322*(5902), 730–732, doi:10.1126/science.1161910.

Neumann, D., V. Matthias, J. Bieser, A. Aulinger, and M. Quante (2016), Sensitivity of modeled atmospheric nitrogen species and nitrogen deposition to variations in sea salt emissions in the North Sea and Baltic Sea regions, *Atmos. Chem. Phys.*, *16*(5), 2921–2942, doi:10.5194/acp-16-2921-2016.

Phuleria, H. C. (2005), Air quality impacts of the October 2003 Southern California wildfires, *J. Geophys. Res.*, *110*(D7), D07S20, doi:10.1029/2004JD004626.

Riha, K. M. (2013), The Use of Stable Isotopes to Constrain the Nitrogent Cycle, Purdue University.

San Diego County Water Authority (2016), FAQ and Key Facts, Available from: http://www.sdcwa.org/frequently-asked-questions-and-key-facts#t7n654

Savarino, J., S. K. Bhattacharya, S. Morin, M. Baroni, and J.-F. Doussin (2008), The NO+O3 reaction: a triple oxygen isotope perspective on the reaction dynamics and atmospheric implications for the transfer of the ozone isotope anomaly., *J. Chem. Phys.*, *128*(19), 194303, doi:10.1063/1.2917581.

Seinfeld, J. H., and S. N. Pandis (2006), *Atmospheric Chemistry and Physics: From Air Pollution to Climate Change, 2nd Edition* -, 2nd ed.

Sievering, H., J. Cainey, M. Harvey, J. McGregor, S. Nichol, and P. Quinn (2004), Aerosol non-sea-salt sulfate in the remote marine boundary layer under clear-sky and normal cloudiness conditions: Ocean-derived biogenic alkalinity enhances sea-salt sulfate production by ozone oxidation, *J. Geophys. Res.*, *109*(D19), doi:10.1029/2003jd004315.

Sillman, S. (1999), The relation between ozone, NO V and hydrocarbons in urban and polluted rural environments, *Atmos. Environ.*, *33*, 1821–1845.

US EPA, O. (n.d.), Biogenic Emission Inventory System (BEIS),

Val Martín, M., R. E. Honrath, R. C. Owen, G. Pfister, P. Fialho, and F. Barata (2006), Significant enhancements of nitrogen oxides, black carbon, and ozone in the North Atlantic lower free troposphere resulting from North American boreal wildfires, *J. Geophys. Res. Atmos.*, *111*(D23), n/a–n/a, doi:10.1029/2006JD007530.

Valenzuela, C. L., L. S. Evans, and K. Ross (2014), *Imperial County Agricultural Crop & Livestock Report*.

Walters, W. W., and G. Michalski (2015), Theoretical calculation of nitrogen isotope

equilibrium exchange fractionation factors for various NOy molecules, *Geochim. Cosmochim. Acta*, *164*, 284–297, doi:10.1016/j.gca.2015.05.029.

Walters, W. W., B. D. Tharp, H. Fang, B. J. Kozak, and G. Michalski (2015a), Nitrogen Isotope Composition of Thermally Produced NOx from Various Fossil-Fuel Combustion Sources., *Environ. Sci. Technol.*, *49*(19), 11363–71, doi:10.1021/acs.est.5b02769.

Walters, W. W., D. S. Simonini, and G. Michalski (2015b), Nitrogen isotope exchange between NO and NO 2 and its implications for δ 15 N variations in tropospheric NO x and atmospheric nitrate, *Geophys. Res. Lett.*, (2), 1–26.

Walters, W. W., S. R. Goodwin, and G. Michalski (2015c), Nitrogen stable isotope composition (δ15N) of vehicle-emitted NOx., *Environ. Sci. Technol.*, *49*(4), 2278–85, doi:10.1021/es505580v.

Wang, H., and D. Shooter (2001), Water soluble ions of atmospheric aerosols in three New Zealand cities: seasonal changes and sources, *Atmos. Environ.*, *35*(34), 6031–6040, doi:10.1016/S1352-2310(01)00437-X.

Wankel, S. D., Y. Chen, C. Kendall, and A. F. Post (2010), Sources of aerosol nitrate to the Gulf of Aqaba: Evidence from δ15N and δ18O of nitrate and trace metal chemistry, *Mar. Chem.*, *120*(1), 90–99, doi:10.1016/j.marchem.2009.01.013.

Williams, J. et al. (2016), Opposite OH reactivity and ozone cycles in the Amazon rainforest and megacity Beijing: Subversion of biospheric oxidant control by anthropogenic emissions, *Atmos. Environ.*, *125*, 112–118, doi:10.1016/j.atmosenv.2015.11.007.

Zatko, M., L. Geng, B. Alexander, E. Sofen, and K. Klein (2016), The impact of snow nitrate photolysis on boundary layer chemistry and the recycling and redistribution of reactive nitrogen across Antarctica and Greenland in a global chemical transport model, *Atmos. Chem. Phys*, *16*, 2819–2842, doi:10.5194/acp-16-2819-2016.